Defense Threat Reduction Agency
8725 John J. Kingman Road, MS
6201 Fort Belvoir, VA 22060-6201

DTRA-TR-12-72

TECHNICAL REPORT

Inactivation of Aerosolized Biological Agents using Filled Nanocomposite Materials

Approved for public release, distribution is unlimited.

February 2013

HDTRA1-08-1-0012

S.A. Grinshpun et al.

Prepared by:
University of Cincinnati
51 Goodman Drive
University Hall Suite 530
P.O. Box 210222
Cincinnati, OH 45221

DESTRUCTION NOTICE:

Destroy this report when it is no longer needed.
Do not return to sender.

PLEASE NOTIFY THE DEFENSE THREAT REDUCTION AGENCY, ATTN: DTRIAC/ J-3 ONIUI , 8725 JOHN J. KINGMAN ROAD, MS-6201, FT BELVOIR, VA 22060-6201, IF YOUR ADDRESS IS INCORRECT, IF YOU WISH THAT IT BE DELETED FROM THE DISTRIBUTION LIST, OR IF THE ADDRESSEE IS NO LONGER EMPLOYED BY YOUR ORGANIZATION.

REPORT DOCUMENTATION PAGE

Form Approved
OMB No. 0704-0188

1. REPORT DATE *(DD-MM-YYYY)*	**2. REPORT TYPE**	**3. DATES COVERED** *(From - To)*
00-02-2013	Technical	01/28/2008 - 08/07/2011

4. TITLE AND SUBTITLE

Inactivation of Aerosolized Biological Agents using Filled Nanocomposite Materials

5a. CONTRACT NUMBER

5b. GRANT NUMBER
HDTRA1-08-1-0012

5c. PROGRAM ELEMENT NUMBER

6. AUTHOR(S)

S.A. Grinshpun, M.Schoenitz, E. Dreizin, A. Adhikari, T. Reponen, and M. Yermakov

5d. PROJECT NUMBER

5e. TASK NUMBER

5f. WORK UNIT NUMBER

7. PERFORMING ORGANIZATION NAME(S) AND ADDRESS(ES)

University of Cincinnati, 51 Goodman Drive University Hall Ste 530, PO Box 210222, Cincinnati, OH 45221-0222
New Jersey Institute of Technology, 323 Dr. ML King Jr Blvd, Newark, NJ 07102
Reactive Metals International, Inc., 340 E. Church Road, King of Prussia, PA 19406

8. PERFORMING ORGANIZATION REPORT NUMBER

9. SPONSORING / MONITORING AGENCY NAME(S) AND ADDRESS(ES)

Defense Threat Reduction Agency
8725 John J. Kingman Road STOP 6201
Fort Belvoir, VA 22060

10. SPONSOR/MONITOR'S ACRONYM(S)

DTRA

11. SPONSOR/MONITOR'S REPORT NUMBER(S)

DTRA-TR-12-72

12. DISTRIBUTION / AVAILABILITY STATEMENT

Approved for public release; distribution is unlimited.

13. SUPPLEMENTARY NOTES

14. ABSTRACT

In this multi-institutional grant, a new method for inactivating aerosolized biological agents was developed utilizing a new class of energetic materials: filled nanocomposite materials. The implemented approach enabled a controllable release of iodine-based oxidizing species in the combustion environment to inactivate viable airborne bio-agents, such as stress-resistant bacterial spores and viruses. Composites with adjustable Al/I2 ratios were produced. A state-of-the-art experimental facility was developed for studying how novel energetic formulations and their combustion products affect the viability of aerosolized spores and viruses during a short (< 1 s) exposure times. Controlled bioaerosol dispersal and sample collection protocols were developed and optimized. The dry-heat inactivation of aerosolized spores was quantified separately from chemical effects and linked to DNA repair mechanisms. It was concluded that the iodine-containing powder provided significantly more effective inactivation of airborne spores than non-iodinated powders. The results of this research help to better understand physical, physicochemical, and biological properties associated with inactivation of aerosolized bio-agents in combustion environments.

15. SUBJECT TERMS

Bioaerosol inactivation, spore, virus, bio-agent defeat, energetic material, iodine

16. SECURITY CLASSIFICATION OF:			**17. LIMITATION OF ABSTRACT**	**18. NUMBER OF PAGES**	**19a. NAME OF RESPONSIBLE PERSON**
a. REPORT	**b. ABSTRACT**	**c. THIS PAGE**	SAR	139	Dr. Sergey Grinshpun
Unclassified	Unclassified	Unclassified			**19b. TELEPHONE NUMBER** *(include area code)* (513) 558-0504

Standard Form 298 (Rev. 8-98)
Prescribed by ANSI Std. Z39.18

CONVERSION TABLE

Conversion Factors for U.S. Customary to metric (SI) units of measurement.

MULTIPLY →	BY →	TO GET
TO GET ←	BY ←	DIVIDE
angstrom	1.000 000 x E -10	meters (m)
atmosphere (normal)	1.013 25 x E +2	kilo pascal (kPa)
bar	1.000 000 x E +2	kilo pascal (kPa)
barn	1.000 000 x E -28	meter^2 (m^2)
British thermal unit (thermochemical)	1.054 350 x E +3	joule (J)
calorie (thermochemical)	4.184 000	joule (J)
cal (thermochemical/cm^2)	4.184 000 x E -2	mega joule/m^2 (MJ/m^2)
curie	3.700 000 x E +1	*giga bacquerel (GBq)
degree (angle)	1.745 329 x E -2	radian (rad)
degree Fahrenheit	$t_k = (t^\circ f + 459.67)/1.8$	degree kelvin (K)
electron volt	1.602 19 x E -19	joule (J)
erg	1.000 000 x E -7	joule (J)
erg/second	1.000 000 x E -7	watt (W)
foot	3.048 000 x E -1	meter (m)
foot-pound-force	1.355 818	joule (J)
gallon (U.S. liquid)	3.785 412 x E -3	meter^3 (m^3)
inch	2.540 000 x E -2	meter (m)
jerk	1.000 000 x E +9	joule (J)
joule/kilogram (J/kg) radiation dose absorbed	1.000 000	Gray (Gy)
kilotons	4.183	terajoules
kip (1000 lbf)	4.448 222 x E +3	newton (N)
kip/inch^2 (ksi)	6.894 757 x E +3	kilo pascal (kPa)
ktap	1.000 000 x E +2	newton-second/m^2 ($N-s/m^2$)
micron	1.000 000 x E -6	meter (m)
mil	2.540 000 x E -5	meter (m)
mile (international)	1.609 344 x E +3	meter (m)
ounce	2.834 952 x E -2	kilogram (kg)
pound-force (lbs avoirdupois)	4.448 222	newton (N)
pound-force inch	1.129 848 x E -1	newton-meter (N-m)
pound-force/inch	1.751 268 x E +2	newton/meter (N/m)
pound-force/foot^2	4.788 026 x E -2	kilo pascal (kPa)
pound-force/inch^2 (psi)	6.894 757	kilo pascal (kPa)
pound-mass (lbm avoirdupois)	4.535 924 x E -1	kilogram (kg)
pound-mass-foot^2 (moment of inertia)	4.214 011 x E -2	kilogram-meter^2 ($kg-m^2$)
pound-mass/foot^3	1.601 846 x E +1	kilogram-meter^3 (kg/m^3)
rad (radiation dose absorbed)	1.000 000 x E -2	**Gray (Gy)
roentgen	2.579 760 x E -4	coulomb/kilogram (C/kg)
shake	1.000 000 x E -8	second (s)
slug	1.459 390 x E +1	kilogram (kg)
torr (mm Hg, 0^0 C)	1.333 22 x E -1	kilo pascal (kPa)

*The bacquerel (Bq) is the SI unit of radioactivity; 1 Bq = 1 event/s.

**The Gray (GY) is the SI unit of absorbed radiation.

CONTENTS

ABSTRACT

In this multi-institutional grant, a new method for inactivating aerosolized biological agents was developed utilizing a new class of energetic materials: filled nanocomposite materials. The implemented approach enabled a controllable release of iodine-based oxidizing species in the combustion environment to inactivate viable airborne bio-agents, such as stress-resistant bacterial spores and viruses. Composites with adjustable Al/I_2 ratios were produced. A state-of-the-art experimental facility was developed for studying how novel energetic formulations and their combustion products affect the viability of aerosolized spores and viruses during a short (< 1 s) exposure times. Controlled bioaerosol dispersal and sample collection protocols were developed and optimized. The dry-heat inactivation of aerosolized spores was quantified separately from chemical effects and linked to DNA repair mechanisms. It was concluded that the iodine-containing powder provided significantly more effective inactivation of airborne spores than non-iodinated powders. The results of this research help to better understand physical, physicochemical, and biological properties associated with inactivation of aerosolized bio-agents in combustion environments.

Summary of accomplishments

Major milestones:

- Development and validation of methods for assessing biocidal properties of new composites designed for agent defeat
- Development of new FNM with targeted properties
- Evaluation of microbial inactivation due to exposure of airborne spores and viruses to dry heat and products of combustion
- Establishing association between the heat-induced inactivation of airborne bacterial spores and the DNA mutational frequency
- Establishing feasibility of the new iodine-based FNM for agent defeat applications

Publications & meetings: 6 papers were published in major peer-reviewed journals and two are under preparation; 16 papers were presented at national/international meetings and two more were accepted for presentation.

Personnel support: 5 faculty members, 4 research associates, 2 postdoctoral fellows, and a PhD student have been supported.

Educational mission: Counter-WMD research subjects were incorporated in the program for mentoring graduate students.

List of individuals contributing to the grant

UNIVERSITY OF CINCINNATI:

Grinshpun, S.A.
Reponen, T.
Adhikari, A.
Yermakov, M.
Indugula, R.
Li., C.
Johansson, E.
Reponen, L.

NEW JERSEY INSTITUTE OF TECHNOLOGY:

Schoenitz M.
Dreizin E.L.
Zhang, S.

RMI:

Trunov M.
Mohan, S.
Hoffmann, V.

Peer-reviewed journal publications resulted from the grant activities

1. Grinshpun, S.A., Adhikari, A., Li C., Reponen, T., Yermakov, M., Schoenitz, M., Dreizin, E., Trunov M., Mohan, S. (2010) Thermal Inactivation of Airborne Viable *Bacillus Subtilis* Spores by Short-term Exposure in Axially Heated Air Flow, *Journal of Aerosol Science*, 41:352-363.

2. Grinshpun, S.A., Adhikari, A., Li C., Yermakov, M., Reponen, L., Johansson, E., Trunov M. (2010) Inactivation of Aerosolized Viruses in Continuous Air Flow with Axial Heating, *Aerosol Science and Technology*, 44:1042-1048.

3. Grinshpun, S.A., Li C., Adhikari, A., Yermakov, M., Reponen, T., Schoenitz, M., Dreizin, E., Hoffmann, V., Trunov M. (2010) Method for Studying Survival of Airborne Viable Microorganisms in Combustion Environments: Development and Evaluation, *Aerosol and Air Quality Research*, 10: 414-424.

4. Zhang, S., Schoenitz, M., Dreizin, E.L. (2010) Iodine Release, Oxidation, and Ignition of Mechanically Alloyed Al−I Composites. *Journal of Physical Chemistry C*, 114 (46): 19653-19659.

5. Zhang S., Schoenitz, M., and Dreizin, E.L. (2010) Mechanically Alloyed Al–I Composite Materials. *Journal of Physics and Chemistry of Solids*, 71: 1213-1220.

6. Johansson, E., Adhikari, A., Reponen, T., Yermakov, M., Grinshpun, S.A. (2011) Association between Increased DNA Mutational Frequency and Thermal Inactivation of Aerosolized *Bacillus* Spores Exposed to Dry Heat, *Aerosol Science and Technology*, 45: 376-381.

Note: Three more papers are being prepared for submission to peer-reviewed journals.

Presentations at national/international scientific conferences and seminars resulted from the grant activities

1. Grinshpun S.A., Adhikari A., Li C., Reponen T., Schoenitz M., Dreizin E., Trunov M. (2008). Method and Experimental Facility for Evaluating the Inactivation of Aerosolized Microorganisms by a Halogen-enriched Filled Nanocomposite Material. Presented at the Annual Conference of the American Association for Aerosol Research (Orlando, FL, October 20– 24, 2008).

2. Schoenitz M., Dreizin, E., Stamatis, D., Grinshpun, S.A., Adhikari, A., Li, C., Reponen, T. (2008). Filled Nanocomposite Naterials for Biocidal Applications. Presented at the Annual Conference of the American Institute of Chemical Engineers (Philadelphia, PA, November 16-21, 2008).

3. Adhikari A., Grinshpun S.A., Li C., Reponen T., Schoenitz M., Dreizin E., Trunov M. (2009). Inactivation of Airborne *Bacillus* Endospores Resulting from Combustion of Iodinated and Non-iodinated Nanocomposite Energetic Materials. Presented at the 109th General Meeting of the American Society for Microbiology (Philadelphia, PA, May 17–21, 2009).

4. Grinshpun S.A., Adhikari A., Li C., Reponen T., Schoenitz M., Dreizin E., Trunov M. (2009). Collection of Airborne Spores from Combustion Environments. Presented at the European Aerosol Conference (Karlsruhe, Germany, September 6–11, 2009).

5. Grinshpun S.A., Adhikari A., Li C., Reponen T., Schoenitz M., Dreizin E., Mohan S., Trunov M. (2009). Survival of *Bacillus Subtilis* Endospores In an Air Flow With Axial Heating. Presented at the Annual Conference of the American Association for Aerosol Research (Minneapolis, MN, October 26–30, 2009).

6. Zhang, S., Schoenitz, M., Dreizin, E.L., Preparation and Characterization Al-I Nanocomposite Powders as Fuel Additives with Biocidal Combustion Products. Presented at the 48th AIAA Aerospace Sciences Meeting (Orlando, FL, January 4–7, 2010).

7. Grinshpun S.A., Reponen T., Adhikari A., Yermakov, M., Johansson, L., Schoenitz M., Dreizin E. (2010). Filled Nanocomposite Materials against Aerosolized Agents. Presented at the DTRA Meeting (Eglin Air Force Base, FL, February 2010).

8. Grinshpun S.A., Yermakov, M., Adhikari A., Li C., Reponen T., Johansson, L., Schoenitz M., Dreizin E. (2010). Inactivation of Aerosolized Bacterial Spores and Viruses in Combustion Environments. Presented at the TTCP Meeting, Defense Science and Technology Laboratory (DSTL, Porton Down, UK, March 8–9, 2010).

9. Grinshpun, S.A., Adhikari, A., Yermakov, M., Li, C., Reponen, L., Johansson, E., Reponen, T., Trunov, M. (2010) Inactivation of Aerosolized Viruses by a Short-Term Exposure in a Heated Air Flow. Presented at the International Aerosol Conference (Helsinki, Finland, August 29 – September 3, 2010).

10. Johansson, E., Adhikari, Reponen, T., Yermakov, M., Grinshpun, S.A., (2010) Viability Loss in Heat-Exposed Aerosolized *Bacillus subtilis* Spores is Strongly Correlated with Mutational Frequency. Presented at the International Aerosol Conference (Helsinki, Finland, August 29 – September 3, 2010).

11. Grinshpun, S.A. (2010) PLENARY: Recent Advances in Biological Aerosol Research. Presented at the 29th Annual Conference of the American Association for Aerosol Research (Portland, Oregon, October 25-29, 2010).

12. Grinshpun, S.A., Adhikari, A., Yermakov, M., Reponen, L., Reponen, T., Dreizin, E., Schoenitz, M., Zhang, S., Hoffmann, V. (2010) Short-term Exposure of Aerosolized Bacillus Endospores to Combustion of Energetic Materials. Presented at the 29th Annual Conference of the American Association for Aerosol Research (Portland, Oregon, October 25-29, 2010).

13. Dreizin, E.L. and Zhang, S. (2011) Reactive Materials for Enhanced Blast Explosives. JANNAF paper; 58th JANNAF Propulsion Meeting (Arlington, VA, April 18-21, 2011).

14. Badiola, C, Zhang, S., Aly, Y., Dreizin, E.L. (2011) Combustion Rates and Temperatures of Reactive Material Particles. 7th US National Technical Meeting of the Combustion Institute (Atlanta, GA, March 20-23, 2011).

15. Aly, Y., Schoenitz, M., Dreizin, E.L. (2011) Aluminum-Boron-Halogen Ternary Reactive Composite Powders. 7th US National Technical Meeting of the Combustion Institute (Atlanta, GA, March 20-23, 2011).

16. Zhang, S., Badiola, C., Schoenitz, M., Dreizin, E.L. (2011) Al•I2 Composite as Fuel Additives with Biocidal Combustion Products. 7th US National Technical Meeting of the Combustion Institute (Atlanta, GA, March 20-23, 2011).

Note: The above list does not include four annual presentations delivered at the DTRA Technical review Meetings in 2008, 2009, 2010, and 2011.

Chapter 1. Method for studying survival of airborne viable microorganisms in combustion environments: development and evaluation

Paper published: Grinshpun, S.A., Li C., Adhikari, A., Yermakov, M., Reponen, T., Schoenitz, M., Dreizin, E., Hoffmann, V., and Trunov M. (2010) Method for Studying Survival of Airborne Viable Microorganisms in Combustion Environments: Development and Evaluation, *Aerosol and Air Quality Research*, 10(5):414-424.

Introduction

Technologies based on thermal and chemical air treatment have demonstrated success in inactivating airborne microorganisms (Lee and Lee, 2006; Ma *et al.*, 2008; Wood *et al.*, 2008; Jung *et al.*, 2009a,b). The development of methods for effective destruction of aerosolized biological agents remains an integral part of defense research programs in the US (Henderson, 2004; Hitchcock *et al.*, 2006; Koch, 2006) and abroad (Tan *et al.*, 2006; Nadasi *et al.*, 2007). Combustion product environments are of particular relevance to military and counterterrorism situations. If bio-agents released as a result of explosion or fire in a bio-weapon facility survive the stress and remain pathogenic, they may be subjected to short- or long-range atmospheric transport and contaminate large areas, which would pose a major threat to the public and infrastructure (Nelson, 2004).

An effective agent defeat weapon to counter biological agents should prevent the undesirable effect of dispersing live agents. Energetic materials are being developed with the added capability to effectively inactivate stress-resistant microorganisms when, e.g., a stockpile of stored bio-weapon agents is targeted. For instance, filled nanocomposite materials (FNMs) with specific combinations of halogen compounds are being presently explored because of their potential to defeat highly pathogenic airborne bacteria and viruses (Zhang *et al.*, 2010). Most of such materials are manufactured as powders to be added to

energetic formulations and aerosolized upon blast (Johnson *et al.*, 2008; Obrey *et al.*, 2008). Inactivation of *aerosolized* agents, especially those dispersed in a military situation, should occur during the short time of their exposure to biocidal materials (e.g., during explosion and post-explosion combustion). Therefore, biocidal effects of combustion products are to be intimately coupled with thermal and pressure effects produced by the blast. Understanding such coupled effects represents a major challenge for the development of new energetic materials with biocidal capabilities. Equally important and challenging is the development of an adequate experimental method for testing the effectiveness of different energetic materials with biocidal reaction products.

The key component of an adequate assessment of bioaerosol inactivation is the ability to identify and enumerate microorganisms in air. Various knowledge gaps and non-standardized protocols used by researchers in diverse disciplines have triggered the need for a standard and scientifically robust approach to measuring aerosolized bio-agents which are being inactivated. There is a lack of peer-reviewed and publically accessible reports on the investigation of destruction of biological agents in aerosol phase. Available experimental methods are often too simplistic and/or do not allow quantifying inactivation with appropriate detection limit. Additionally, to our knowledge, no method has yet been developed that would discriminate between different effects causing inactivation, such as heat and combustion products. Considering that the targeted inactivation level for bio-agents is usually very high, the study design must provide sufficiently high bioaerosol concentration in control tests and sufficiently low detection limit of microorganism enumeration from the treated/exposed samples. This enables testing formulations producing combustion products that cause substantial viability losses (e.g., 99.99% or greater). As newly-developed materials are often expensive to manufacture and available in limited amounts, a preferred evaluation method should be capable of generating credible inactivation data from combustion of small amounts of material. Finally, conventional experimental protocols for assessing microbial inactivation often measure the viability decrease over relatively long exposure time periods, which has a limited relevance to many agent defeat applications (particularly, for aerosolized agents) because the latter are often characterized by exposure time from milliseconds to about 1 s.

In this study, we designed and built a state-of-the-art experimental facility and developed a method for investigating the inactivation of airborne viable microorganisms exposed to combustion of various materials over a short period of time, ~0.01 – 1 s. The test protocol is capable of quantifying viability losses of about 99.998% (with the upper detection limit as high as 99.9995%) and has a potential to target even higher levels. The newly-developed facility and method were evaluated and used for determining the inactivation of aerosolized *Bacillus subtilis* endospores exposed to combustion of energetic powders, including a novel metastable aluminum-iodine composite.

Method description

Quantitative characterization of inactivation

The efficacy of a method aiming at controlling viable microorganisms can be determined by comparing the concentrations of these microorganisms with and without their exposure to a specific treatment ("control-to-test" comparison). The bioaerosol viability is usually represented by culturable count from an air sample. Thus, the loss in culturability serves as a surrogate for the viability loss, which can be quantified by the inactivation factor:

$$IF = \frac{C_{culturable}(CONTROL)}{C_{culturable}(TEST)} \tag{1.1}$$

where $C_{culturable}(CONTROL)$ and $C_{culturable}(TEST)$ are the culture-based concentrations of microorganisms measured without exposure and with exposure, respectively. If the challenge microorganisms are, e.g., bacterial spores, the values are expressed in colony forming units (CFU) per m^3 of air. In microbiology, microbial inactivation is often quantified in terms of log reduction, e.g., IF=0.001 would be referred to as a 3-log reduction. The viability loss (VL) — an alternative measure of inactivation used by some investigators (Green *et al.*, 1968; Lee and Lee, 2006; Jung *et al.*, 2009a,b) — can be expressed through the inactivation factor IF as

$$VL = \left(1 - \frac{1}{IF}\right) \times 100\% \qquad (1.2)$$

Generally, Eq. (1.1) assumes that all the microorganisms treated by the method under evaluation were exposed to the same stress during the same time interval.

Experimental facility

Figure 1.1 presents the experimental setup developed for studying the inactivation of aerosolized microorganisms.

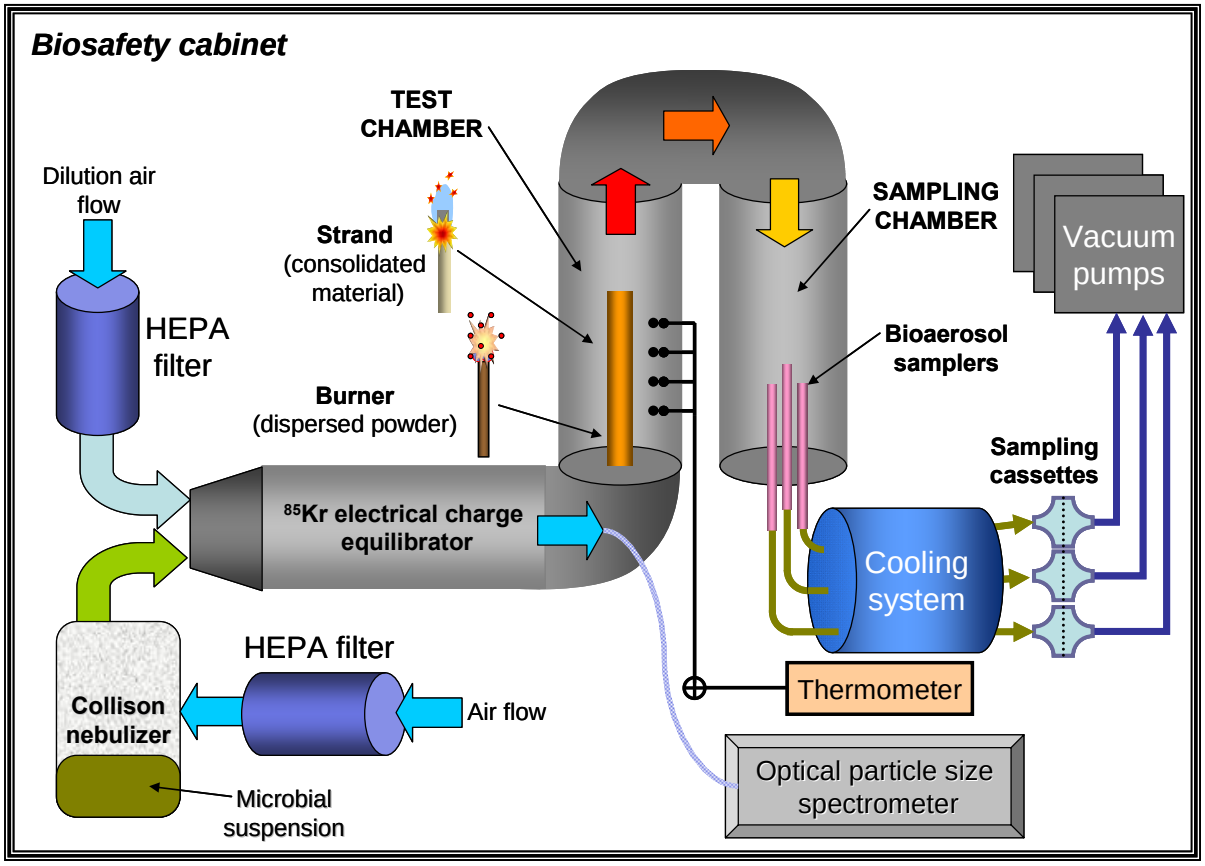

Figure 1.1 Experimental facility for the evaluation of the bioaerosol inactivation due to exposure to combustion.

The challenge bioaerosol – a specific bio-agent or its simulant – is generated from a surfactant-free, de-ionized water suspension using a six-jet Collison nebulizer (BGI Inc., Waltham, MA, USA) at its nominal operational flow rate, Q_{neb}=6 L min^{-1}. Strong shear forces inside the nebulizer created by the high-velocity air jet enhance spore de-agglomeration. The bioaerosol generation protocol has previously been validated and used in several studies (Mainelis *et al.*, 1999; Lin *et al.*, 2000; Grinshpun *et al.*, 2005; Grinshpun *et al.*, 2007). Alternatively, several other methods can be utilized for generating biological particles (Reponen *et al.*, 1997; Ulevicius *et al.*, 1997; Eninger *et al.*, 2009; Jung *et al.*, 2009a). The bioaerosol is diluted with HEPA-filtered dry air at different flow rates, which enables testing different flow regimes and different exposure times.

After passing through a 10-mCi ^{85}Kr charge equilibrator (model 3012, TSI Inc., St. Paul, MN, USA), the bioaerosol enters the test (combustion) chamber – a vertical cylindrical channel of 50 mm inner diameter and 320 mm height. Combustion products are generated by two alternate configurations: (1) by a burning solid fuel strand or (2) from an aerosol burner located in the center of the combustion chamber. The solid fuel strand, or "candle," was first used to test consolidated energetic materials. Materials studied in this configuration included nanocomposite powders of metallic fuel (Al) and an oxidizer (MoO_3) prepared by arrested reactive milling (ARM) (Dreizin and Schoenitz, 2009). Iodine was added to selected mixed composites to produce biocidal combustion products. The strands were ignited at the top and flames propagated downward.

Due to very rapid reaction rates of nanocomposite materials, a strand manufactured exclusively from the nanocomposite would be consumed over a very short period, which was found impractical. Therefore, the nanocomposite powders were mixed with a slower burning organic binder, paraffin wax.

The strand itself consisted of –8 +20 mesh (approximately 0.8 – 2.4 mm) granules of the nanocomposite material with binder, which was contained in a wire mesh cage. To prepare the granules, the nanocomposite powder was blended with paraffin wax, consolidated, crushed, and subsequently size classified. Characteristic dimensions of the cylindrical

strand were 12.5 mm (1/2") in diameter and 250 mm in height and characteristic burn times varied from 1.5 to 2.5 min. Due to variability in the packing density of the tested materials, the total mass subjected to combustion in an individual test (an energetic compound plus wax) ranged from 20 to 28 g; however, in most cases the strand mass was rather consistent: 25 g with variability of ~2%. This strand-based design allows for testing at relatively high combustion rates. The latter is important for exploratory studies when the potential of a tested formulation to produce appreciable inactivation over short time is unknown. An electro-chemical igniter with a 300 mg load of boron-titanium ARM nanocomposite (2B·Ti) was used to initiate combustion. The burn time of the electro-chemical igniter was ~0.01 s. To remove combustion products of the electrochemical igniter from the setup, the bioaerosol sampling was started five seconds after initiating the combustion.

While sufficient for initial inactivation assessment, the strand burner is associated with some operational shortcomings. For instance, the use of an organic binder causes substantial formation of soot, exhibiting an undesirable effect on the bioaerosol particles passing by the flame as well as on those collected on the filter, as discussed in detail below. As an alternative to the strand burner, an aerosol burner was developed in which the energetic materials under investigation are fed as additives into a gaseous hydrocarbon flame (Fig. 1.2). In this design, the gaseous hydrocarbon flame largely determines the flame temperature and structure. While the powder additives generally change the flame characteristics, their influence is limited, which provides reproducible experimental conditions for different energetic materials tested.

Although methane flame was utilized in the present experiments, a different hydrocarbon fuel (e.g., butane, acetylene, etc.) can be readily used to adjust the flame temperature and structure. Operation of the gaseous flame also enables one to readily control the soot formation with a small auxiliary oxygen flow.

The tested powder is loaded into a cylindrical channel in the center of the burner and fed into a built-in aerosolization chamber at a nominally constant rate using a cylindrical plunger, which is pushed at a controllable speed by a syringe pump. Upon entering the

aerosolization chamber, the powder is lifted by three tangential jets of a methane/nitrogen mixture. Further downstream, oxygen is introduced to generate a flammable mixture. Inserted into the test chamber, the burner is capable of generating a flame with dimensions similar to that obtained with the solid fuel strand.

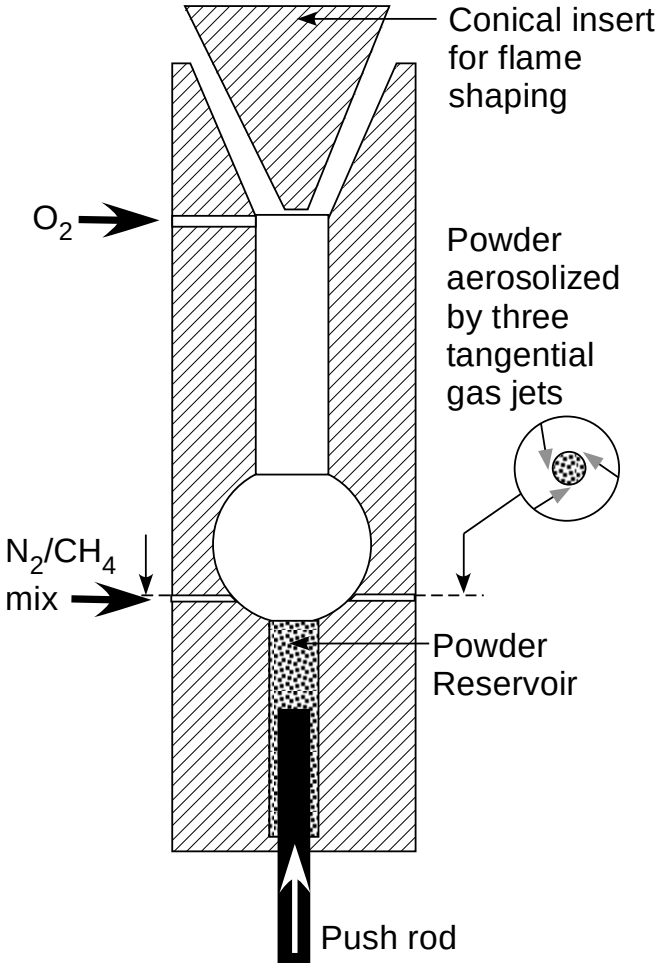

Figure 1.2. Schematic diagram of the aerosol burner for generating a hydrocarbon flame seeded with energetic particles. Only the top part of the burner protrudes into the test chamber through which the bioaerosol is flown.

At a total air flow rate through the test chamber ranging from 18 to 36 L min^{-1} and the flame vertical dimensions ranging from ~30 to 100 mm (depending on operational conditions), the residence time of a bioaerosol particle in the combustion zone is ~0.1 – 1 s. Increased air flow rates (not validated in this study) could allow testing shorter-term

exposures (~0.01 s). Overall, the combustion chamber is capable of accommodating different energetic formulations and conducting tests with both consolidated (the strand-based design) and dispersed (the burner) powders at sub-second exposure time intervals.

After passing the test chamber and a U-shaped transportation line (50 mm diameter and 500 mm length), the aerosol is sampled into three identical cylindrical probes and transported through a 300-mm long cooling system, which reduces the air flow temperature to the initial (room temperature) level. The probes are oriented isoaxially to the incoming air flow but may not necessarily sample isokinetically. Considering the ranges of operational parameters of the newly-developed experimental facility, non-isokinetic aspiration does not introduce measurable bias. The particles of interest (e.g., bacterial endospores) are small enough to follow the air streamlines, which provides an aspiration efficiency of 100%. The wall losses inside the sampling system are below 5% based on the estimate involving impaction, gravitation, and diffusion. The particles from each probe are collected for a subsequent culture-based analysis (AIHA, 2005). The present version of the experimental facility utilizes sterile 25-mm filter cassettes (SKC Inc., Eighty Four, PA, USA) equipped with a 25-mm diameter autoclaved polycarbonate filters (Millipore Corp., Billerica, MA, USA) (pore size=0.4 μm), which provide effective collection of bacterial spores, which are usually close to 1 – 3 μm in diameter. The sampling flow rate of 5 L min^{-1} (for each of the three sampling lines) was found to be high enough to achieve sufficient microorganism counts on the collection filters and, at the same time, sufficiently low to minimize the desiccation-induced viability loss on filters during collection.

The temperatures on the wall of the test chamber are measured using surface thermocouple probes (Model 5TC-GG-20, Omega Engineering, Inc., Stamford, CT, USA) with a digital thermometer (Model HH12A, Omega Engineering, Inc., Stamford, CT, USA). The air temperature profiles inside the test chamber are determined with non-sheathed thermocouple probes (Type J, Model 5J36-ICIN-116, Omega Engineering, Inc., Stamford, CT, USA). The air temperature monitoring assembly allows for a cross-sectional spatial resolution as low as 1 mm. The relative humidity is measured with a thermohygrometer

pen (Fisher Scientific, Pittsburgh, PA, USA). To monitor the ignition and combustion, a thermo-stable glass window is installed at the top of the test chamber.

The test chamber as well as the other sections of the experimental setup was made of stainless steel. The setup was assembled and operated inside a class II biosafety cabinet (Model 6TX, Baker Co., Inc., Sanford, ME, USA).

The above experimental design does not aim at exposing bioaerosol particles exclusively to the flame zone. Given that the adiabatic flame temperature for hydrocarbon fuels is about 1900–2200°C and may be somewhat higher when metal-based energetic composites are deployed in a practical configuration, it is likely that even stress-resistant bacterial spores and viruses are completely inactivated (or disintegrated) by heat if passing directly through the flame zone (Grinshpun *et al.*, 2010a; Grinshpun *et al.*, 2010b). The effect on bioaerosol passing in the proximity of the flame is less clear-cut. In addition, when testing a composite containing biocidal additives that are released during combustion, it is important to be able to compare the combustion-induced inactivation level of this composite to the one offered by its non-biocidal analog. From this perspective, an appreciable fraction of bioaerosol particles in the combustion test should be allowed to pass through an area between the flame zone and the wall of the combustion chamber so that the bio-particles are exposed to the tested products but not combusted themselves. These considerations were taken into account when choosing the dimensions of the experimental setup and the operational conditions.

Microbiological procedures used in the method evaluation

The experimental method was evaluated with *Bacillus subtilis* var. *niger* endospores, also known as *Bacillus globigii* (BG) and *Bacillus atrophaeus*, which are widely used as simulants of biological warfare agents (Johnson *et al.*, 1994; Franz *et al.*, 1997; Hill *et al.*, 1999; Laflamme *et al.*, 2004). The *B. subtilis* stock used in this study was obtained from the US Army Edgewood Laboratories (Aberdeen Proving Ground, MD, USA). The suspension was prepared for aerosolization with freeze dried *B. subtilis* spores in sterile

deionized water. The suspension was washed two times by vortexing and centrifuged at 7,000 rpm for 7 min at room temperature. The total bacterial concentration in suspension was adjusted to 10^7–10^9 mL^{-1} using a hemacytometer (Bright-Line Hemacytometer, Hausser Scientific, Horsham, PA, USA). The culturable concentration [enumerated after incubation on Trypticase Soy agar (TSA) at 30°C for 18 hours] was 10^7–10^9 CFU mL^{-1}. Immediately after aerosolized spores were collected, they were extracted from the collection filters with 10 mL of sterile filtered de-ionized water. Aliquots of filter extract ranging from 200 μL to 5 mL were used for cultivation. As control samples were very concentrated, the smaller aliquot of 200 μL was used with appropriate dilutions (up to 10^4). In the test samples (collected from combustion air environments), the spore recovery was low, which necessitated cultivating larger liquid volumes with no dilution. In some cases (corresponding to high inactivation), a 1-, 2-, and 5-mL aliquots were filtered through sterile filters (mixed cellulose esterase with diameter of 37 mm and pore size of 0.4 μm), which were placed face up on the agar plate. After incubation, the CFUs were counted to obtain the airborne concentration of culturable spores (CFU m^{-3}).

For each experiment, three collection filters operating in parallel in the test trial and three filters from the control trial were analyzed. Arithmetic average values were calculated for $C_{culturable}(CONTROL)$ and $C_{culturable}(TEST)$, and *IF*-value was determined as their ratio using Eq. (1.1). Each experiment was repeated at least three times, and the geometric mean of *IF*-value as well as the geometric standard deviation was calculated.

An average CFU value was determined from at least three replicate counts. The lowest countable number was 1 CFU per plate while some plates showed zero count. When averaging from a set of plates containing zero and non-zero counts, ½ CFU was designated for the former. The limit of detection (LOD) was calculated using 1 CFU per 5 mL aliquot sample, which is the largest aliquot transferred in the study on a single agar plate. This results in the LOD of 2 CFU per filter sample (1 CFU/5 mL=2 CFU/10 mL of total extraction volume). Similar to our recent study (Grinshpun *et al.*, 2010a), we adopted the Practical Quantification Limit (PQL)=5×LOD=10 CFU/sample as the lowest level that can be reliably achieved within specific precision and accuracy limitations provided by routine

laboratory operating conditions (McBean *et al.*, 1998; Wayman *et al.*, 1999; Benjamin and Belluck, 2001).

The upper limit of the detectable *IF* was determined as the ratio of $C_{culturable}(CONTROL)$ to the counting LOD and referred to as the Highest Detection Limit (HDL). Similarly, the upper limit of the reportable *IF* was derived from PQL=5×LOD and referred to as the highest practical quantification limit (HPQL).

The maximum viable *B. subtilis* count on the control filter can be reached by aerosolizing spores from a single Collison nebulizer charged with suspension of the highest achievable concentration of 10^8 per mL (which is still below the aggregate-producing level) and mixing it with dry air at the lowest dilution ratio of 1:2 (which is sufficient to provide adequate water evaporation). Based on this maximum and the above-listed LOD and PQL, the following upper limits of the detectable *IF* were calculated: HDL of ~2.2×10^5 (~99.9995% viability loss) and HPQL of ~4.4×10^4 (~99.998% viability loss). It is feasible to achieve ~10^1- to 10^2-fold higher bioaerosol concentrations by using alternative bioaerosol generation and air mixing systems. It is also possible to increase HDL and consequently HPQL, at least within an order of magnitude, by adjusting the sampling conditions such as time and/or flow rate. Therefore, the HPQL can be potentially further increased allowing for quantifying *IF*-values as high as ~10^7.

Evaluation results

In the course of evaluating the newly-developed method and experimental facilities, the following topics were covered:

(i) Characterization of the challenge aerosol and particle losses in the system;
(ii) Effectiveness of the facility decontamination conducted between the tests;
(iii) Inactivation of spores exposed to combustion of strands filled with conventional and potentially biocidal energetic materials (pilot data on comparison);

(iv) Inactivation of spores collected on filters exposed to combustion products during the test;
(v) Role of metal powder dispersed into hydrocarbon flame in inactivating spores (pilot data).

Characterization of the challenge aerosol and particle losses in the system

First, it was verified whether the particles aerosolized by the nebulizer and dried by the HEPA-filtered air flow represented single *B. subtilis* spores. The aerosol particle size distribution was measured with an optical particle size spectrometer (Dust Monitor 1.108, Grimm Technologies, Inc., Douglasville, GA, USA) approximately 640 mm downstream of the nebulizer, at the entrance to the test chamber. The real-time aerosol measurements were conducted at four dilution flow rates, $Q_{dilution}$, of 12, 18, 24, and 30 L min^{-1}. Thus, the total flow rate through the system, $Q=Q_{neb}+Q_{dilution}$, was 18, 24, 30, and 36 L min^{-1}, respectively. Figure 1.3A shows the particle size distributions measured over a 1-min time period initiated 5 min after the nebulization began. The peaks of these distributions occurred at approximately the same particle size, D_p =0.71 μm, representative of intact *B. subtilis* endospores [existing literature refers to the aerodynamic diameters of these spores ranging from 0.7 to 0.9 μm (Li *et al.*, 1999; Aizenberg *et al.*, 2000) and microscopic optical diameter of ~1 μm for non-germinated endospores (Daniels *et al.*, 2006)]. These data suggest that the tested dry dilution flows were sufficient to shrink the nebulizer-generated particles to the spore size as water content evaporated between the aerosolization point (nebulizer) and the chamber's entry point. The particle number concentration decreased with increasing dilution ratio. Thus, it was concluded that the aerosol entering the test chamber was representative of the intended bioaerosol with respect to its particle size and concentration characteristics.

Second, by tracking the peak aerosol concentration in 6-second increments, 50% variability was observed during the first 30 s of nebulization. While decreasing with time, the variability remained relatively high (approximately 15%) for the next 2-3 min. It was determined that the concentration stabilized approximately by the 4th minute and remained

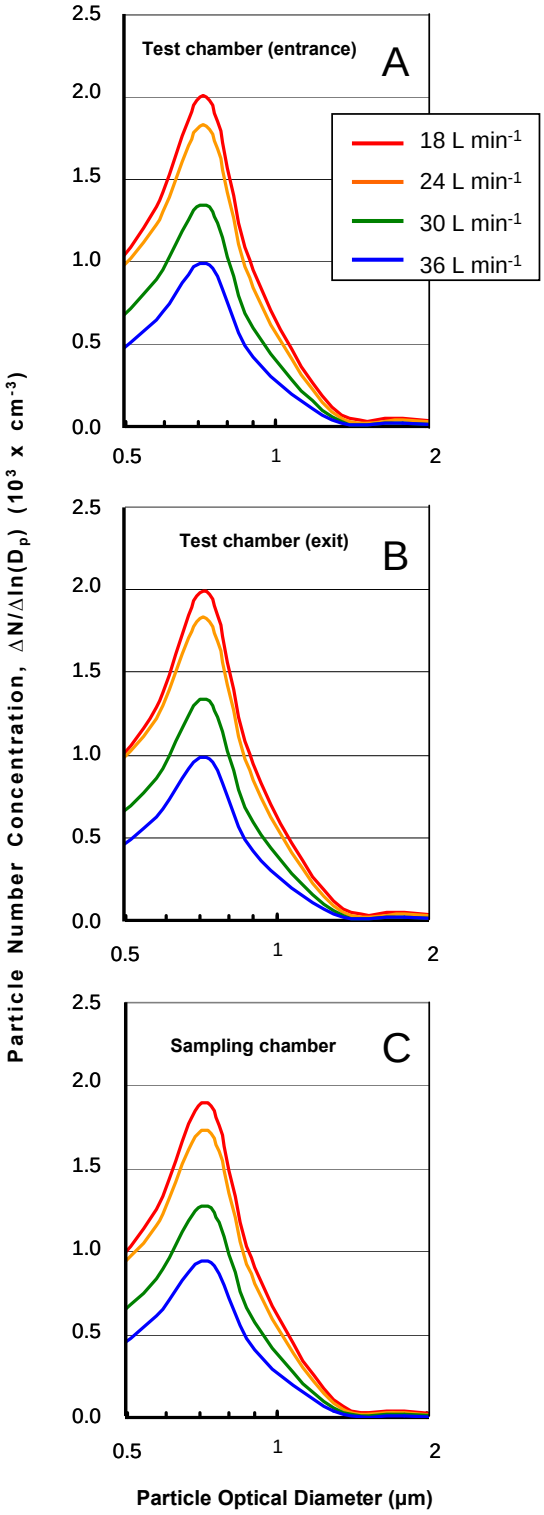

Figure 1.3. The particle size distributions of aerosolized *B. subtilis* endospores measured at three different points of the experimental system and at four different air flow rates.

essentially constant (variability <4%) during at least 30-45 min of continuous aerosol generation. The data suggest that the nebulizer should be turned on at least 5 min prior to the test, and the single test time should generally not exceed 30 min.

Third, the dimensions of the elements of the experimental setup and the air flow conditions were selected to assure that the particle losses inside the system are minimal. To test whether this was actually achieved, the particle concentrations and size distributions measured at the entrance of the test chamber were compared to those measured at its exit and in the sampling chamber. The latter are shown in Figs. 1.3B and 1.3C, respectively. The measurements were conducted with the combustion strand installed in the test chamber but not ignited (having approximately the same dimensions as the strand, the burner represents the same obstacle in the air flow causing about the same particle deposition). We found that the particle losses inside the test chamber (including the deposition on the strand surfaces) did not exceed 3.9% by number; the particle transport to the sampling point caused no more than 5.2% losses. This low internal deposition is considered acceptable for the purpose of the present study.

Effectiveness of the facility decontamination conducted between the tests

To ensure that the results of a subsequent experiment were not affected by the residual contamination of the system from a previous experiment, the system was cleaned between consecutive trials by blowing HEPA-filtered air at 85 L min^{-1} for 20 min. In addition, the internal surfaces were sprayed and wiped with 70% ethanol. The effectiveness of these procedures was assessed through a post-cleaning air sampling conducted during a 10-min period at 5 L min^{-1}. From a total of nine collection filters analyzed, only two developed any colonies (with 2 and 1 CFUs in 5-mL samples). The average count from these nine filters translates into the culturable concentrations lower than the one derived from the LOD=2 CFU per filter established in the experimental protocol of this study. Thus, it was concluded that the implemented decontamination procedures were appropriate.

Inactivation of spores exposed to combustion of solid fuel strands filled with conventional and potentially biocidal energetic materials (pilot data on comparison)

The newly-developed experimental facility and method were deployed to generate pilot data on the inactivation of *B. subtilis* endospores passing the test chamber, in which a strand filled with a consolidated energetic material ($12Al{\cdot}MoO_3$ nanocomposite powder with about 20 wt-% paraffin wax) was burned. The $12Al{\cdot}MoO_3$ nanocomposite powder was prepared in a shaker mill according to a procedure described elsewhere (Umbrajkar *et al.*, 2008). The iodine was incorporated by adding 5 wt-% at the preparation phase. The tests were conducted at a total flow rate (nebulizer flow plus dilution flow) of 36 L min^{-1}. Following the first 5 s, during which the flame was stabilizing, the sampling was initiated. The combustion continued for approximately 2 min with a mass burn rate ranging approximately from 200 to 300 mg s^{-1}. The sampling was stopped when the entire strand had burned out or when 2 min sampling time limit was reached (whatever occurred first).

Noticeable differences were observed in the structure and consistency of the flames generated by burning different solid fuels; furthermore, using organic binders resulted in substantial generation of soot. The collection filters were covered with soot, which caused additional concern regarding the continuing soot effect on the collected bioaerosol particles.

The spore exposure to the burning strand containing $12Al{\cdot}MoO_3$ nanocomposite with no iodine produced relatively low *IF*-values: geometric mean (GM)=52.3, geometric standard deviation (GSD)=1.51, number of replicates n=5. The solid-strand combustion of the same nanocomposite with embedded iodine produced much higher *IF*-values: GM=9,849, GSD=4.9, n=6. It is acknowledged that a part of the above difference occurred due to the temperature effect because combustion of the iodinated formulation created a higher temperature in the test chamber. As a reference, the average wall temperature measured at the end of the 2-min experiment was ~150ºC (varied from 109ºC to 160ºC) while testing $12Al{\cdot}MoO_3$ without iodine, and ~240ºC (varied from 200ºC to 253ºC) while testing the iodinated nanocomposite. In the latter case, the air temperature profiles measured in the test chamber identified the space in the vicinity of the wall (~1–2 mm wide at Q=36 L min^{-1})

with temperatures of ~200–300ºC. These temperatures are not nearly as high to produce the spore inactivation of *IF*~10^3–10^4 exclusively due to heat. Based on the previously reported findings (Grinshpun *et al.*, 2010a), close to 10% of spores should have remained viable after exposure to a heated air flow (no combustion) at the above-specified temperatures in the pre-wall layer. After accounting for the cross-sectional area represented by this layer relative to the total cross-section area of the flow, we estimate that at least ~1% of spores passing the test chamber should have survived if viability loss was caused only by the heat exposure. This translates into *IF* of ~10^2. The experimental values obtained with the strand containing the iodinated nanocomposite revealed much higher inactivation levels, thus pointing to additional (non-thermal) contribution. The latter is believed to be associated with the products released during combustion of the solid strand containing $12Al{\cdot}MoO_3$ nanocomposite with iodine. In contrast, combustion of the non-iodinated composite produced the viability losses closer to the levels, which can be explained exclusively by the heat-induced stress.

To summarize, the almost 200-fold difference in *IF*-values between the iodinated and non-iodinated composites obtained in these pilot tests can be explained, at least to a significant extent, by the effect of released iodine on airborne viable spores of *B. subtilis* passing the test chamber. Generally, there is a need in developing appropriate approaches to separate the thermal and chemical effects causing inactivation of airborne microorganisms. Nevertheless, these results show the feasibility of iodine-containing energetic material for agent defeat applications.

Inactivation of spores collected on filters exposed to combustion products during tests

While the pilot data generated in this study provide evidence that iodine in the FNM enhances the inactivation of spores exposed to combustion, there is an important limitation in attributing this effect solely to the *aerosol* interaction. Indeed, the spores, which remain viable after passing through the system, are collected on filters and continue being exposed to combustion products including smoke and soot until the test ends (the cooling system eliminates exposure of the collected spores to hot air but does not remove the combustion

products from the incoming air flow). To quantify the survival of spores, which are exposed to combustion products on the collection filter, we performed the following experiment. First, the originally aerosolized *B. subtilis* spores passed through the system (at a total air flow rate of 36 L min^{-1}) and were collected on five polycarbonate filters with no combustion in the chamber. Two of these five pre-loaded filters served as controls, while three others were exposed to combustion products released when a strand filled with the $12Al{\cdot}MoO_3$ nanocomposite and paraffin wax was burned in the test chamber at a mass rate (R), of approximately 250 mg s^{-1} with clean air supplied at 36 L min^{-1}. The exposure time (equal to the established collection time period) varied approximately from 20 to 80 s. Combustion products were aluminum oxide, molybdenum oxide, water, carbon oxides and soot [further details on this material and its products are given in (Umbrajkar *et al.*, 2008)]. The spores were extracted from the filters using a standard extraction method using a vortex touch mixer (Fisher Scientific, Pittsburgh, PA, USA), serially diluted, and subjected to the culture-based analysis using Trypticase Soy agar media (Grinshpun *et al*., 2010a). The survived spore fraction was calculated based on the bacterial colony forming units counted from the control and treated samples.

The microbial inactivation occurring on the collection filters was found to depend on the time during which the filter was exposed to combustion products. The survived fraction decreased exponentially with time and fell below 10% within a minute due to the high amount of combustion products released when a $12Al{\cdot}MoO_3$ strand was burned (Fig. 1.4).

Unlike in a strand of consolidated FNM, the aerosol burner design provides a slow feeding of the tested material in powder form directly to a hydrocarbon flame, thus producing much lower mass burn rates (in our tests conducted at a total air flow rate of 36 L min^{-1}, R varied from 12 to 22 mg s^{-1}). The filter samples obtained in 1-min experiments involving the aerosol burner did not have a distinctive black/grey deposit that was observed when burning solid strands, apparently due to an extensive generation of soot. Figure 1.4 shows that when testing with the aerosol burner, the detrimental effect associated with the viability loss on the collection filter was smaller as compared to the tests conducted with the solid strand. The difference between the respective slopes, k=0.0034 s^{-1} (burner, $R\approx$20 mg s^{-1}) versus

k=0.0538 s^{-1} (strand, R≈250 mg s^{-1}), is clearly appreciable. By using the aerosol burner, the time of bioaerosol collection from combustion air environments could be at least 1 min.

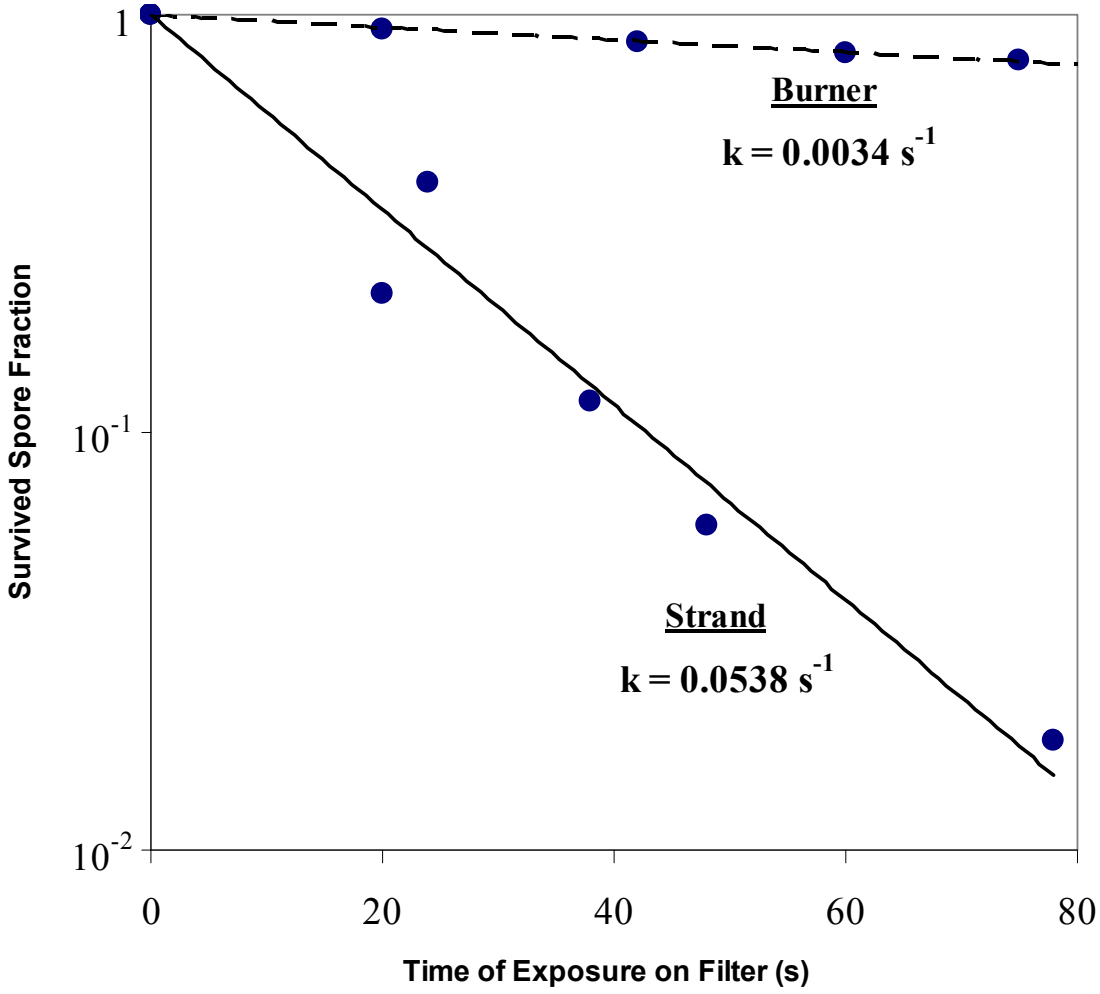

Figure 1.4. Survival of *B. subtilis* endospores on a 25-mm polycarbonate collection filter (pore size: 0.4 µm) exposed to combustion products of 12Al·MoO_3 while burning a dispersed powder (aerosol burner) and a pellet of consolidated material (solid strand).

This sampling time is considered reasonably practical while still short enough to avoid a loss of viability on the filter. At the same time, the experiment with pre-loaded filters produces a conservative estimate of the collection time limit because in a routine test the spores collected at the end of the sampling period have much shorter exposure to combustion products on the filter than those collected at the beginning of the sampling period. The aerosol burner demonstrated several advantages over the strand design as the

former provides a more stable/uniform combustion at a sufficiently low mass burn rates. The measured viability loss is more representative of the spore *aerosol* exposure. The test conditions established by this validation study are applicable to stress-resistant bacterial spores. Microorganisms that are more susceptible to environmental stress may require establishing different test conditions, in particular shorter collection time periods.

Role of metal powder dispersed into hydrocarbon flame in inactivating spores (pilot data)

The aerosol burner is capable of providing two combustion environments:

(i) a gaseous (e.g., hydrocarbon) flame and

(ii) the flame seeded with particles of an energetic material.

In both cases, exposure to the heat and combustion products may cause significant inactivation of the aerosolized *B. subtilis* endospores. However, the presence of a dispersed energetic material (e.g., seeded metal particles) in the aerosolization chamber of the burner has a potential to enhance inactivation due to higher energy input. The new method developed in this study was evaluated with respect to its ability to obtain a measurable difference in *IF*-values associated with metal particles in the flame. Identical tests were performed using the burner producing a hydrocarbon flame with and without spherical aluminum particles (Alfa Aesar, 97.5%, nominal diameter 3–4.5 μm) burned at R≈20 mg s^{-1}. At a total air flow rate of 36 L min^{-1}, the pure flame expanded 10–20 mm downstream from the top edge of the burner and about 6 mm radially. The flameless area along the wall was also about 6 mm wide. When feeding aluminum powder particles, the flame configuration did not change appreciably. Luminous streaks of heated and burning particles were apparent in the flame zone and above the gaseous flame. In these tests, a 1-min sampling period was established for collecting spores on filters.

The spore exposure to the pure flame produced moderate inactivation: GM of *IF* was 50.2 (GSD=1.49; n=3), which corresponds to approximately 2% survival. Dispersing of aluminum powder enhanced the inactivation considerably: GM=857 (GSD=1.58; n=3), which translates to approximately 0.12% survival. This substantial difference between the

*IF*s determined with and without the aluminum powder reflects an enhancement in inactivation taking place in the aerosol phase (as shown above, a low rate provided by the aerosol burner and a short sampling time of 1 min minimize the influence of the powder combustion on the representativeness of the filter samples). The difference brought in by dispersing aluminum powder in the flame can be attributed to a combination of two factors: (i) increase of air temperature due to the energy output from combustion of aluminum particles in the gas mixture and (ii) aerosolized combustion products (alumina smoke). Both may directly affect the viability of the exposed bioaerosol particles.

Conclusions

In summary, we designed and built a state-of-the-art experimental facility and developed a method for assessing the survival of aerosolized microorganisms exposed to combustion for a short time (<1 s). In spite of its ability to measure high inactivation levels, the newly-developed method does not aim at exposing bioaerosol particles exclusively to the flame zone, in which even stress-resistant microorganisms are expected to be completely inactivated (or disintegrated) by heat. The design allows assessing the bioaerosol inactivation in the periphery or in close proximity to the flame zone. It is particularly advantageous when testing fuels modified with biocidal additives, which are released during combustion, against their unmodified analogs. The method and experimental facility were evaluated with aerosolized *B. subtilis* endospores exposed to a pure hydrocarbon flame and to combustion of different aluminum-based energetic composites (including novel compositions with added iodine). The method was used in establishing feasibility of the new iodine-containing material for microbial agent defeat applications. Although in this study we tested the new method with bacterial spores, its use can be expanded to other challenge bioaerosols (including viruses).

Chapter 2. Thermal inactivation of airborne viable *Bacillus subtilis* spores by short-term exposure in axially heated air flow

Paper published: Grinshpun, S.A., Adhikari, A., Li C., Reponen, T., Yermakov, M., Schoenitz, M., Dreizin, E., Trunov M., and Mohan, S. (2010) Thermal Inactivation of Airborne Viable *Bacillus Subtilis* Spores by Short-term Exposure in Axially Heated Air Flow, *Journal of Aerosol Science*, 41:352-363.

Introduction

Viable biological aerosol particles can be controlled by implementing two approaches: (1) physical particles removal from the targeted air environment [by air filtration (Kwabata and Kawato, 1998) or other methods] and (2) inactivation of viable microorganisms [e.g., through exposure to ultraviolet germicidal radiation (Lin and Li, 2002), toxic chemicals (Burton *et al*., 2008), or heat treatment (Mullican *et al*., 1971; Lee and Lee, 2006; Jung *et al*., 2009b,c), etc.]. Different microorganisms exhibit different response to a specific stress; which determines the efficiency of a specific inactivation method. For instance, unlike vegetative cells, spores are generally resistant to heat stress (Setlow, 2006). While the spore inactivation by high temperatures has been extensively investigated, most of these studies involved microorganisms in aqueous or on solid media (Molin and Östlund, 1975; Pfeifer and Kessler, 1994; Nicholson *et al*., 2000; Setlow, 2006), with very few experiments conducted with airborne spores [e.g., a study by Jung *et al*. (2009c) with fungal spores]. Aerosolized microorganisms have generally different response to environmental stresses as compared to those suspended in liquid or attached to solid surfaces. Thus far, the effect of thermal inactivation of aerosolized viable spores has not been sufficiently characterized and understood, particularly for exposure periods as short as $10^{-2} – 10^{0}$ s.

Short-term heat exposure of airborne spores has important applications. One relates to biodefense/counterterrorism involving biological warfare agents that are exceptionally resistant to various stresses, including “dry” and “wet” heat (Setlow, 1995). For instance, pathogenic bacterial spores aerosolized under high-temperature conditions, which have been applied over seconds or fraction of a second (e.g., as a result of explosion), may

survive and remain viable in the atmosphere, thus posing a threat. It has not yet been adequately investigated how the viability of aerosolized spores depends on the temperature, exposure time and other parameters. The other area of application is indoor air quality. Thermal processes are believed to be effective, safe and environmentally-friendly for controlling viable biological particles in continuous-flow settings, including heating, ventilation, and air-conditioning systems (Jung *et al*., 2009c). Thus, data are needed on the survival of airborne spores under specific temperature and air flow conditions.

Two innovative studies published in 2009 by researchers from the Republic of Korea addressed inactivation of airborne fungi and bacteria by short-term heat exposure in a continuous air flow inside an externally-heated cylindrical tube. The investigators reported that more than 99% of fungal spores of *Aspergillus versicolor* and *Cladosporium cladosporioidis* lost their viability (determined by cultivation) in about 0.2 s when the surrounding temperature exceeded 350 and 400°C, respectively (Jung *et al*., 2009c). It was also reported that bacterial vegetative cells of Gram-negative *Escherichia coli* and Gram-positive *Bacillus subtilis* were rendered more than 99.9% inactive as a result of a <0.3-s exposure to surrounding temperature of 160°C and 350°C, respectively (Jung *et al*., 2009b). While acknowledging the complexity of the longitudinal and cross-sectional air temperature profiles in the thermal tube used in their study, the authors defined the cell exposure temperature in a somewhat simplistic way – as the "surrounding temperature" equal to the tube's wall temperature. In general, the wall temperature is not fully representative of the inactivation process involving microorganisms in a heated air flow. A much more relevant parameter – the temperature adapted by a bioaerosol particle moving in the heated air – was not considered in above-referred studies. In addition, while providing important information, these studies had several limitations associated with the experimental design and appropriate data resolution at inactivation levels exceeding $10^2 – 10^3$.

The study design developed in this grant allowed measuring microbial inactivation levels of up to ~10^5, which resulted from a short-term heating of aerosolized microorganisms to a broad range of temperatures. The tests were conducted with *B. subtilis* var. *niger* endospores [also known as *Bacillus globigii* (BG)], which are widely used as simulants of

biological warfare agents (Johnson *et al*., 1994; Franz *et al*., 1997; Hill *et al*., 1997; Laflamme *et al*., 2004).

Experimental

Experimental setup

The experimental setup is shown schematically in Fig. 2.1 (this is a modification of the facility presented in Fig. 1.1 and discussed in Chapter 1). The challenge bioaerosol – bacterial endospores of *B. subtilis* var. *niger* (obtained from the US Army Edgewood Chemical Biological Center, Aberdeen Proving Grounds, MD, USA; courtesy of Ms. A. Akiyemi and Dr. E.W. Stuebing) – was generated from a surfactant-free, de-ionized water suspension using a six-jet Collison nebulizer (BGI Inc., Waltham, MA, USA) operated at 6 L min^{-1}. Strong shear forces inside the nebulizer created by the high-velocity air jet enhanced spore de-agglomeration. The aerosol generation protocol has previously been validated and used in several studies (Mainelis *et al*., 1999; Lin *et al*., 2000; Grinshpun *et al*., 2005, 2007).

The bioaerosol was diluted with HEPA-filtered dry air at flow rates of 12 and 30 L min^{-1} producing the total flows of Q=12+6=18 L min^{-1} and Q=30+6=36 L min^{-1}, which respectively represent two different thermal flow regimes – fully developed and developing (Holman, 2002). After passing through a 10-mCi ^{85}Kr charge equilibrator (model 3012, TSI Inc., St. Paul, MN, USA), the bioaerosol entered the test chamber – a vertical cylindrical channel of 50 mm inner diameter and 320 mm height. A cylindrical electric heating element (Mighty Watt Heater, Gordo Sales, Inc., Layton, UT, USA) of 10 mm diameter and 230 mm height was installed along the axis of the test chamber on a flat holder placed 16 mm into the chamber.

The axial geometry was chosen because it is relevant to a parallel laboratory study investigating the bio-agent defeat during explosion and combustion. Besides, this design is being explored for heating-based air purifiers.

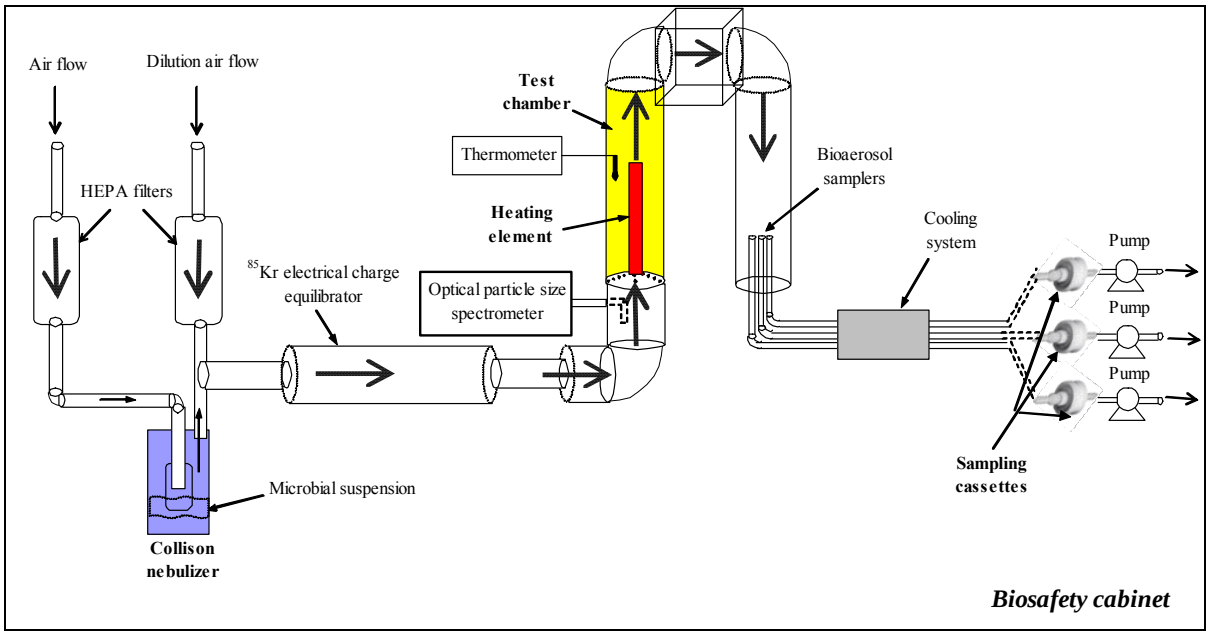

Figure 2.1. Experimental setup.

Connected to a variable voltage source (Staco Energy Products, Co., Dayton, OH, USA) through a general purpose transformer (Acme Electric Corp., Lumberton, NC, USA), the heating element was operated at 50 – 240 V producing heater surface temperatures ranging from ~550 to 1250°C. Depending on the applied voltage and the air flow rate, it took approximately 30 – 60 min to achieve a steady-state temperature distribution, when the temperature measured at a specific location of the test chamber wall, T_{wall}, did not anymore change with time. This T_{wall} was regarded as a target temperature; in our tests, it ranged from 150 to 460°C.

The residence time of spores in the heated zone (representing their thermal exposure in the air flow) was characterized for each of the two test flow rates taking into account the air velocity and temperature profiles in the space between the heater and the test chamber wall.

The aerosol concentration and particle size distribution were determined in real time at the inlet and the outlet of the test chamber using an optical particle size spectrometer (Model 1.108, Grimm Technologies, Inc., Douglasville, GA, USA), which operated at a flow rate of 1.2 L min^{-1} and counted particles in 15 channels covering the optical size range of 0.3

to >10 μm. Following a 10-min nebulization period, a stable concentration of the challenge aerosol was achieved with the particle size distribution peaking at 0.7 – 0.8 μm. This peak corresponds to the optical size of intact *B. subtilis* endospores (An *et al*., 2004).

After passing the test chamber and a U-shaped transportation line (50 mm diameter and 500 mm length), the aerosol was sampled into three identical cylindrical probes and transported through a 300-mm long cooling system, which reduced the air flow temperature to the initial (room temperature) level. Subsequently, the spores from each probe were collected on a sterile 25-mm filter cassette (SKC Inc., Eighty Four, PA, USA) equipped with a 25-mm polycarbonate filter (Millipore Corp., Billerica, MA, USA) (pore size=0.4 μm). The sampling time was 60 s, and the sampling flow rate was 5 L min^{-1}. The filters were then removed; spores were extracted and analyzed by cultivation.

The test chamber as well as the other sections of the experimental setup was made of stainless steel. The setup was assembled and operated inside a class II biosafety cabinet (Model 6TX, Baker Co., Inc., Sanford, ME, USA).

The concentration of culturable spores was determined as an average from the three filter samples obtained in each run. The experiments were conducted with no voltage applied to the heating element (control) as well as at various voltage levels representing specific thermal exposures of the aerosolized spores in the chamber (tests). The culturable counts were compared for each test-control combination to determine the loss in spore culturability due to their specific thermal exposure. Thus, the loss in culturability served as a surrogate for the viability loss. It is acknowledged that culturable count may be lower than the viable count. Culturability, however, is conventionally used as a surrogate for viability, which is especially relevant when dealing with pathogenic microorganisms because their hazard level is usually associated with their ability to multiply.

Applying the test-control comparison described in Chapter 1, microbial inactivation can be calculated by relating the concentration of culturable airborne microorganisms (e.g., spores),

originally aerosolized at a normal temperature (T_0=20°C), to that of microorganisms exposed to a temperature (T) during the air flow heating:

$$IF = \frac{C_{culturable}(T_0)}{C_{culturable}(T)} \tag{2.1}$$

where $C_{culturable}(T_0)$ and $C_{culturable}(T)$ are the concentrations of culturable spores collected after they passed the test chamber with no air flow heating and with heating, respectively. The spore viability loss (VL) due to high-temperature exposure — an alternative measure of inactivation used by other investigators, including Jung *et al*. (2009b,c) — can be expressed through the inactivation factor IF as

$$VL = \left(1 - \frac{1}{IF}\right) \times 100\% \tag{2.2}$$

Equation (2.1) assumes that all the spores were exposed to the same temperature during the same time interval. In this sense, it is appropriate for the IF definition but provides limited information in practical situations with gradients of air temperature and velocity. In the axially heated flow used in this study, the air temperature varies longitudinally and radially. Pilot measurements showed that the radial temperature gradient was significant in close proximity to the heater but became smaller at greater distance from the heating element. Consequently, the spores moving close to the heater are expected to be inactivated much more efficiently than those moving further from the heater and closer to the wall. Therefore, the inactivation factor determined experimentally according to Eq. (2.1) represents some integral value, which does not refer to a single specific temperature T. Based on the longitudinal and cross-sectional air temperature profiles, we defined the characteristic temperature and introduced an appropriate correction for the experimentally determined IF, which established its conservative estimate, as explained below.

Microbiological procedures: suspension preparation and analysis of collected spores

To prepare suspension for aerosolization, freeze dried *B. subtilis* spores were suspended in sterile deionized water and then washed two times by vortexing followed by centrifugation at 7,000 rpm for 7 min at room temperature. The total bacterial concentration in suspension was adjusted to 10^7–10^9 mL^{-1} using a hemacytometer. The culturable bacteria were

enumerated by using Trypicase Soy agar (TSA) incubated at 30°C for 18 hours. The culturable concentration in the nebulizer suspension was of the same order of magnitude as the total concentration, i.e., 10^7–10^9 CFU mL^{-1} (CFU=colony-forming unit). Aerosolized spores collected on filters were extracted using sterile filtered de-ionized water, and aliquots of filter extract ranging from 200 μL to 5 mL were used for cultivation. As control samples and test samples obtained under low inactivation conditions were very concentrated, the smaller aliquot of 200 μL was used with appropriate dilutions (up to 10^4). At higher temperatures, microorganism recovery was very low, which necessitated cultivating larger liquid volumes with no dilution. In these cases, a 5 mL aliquot was filtered through sterile filters (Mixed cellulose esterase with diameter of 37 mm and pore size of 0.4 μm) and the entire filter was placed face up on the agar plate. After incubation, the CFUs were counted to obtain the airborne concentration of culturable spores (CFU m^{-3}).

An average CFU value was determined from at least three replicate counts. The lowest countable number was 1 CFU per plate while some plates (representing high thermal exposure conditions) showed zero count. The limit of detection (LOD) was calculated using 1 CFU per sample and a total suspension volume of 10 mL. Available analytical guidelines recommend the Practical Quantification Limit (PQL) calculated as 5×LOD as the lowest level that can be reliably achieved within specific precision and accuracy limitations provided by routine laboratory operating conditions (McBean and Rovers, 1998; Wayman *et al*., 1999; Benjamin and Belluck, 2001). Following these guidelines, we adopted PQL=5×CFU as the quantification limit for data analysis.

Characteristic exposure temperature

Due to pronounced spatial non-uniformity of the air temperature, it is not a trivial task to characterize the microbial inactivation process by a single value of air temperature. Unlike confined thermal systems used for sterilizing food and liquids, a continuously heated air flow system cannot, in principle, maintain a single temperature because of continuous longitudinal and cross-sectional energy transfer (Jung *et al*., 2009c). At the same time, a specific ("characteristic") temperature can be defined to characterize the inactivation

process in the heated air flow. This challenge was addressed in the following way. First, we measured the air temperature profiles – longitudinal (T_y) and cross-sectional/radial (T_x) – within the annular space between the heater and the chamber wall. Second, within this space, we selected a narrower annular zone representing the lowest heat exposure of particles in the air flow, thus implementing a conservative approach for determining the efficiency of the heat-induced spore inactivation in the air flow. It was postulated that if the microorganisms moving through this zone (characterized by lower air temperatures) did not survive, those moving through a more heated zone (e.g., close to the heater) would not survive either. In processing the final results, only a part of the aerosol flow passing through the selected characteristic zone was accounted for. The characteristic air temperature profile was determined for each combination of the voltage applied to the heater and the air flow rate. Third, we quantified the thermal equilibration time ($\tau_{eq.}$) needed for a spore to adapt to the temperature of the surrounding air. All of the above allowed us to define the characteristic spore exposure temperature (T_e) for each set of conditions and plot the inactivation factor against this temperature.

Temperature measurement and correction procedure

For each combination of the air flow rate (18 and 36 L min^{-1}) and the voltage applied to the heating element, a specific temperature regime was achieved. The temperatures on the heater surface and on the wall of the test chamber were measured using surface thermocouple probes (Model 5TC-GG-20, Omega Engineering, Inc., Stamford, CT, USA) with a digital thermometer (Model HH12A, Omega Engineering, Inc., Stamford, CT, USA). The target temperature T_{wall} was established as a function of the heater voltage and the air flow rate, which produces a specific temperature on the heater surface, T_{heater}.

The surface-measured temperature was regarded as the air temperature of the pre-surface layer (x=0 for the heater and x=20 mm for the wall, as demonstrated in Fig. 2.2). In addition, the air temperature profiles inside the test chamber were determined with non-sheathed thermocouple probes (Type J, Model 5J36-ICIN-116, Omega Engineering Inc., Stamford, CT, USA) positioned at specific points (x, y) shown in Fig. 2.2. The

measurement precision was $\Delta T = \pm 15°C$ representing variations associated with positioning the thermocouple inside the chamber as a specific distance from the wall. It derives from the dimensions of the thermocouple, the distance between the heater and the chamber wall, and other factors.

The thermocouple-measured air temperature profiles were subjected to correction for radiation. Indeed, the temperature value obtained with a thermocouple placed in an air flow ($T_{air,\ measured}$) may differ from the actual air temperature (T_{air}) at the measured location. This difference reflects two modes through which the thermocouple gains or looses energy: forced convection from air and radiation from surrounding objects. The correction derived from a simplified heat balance equation:

$$\pi d_{tc}^{2} h(T_{air,\ measured} - T_{air}) = \dot{Q}_{heater \to tc}^{rad} + \dot{Q}_{wall \to tc}^{rad} - \dot{Q}_{tc \to}^{rad} + \dot{Q}_{heater \to wall \to tc}^{ref} \tag{2.3}$$

where d_{tc} is the diameter of the thermocouple's spherical probe (890 μm); h is the probe heat transfer coefficient due to forced convection; $\dot{Q}_{heater \to tc}^{rad}$, $\dot{Q}_{wall \to tc}^{rad}$ and $\dot{Q}_{tc \to}^{rad}$ are three rates of radiation heat transfer: from the heater to the thermocouple, from the chamber wall to the thermocouple, and from the thermocouple to the surrounding objects, respectively; $\dot{Q}_{heater \to wall \to tc}^{ref}$ is the rate of heat transfer to the thermocouple occurring due to reflection of the heater-emitted radiation from the chamber walls. The convection and radiation terms were determined according to Holman (2002).

Each term in the right part of Eq. (2.3) depends on the emissivity of objects participating in the radiation heat exchange. The terms depend on the temperatures of the heater, wall temperature, and the thermocouple spherical probe ($T_{air,\ measured}$). The emissivity of the probe made of an alloy of nickel, copper, and iron, was estimated to be approximately 0.575 [an average of emissivity values listed for oxidized nickel-copper alloy and oxidized iron (www.omega.com)]. The wall (non-oxidized stainless steel) and the heater (heavily oxidized stainless steel) yielded the emissivity values of 0.57 and 0.87, respectively. As the heater's emissivity is relatively high, it absorbs nearly all the incoming radiation so

reflection from the heater can be neglected. Due to the small size of the thermocouple, we also neglected reflection of the thermocouple radiation from the chamber walls back to the thermocouple.

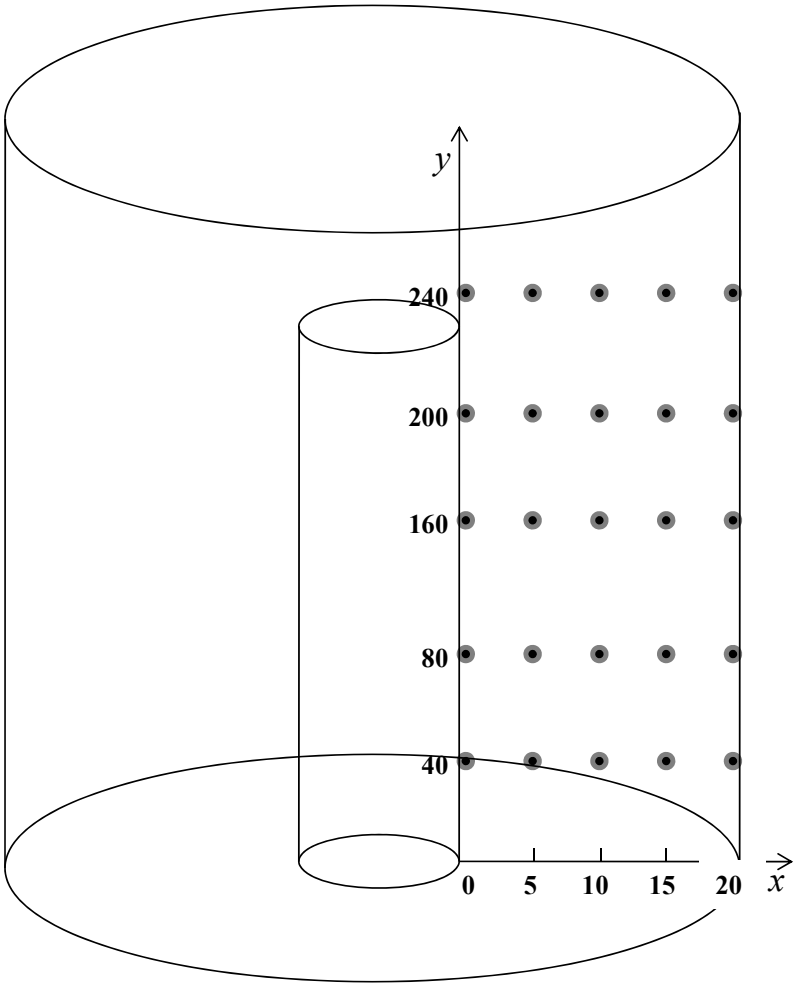

Figure 2.2 Temperature measurement grid.

Data analysis

The mean *IF*-value and the geometric standard deviation were calculated for every test. The upper limit of the detectable *IF* was determined as a ratio of $C_{culturable}(T_0)$ to the counting LOD and referred to as the Highest Detection Limit (HDL). Similarly, the upper limit of the reportable *IF* was derived from PQL=5×LOD and referred to as the highest practical quantification limit (HPQL).

Results and discussion

Air temperature profile: measurement data and modeling

All the measured air temperature values represented some overestimation due to radiation heat exchange. The correction values, calculated as described above, ranged from 12 to 118°C, depending on the air flow rate and the heater temperature. The correction increased with increase in T_{heater}. At a fixed heater temperature, the greatest difference between $T_{air, measured}$ and T_{air} was found for the lowest measured air temperatures suggesting that all the incoming radiation heated the thermocouple while there was practically no radiation energy loss from the thermocouple.

As expected, the air temperature was much higher in close proximity to the heater than further from its surface exhibiting a unique cross-sectional profile for each combination of the target temperature and the flow rate. In most of the tests, T_{heater} exceeded T_{wall} approximately by 500 – 700°C.

Figure 2.3 represents the cross-sectional (radial) temperature profiles obtained at longitudinal coordinates y=40, 80, 160, 200, and 240 mm. For each Q and T_{wall}, the profile evolved as the air passed the heater. At both flow rates, T_{air} rapidly decreased radially within the 5-mm annular area adjacent to the heater and then either continued decreasing at a much lower pace or exhibited a non-monotonic behavior showing some increase close to the wall. For example, at Q=18 L min^{-1}, a monotonic decrease was observed for y=200 mm from x=5 to 20 mm. At the same time, at Q=36 L min^{-1} and y=200 mm, T_{air} increased between x=15 and 20 mm. The latter temperature profile appeared somewhat counter-intuitive as T_{air} was anticipated to gradually decrease within any cross-section along the radial coordinate with the lowest value reached at the chamber wall. However, the temperature of the wall may be higher than that of the surrounding air due to radiation. A gradual temperature profile is established only after the flow is fully thermally developed (Holman, 2002).

The longitudinal coordinate at which this thermal flow development is completed can be calculated (Thomas, 1992) as:

$$y^* = 0.05\, Re\, Pr\, D_H \tag{2.4}$$

where

$$Re = \frac{VD_H}{2\nu} \tag{2.5}$$

is the Reynolds number, V is the air velocity, ν is the air kinematic viscosity,

$$Pr = \frac{\nu}{\alpha} \tag{2.6}$$

is the Prandtl number, α is the thermal diffusivity of air, and

$$D_H = D_{chamber} - D_{heater} = 40 \text{ mm} \tag{2.7}$$

is the hydraulic diameter.

The parameter y^* was calculated for a range of temperatures from 130 to 500°C. At Q=18 L min^{-1}, y^* falls approximately between 155 (corresponds to the highest T_{air}) and 233 mm (corresponds to the lowest T_{air}), suggesting that the flow development had reached completion essentially before the air passed the top of the heater (y^*=230 mm). The data obtained at 18 L min^{-1} show that within the heater-wall space the radial air temperature profiles were monotonic if $y > y^*$ and non-monotonic if $y < y^*$ (Fig. 2.3). At Q=36 L min^{-1}, $y^* \approx 297 - 447$ mm, indicating that the air flow became fully thermally developed only after passing the heater. Consequently, all the radial temperature profiles experimentally determined for 36 L min^{-1} (y=40–240 mm) as well as those for 18 L min^{-1} measured along the first ¾ of its length were non-monotonic. This is evidence that the heat transfer between the heater and the wall took place primarily due to radiation, but not convection. In the area downstream of the heater (y > 230 mm), the thermal conditions change so that the temperature profile readjusts regardless whether the air flow reached the full thermal development stage at y < 230 mm. The data presented in Fig. 2.3 for y=240 mm demonstrate this readjustment.

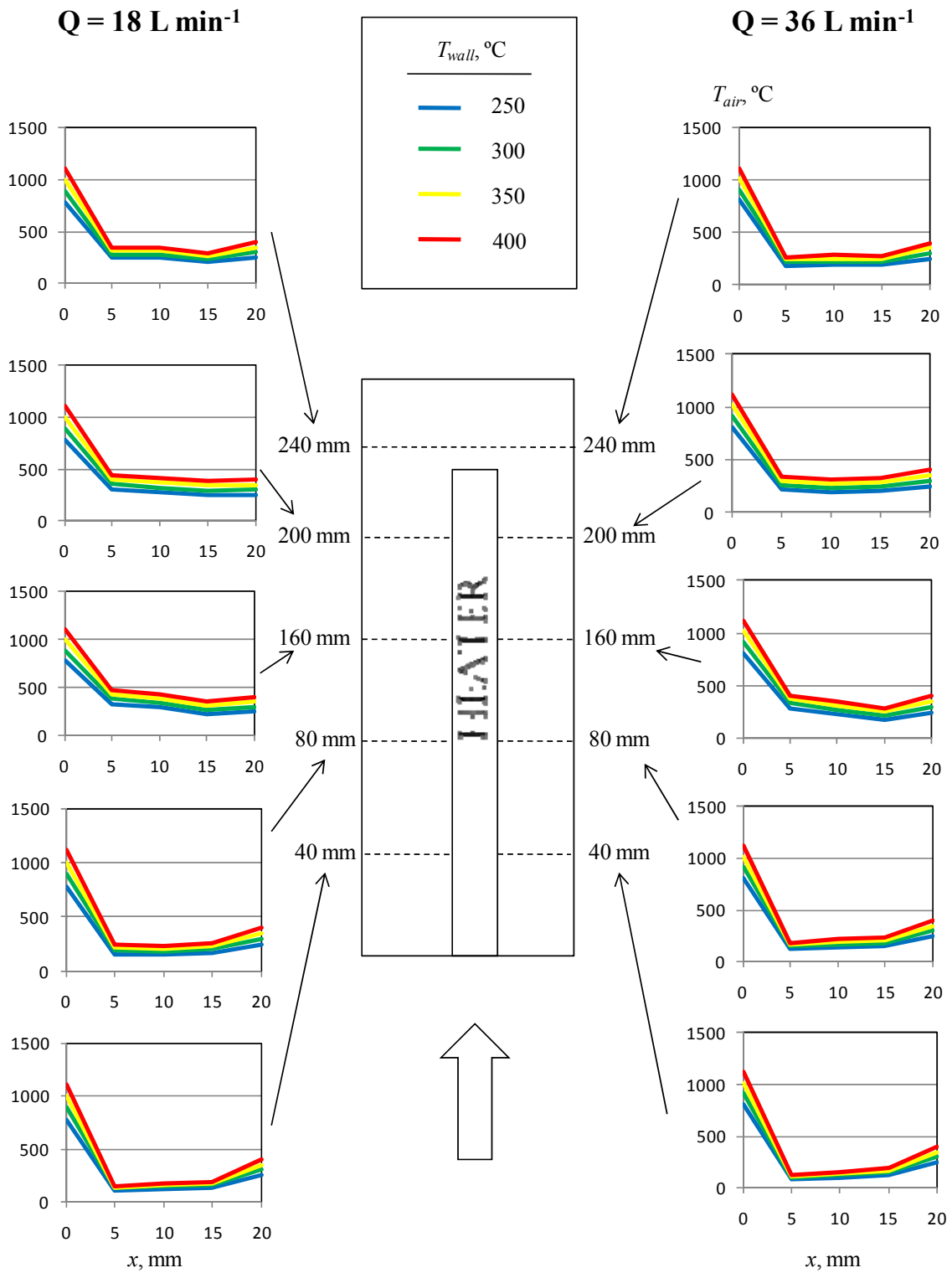

Figure 2.3. Temperature profiles determined in the test chamber for Q=18 and 36 L min^{-1}, T_{wall}=250, 300, 350, and 400°C, and y=40, 80, 160, 200, and 240 mm. All temperature values measured with a thermocouple in the air-flow are corrected for radiation.

The longitudinal profiles of the air temperature (T_y) measured at different distances from the heater showed that initially T_{air} increased along the flow direction, peaking ($T_{y,\,max}$) at $y \approx 160 - 200$ mm, and then decreased. The peak values for x=5, 10, 15, and 20 mm are presented in Fig. 2.4 for different Q and T_{wall}. It is seen that for each set of conditions there was always a minimum of $T_{y,\,max}=f(x)$.

In search of the lowest heat exposure zone and following the analysis of $T_{y,\,max}=f(x)$, we considered four annular zones: x=0 – 5 mm (cross-sectional area = 12.5% of the total), x=5–10 mm (cross-sectional area = 20.8% of the total), x=10–15 mm (cross-sectional area = 29.2% of the total), and x=15–20 mm (cross-sectional area = 37.5% of the total). For each annulus, an equivalent temperature can be defined if the air temperature distribution within this annulus is known. In absence of this information (due to limited special resolution of the air temperature measurement), we defined an equivalent temperature of each annulus in a simplistic way – as an arithmetic average of air temperatures obtained on its boundaries. This definition was applied to all annuli, except for the first one:

$$T_{y,\max}^{x=5-10} = \tfrac{1}{2}\left(T_{y,\max}^{x=5} + T_{y,\max}^{x=10}\right) \tag{2.8a}$$

$$T_{y,\max}^{x=10-15} = \tfrac{1}{2}\left(T_{y,\max}^{x=10} + T_{y,\max}^{x=15}\right) \tag{2.8b}$$

$$T_{y,\max}^{x=15-20} = \tfrac{1}{2}\left(T_{y,\max}^{x=15} + T_{y,\max}^{x=20}\right) \tag{2.8c}$$

Given its steep air temperature change from x=0 to 5 mm, the first annulus could not be adequately approximated using the temperatures on its boundaries. Furthermore, featuring the highest temperatures, the first annulus is definitely not representative of the lowest heat exposure zone, which we aimed to identify.

The equivalent temperatures of adjacent annuli were compared. If the difference fell below 30°C (twice the precision-based uncertainty, ΔT=15°C), no differentiation was made between the two annuli with respect to the heat exposure and they were combined. In all situations but one, the equivalent temperatures of the third (x=10–15 mm) and the forth (x=15–20 mm) annuli differed by <30°C (the single exception exhibited a difference of

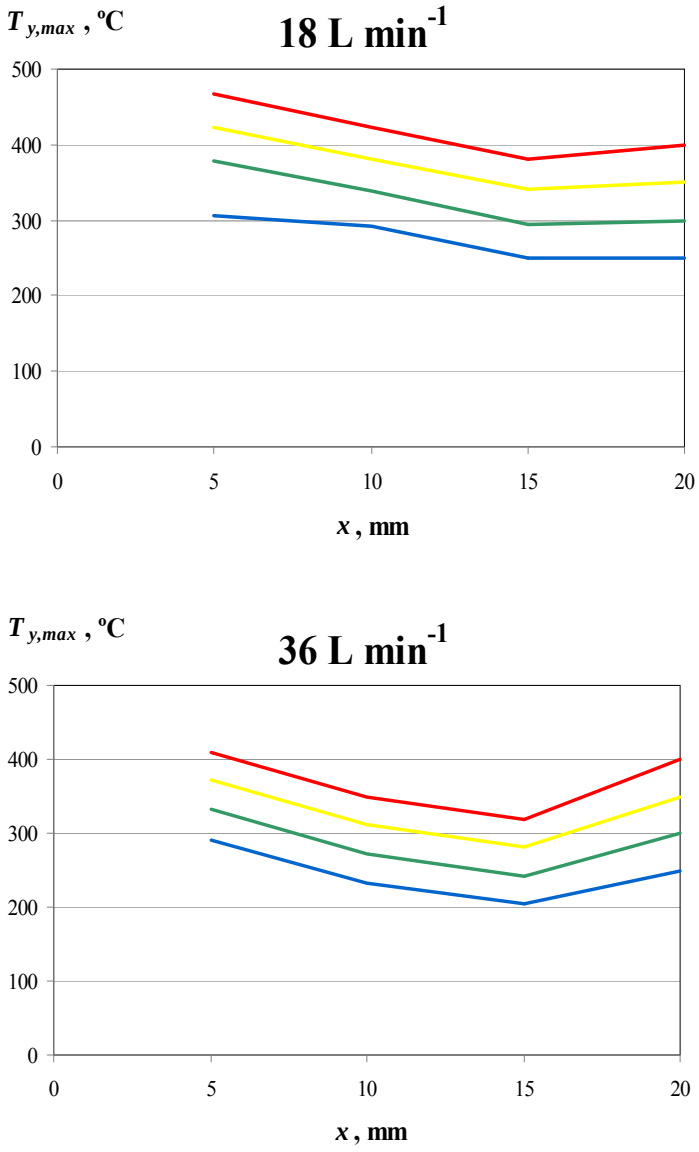

Figure 2.4. Profiles $T_{y,\,max}$ in the test chamber between x=5 and 20 mm for Q=18 and 36 L min^{-1}, T_{wall}=250, 300, 350, and 400°C. All temperature values measured with a thermocouple in the air-flow are corrected for radiation.

34°C). In contrast, the second annulus (x=5–10 mm) was treated as a separate area because the corresponding temperature differences were mostly between 40 to 50°C, i.e., >2ΔT. By combining the third and the fourth annuli, we introduced the annular area accounting for 66.7% of the entire cross-section, which was designated as the lowest heat exposure zone. To characterize the air temperature in this zone, we assigned an interval between the equivalent temperatures representing the combined annuli ($T_{y,\max}^{x=10-15}$ and $T_{y,\max}^{x=15-20}$) extended

to the left and to the right by ΔT=15°C. The mid-point of this interval was regarded as the characteristic air temperature value ($\overline{T}_{air}$). The characteristic interval and the mid-point value were determined for each set temperature and air flow rate.

Thermal equilibration time of a spore in heated air flow

The thermal equilibration of a spore that moves in the axially-heated air flow was quantified using the experimentally determined temperature profiles. To perform a conservative estimation of the equilibration time, the spore was assumed to be a uniform sphere of diameter D_p with the lowest plausible thermal conductivity, k, and the highest plausible heat capacity. For the former, we used 0.05 W/m-K [listed for fiber glass which is less conductive than fat or other biological tissues (Santos *et al*., 2008)]; for the latter, we used 4.18 x 10^6 J/m^3-K (water). The Biot number of such a spherical particle

$$Bi = \frac{h_p D_p}{2k} \tag{2.9}$$

is close to 1, constituting a transient heat transfer problem with a convection boundary condition (here h_p is the particle heat transfer coefficient due to forced convention,). Based on the graphical solution described by Holman (2002), the equilibration time ($\tau_{eq.}$) needed for a spore to adapt to a specific air temperature is less than 1 ms. In this estimation, the adaptation is defined as the condition at which the spore center lags the air temperature by no more than 0.1% of the difference between T_{air} and T_0, which translates to about 1°C or less for the temperatures tested in this study.

The above assessment assumes that T_{air}=const. As a next approximation, we accounted for the continuous change in air temperature along the spore trajectory. By factoring in the temperature effect on the air density, we calculated that at Q=36 L min^{-1} and $T_{y,\,max}$ ~ 500°C, the spore passes the entire length of the heater within 0.3 s, which corresponds to a temperature change of about 1600°C per second, i.e., 1.6°C per millisecond. Considering that τ_{eq} ~ 1 ms, an additional temperature difference between the spore core and the local air flow, which occurs due to the air temperature change, does not exceed 1.6°C. The estimated τ_{eq} is even lower at lower $T_{y,\,max}$.

To summarize, under the test conditions of this study, the spore adapted the air temperature practically instantly. Therefore, we concluded that the characteristic air temperature represents the actual spore exposure temperature T_e.

Size distribution of aerosol particles

Figure 2.5 presents the normalized particle size distributions measured at the entry and exit points of the test chambers at two operational air flow rates while generating aerosol from the suspension containing $10^7 – 10^9$ spores mL^{-1}. During these measurements, the heating element was installed inside the chamber but no voltage was applied.

The distributions shown in Figs. 2.5A and 2.5B peak at the same particle size, D_p=0.73 μm, representative of intact *B. subtilis* spores. These data suggest that both dry dilution flows – 12 L min^{-1} (Fig. 2.5A, Q=18 L min^{-1}) and 30 L min^{-1} (Fig. 2.5B, Q=36 L min^{-1}) – were equally sufficient to shrink the nebulizer-generated particles to the spore size as water content evaporates downstream of the test chamber – between the aerosolization point (nebulizer) and the chamber's entry point. At the same time, the peak concentration values presented in Figs. 2.5A and 2.5B differ by about factor of two, which reflects the dilutions. The dilution-associated difference in the spore concentration is also observed in the curves representing downstream aerosol measurements (Fig. 2.5C versus Fig. 2.5D).

The distribution obtained upstream and downstream of the test chamber are almost identical for both flow rates (Fig. 2.5A versus Fig. 2.5C and Fig. 2.5B versus Fig. 2.5D), which indicates that no substantial particle losses occurred in the test chamber with the axial heater (the concentration difference was below 10% in all tests).

Spore inactivation factor

The measured *IF*-values varied from 1 to $>10^5$. Following the above-described conservative approach, it was postulated that only spores moving through the external

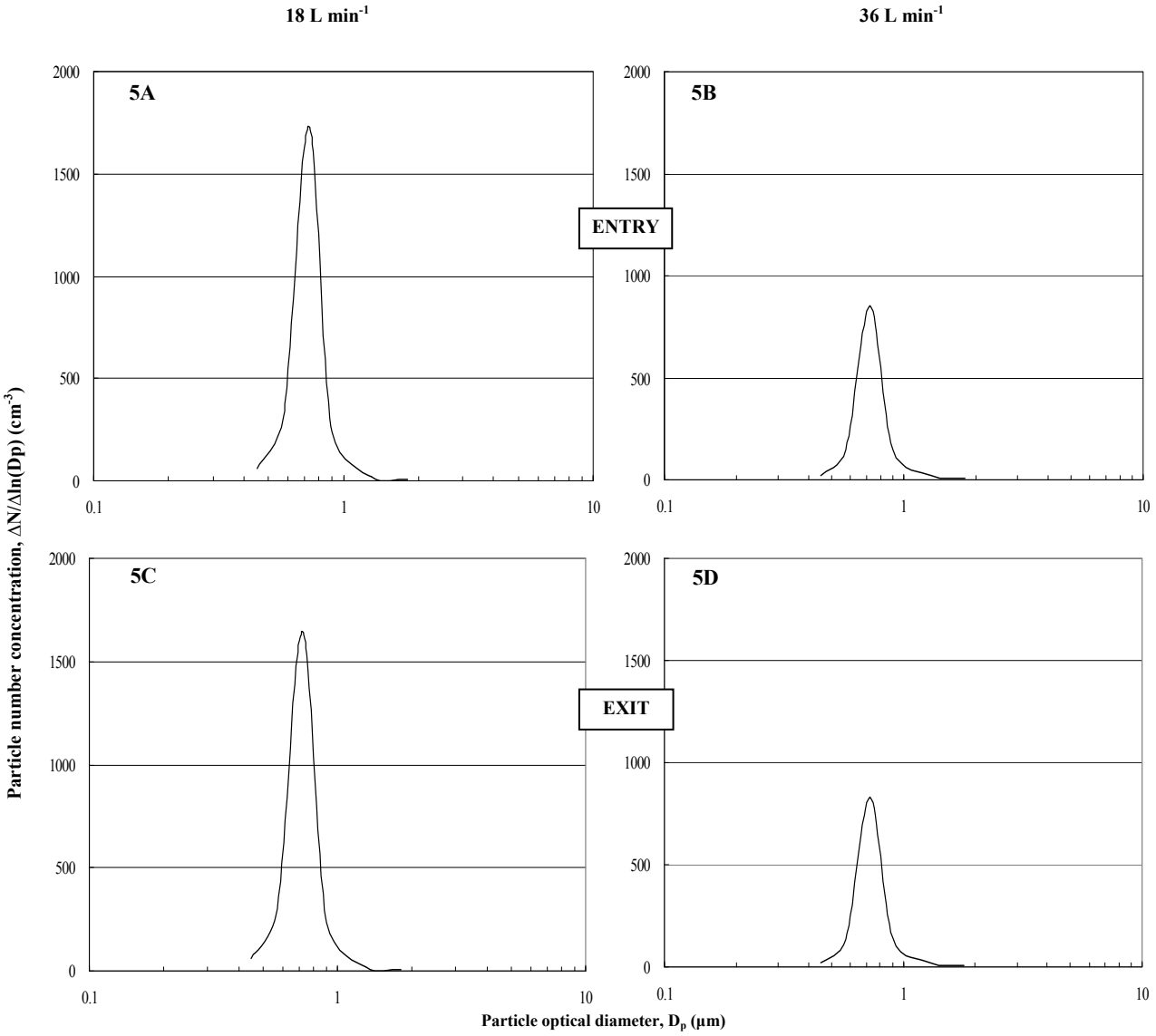

Figure 2.5. Aerosol particle size distributions measured at the entry and exit point of the test chambers at Q=18 and 36 L min^{-1}.

annulus (x=10–20 mm), where they are exposed to lowest air temperatures, could survive the heat-induced stress while those moving in the interior annulus (x=0–10 mm) do not survive because of much higher temperatures in the heater vicinity. It was further assumed that the spores are distributed uniformly in the air flow. To account for the difference between cross-sectional areas corresponding to control samples (x=0–20 mm) and test samples (x=10–20 mm), a correction coefficient of 0.667 (or 66.7 %), referred above, was applied to the measured *IF*-values. The corrected value ($IF_{corrected}$=0.667×$IF_{measured}$)

represents the lowest boundary for the spore inactivation. The actual inactivation falls into the range between $0.667 \times IF_{measured}$ and $IF_{measured}$

Figure 2.6 shows the corrected spore inactivation factor as a function of the characteristic exposure temperature. Horizontal bars represent the characteristic air temperature interval $\overline{T}_{air}$ defined above. The experimentally obtained mean *IF*-values are presented at the mid-point of each temperature interval. The vertical error bars represent the geometric standard deviations. The experimental data were subjected to a combination of non-linear and linear regression analyses. At Q=18 L min^{-1}, a polynomial fit was developed for the function $log_{10}(IF)=f(T_e)$ in the temperature range from 220°C to 290°C (R^2=0.994) with a linear extension beyond 290°C. At Q=36 L min^{-1}, a polynomial fit was developed for 240°C – 350°C (R^2=0.992) and extended linearly for higher temperatures.

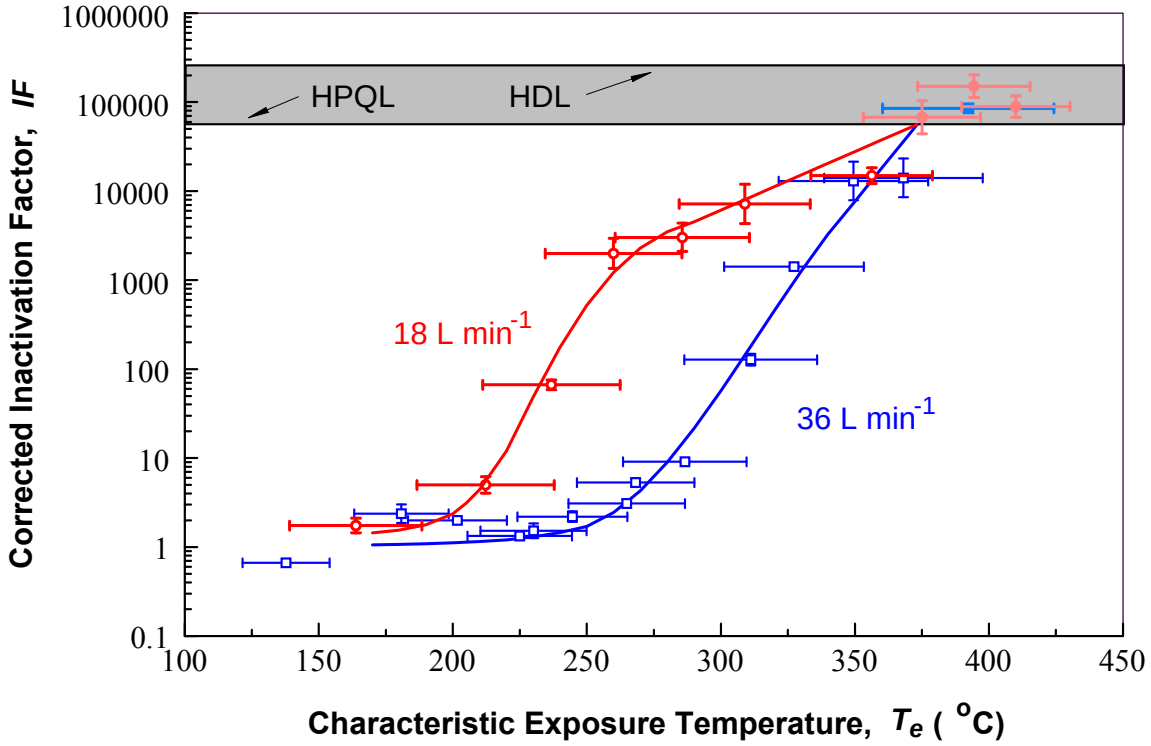

Figure 2.6. Effect of the exposure temperature and flow rate in the corrected spore inactivation for *Bacillus subtilis* spores. Horizontal bars represent the characteristic air temperature interval defied in this Chapter. The experimentally obtained mean *IF*-values are presented at the mid-point of each temperature interval, and the vertical error bars represent the geometric standard deviations. HDL is the Highest Detection Limit, and HPQL is the Highest Practical Quantification Limit (both are defined in this Chapter).

The two data sets obtained at different flow rates represent different exposure conditions. In both cases, the thermal exposure of aerosolized spores produced no effect or only a moderate inactivation when the temperature remained below ~200°C for 18 L min^{-1} and ~250°C for 36 L min^{-1}. The inactivation factor then increased exponentially by about 4 orders of magnitude as T_e rose by about 150°C. As a result, IF obtained for Q=18 L min^{-1} reached mean values of 5.2×10^2 at T_e ≈250°C, 6.2×10^3 at T_e ≈300°C, and above 10^4 at T_e >320°C. For Q=36 L min^{-1}, IF=5.7×10^1 at T_e ≈300°C, 1.3×10^3 at T_e ≈330°C, and 7.7×10^3 at T_e ≈350°C. Both curves reached HPQL≈5.6×10^4 at T_e ≈375°C. The curve corresponding to Q=18 L min^{-1} shows that the effect of temperature on inactivation becomes less dramatic as T_e approaches about 275°C.

The slope representing $log_{10}(IF)$ versus T_e changes from ~6.1×10^{-2}/°C to 1.3×10^{-2}/°C. A similar change cannot be clearly observed from the other curve (Q=36 L min^{-1}) as the data approach HPQL. Both curves come together as the characteristic spore exposure temperature becomes close to 400°C pointing to a biocidal effect that is characterized primarily by the exposure temperature rather than by the time of exposure. At that stage, IF attains ~10^5, thus reaching the limitation of our test protocol (shown as the area between HPQL and HDL). The IF=10^5 translates into a loss of the spore viability of 99.999%.

The time of heat exposure (t_{exp}) was not clearly defined by this study protocol because the spores were exposed to different temperatures as they moved through the "lowest heat exposure zone" making their way from the entrance to the exit of the test chamber. If defined as the spore time of flight from the bottom to the top of the heater (the full length of 230 mm), t_{exp} is estimated to be between 0.2–0.3 and <1 s (depending on the air flow rate and the target temperature). If defined specifically as the time of exposure to the temperature range established for T_e (a much shorter distance), t_{exp} is below or about 0.1 s.

Heat-induced changes in structure and composition of an aerosolized spore

Remarkable heat resistance of dormant *B. subtilis* spores observed at high temperatures is due to their unique structure. The spore consists of multiple layers of resistant coats surrounding the cytoplasm with DNA containing nucleoid (Setlow, 1995, 2006; Zheng *et al*., 1988). We attribute our findings on the dry thermal inactivation of aerosolized *B. subtilis* spores to the following three mechanisms:

1. DNA Damage. Scientific literature contains evidence that spores exposed to dry heat on surface can attain both DNA damage and mutations (Northrop *et al*., 1967; Setlow & Setlow, 1995; Zytkovic *et al*., 1972), which can play a primary role in the spore inactivation.

2. Damage to essential proteins. The inner and outer layer of proteins including coat proteins involved in spore germination as well as proteins involved in protecting spore DNA can be significantly damaged by heat exposure resulting in the spore inactivation.

3. Breaking of the coat layers by the inner pressure. The inner pressure applied to the spore wall increases as the spores adapt to high air temperature. This process may take milliseconds. At certain pressure, the outer coat layers of the spore can break inflicting direct physical damage to the cell membrane with consequent release of inner cytoplasm, and eventual death of the endospore.

No sufficient data are currently available in the peer-reviewed literature to characterize the potency of each of the above-described mechanisms and assess their relative contributions in the thermal inactivation of airborne endospores. The inner pressure change is unlikely to break the coat layers of *B. subtilis* spores and thus is not believed to be a primary factor responsible to a very effective spore inactivation observed in this study. Even vegetative cells of *B subtilis* (which do not have protective coat layers) have been shown to stay intact after exposure to about 700°C, as demonstrated by recently published scanning electron micrographs (Jung *et al*., 2009b). Damages to proteins and DNA are probably more important factors. DNA damage, particularly depurination, is believed to be an important process influencing the heat-induced spore inactivation (Setlow and Setlow, 1995; Setlow, 2006). Small acid soluble proteins bind tightly the DNA and can – to some extent – protect

it from depurination (Setlow and Setlow, 1995). Deactivation of these proteins is expected to accelerate the DNA damage. We can assume that, up to a certain level of the heat exposure, the changes in protein structures are repairable. However, the self-repair capability diminishes with increasing heat exposure resulting in a gradual (exponential) viability loss. Once the heat exposure exceeds a threshold level, the changes in indispensible proteins (vital for bacterial growth on culture media) become irreversible, which causes the spore inactivation. The DNA damage may follow similar pattern because several proteins and enzymes are involved in DNA repair mechanisms. To explore a possible DNA damage in *B. subtilis* spores, a limited number of filter extract samples were stained with acridine orange (a DNA selective metachromatic stain). We found that the samples generated from experiments conducted at a high exposure temperature ($T_e \approx 400$°C) produced much lower number of stained spores as compared to those obtained from samples not subjected to heat treatment. The difference was about 100-fold at 18 L min^{-1} (longer exposure) and about 50-fold at 36 L min^{-1} (shorter exposure). These observations suggest that the DNA damage did occur as a result of the dry heat treatment of airborne spores although their exposure time was a fraction of a second. We believe that this effect may have taken place simultaneously with the damage to essential proteins (especially those involved in the DNA repair mechanisms). The difference observed at two flow rates for temperature ranging from 200 to 350°C confirms that the protein and DNA damage depends on both the exposure temperature and exposure time. Longer exposure to lower temperatures and shorter exposure to higher temperatures can equally act on repair mechanisms of DNA and proteins producing similar inactivation patterns: *IF* changed from 10^1 to 10^3 as the spore exposure temperature increased from 220 to 260°C at 18 L min^{-1} and from 280 to 330°C at 36 L min^{-1}. The similarity of trends observed with the two flow rates suggests that the same mechanisms were involved in the spore inactivation occurring at different exposure time intervals. At the same time, a change in the *IF*-slope observed at Q=18 L min^{-1} around 275°C suggests a possible involvement of an additional phenomenon that has the potential to slow down the spore damage. A separate investigation is needed to develop a more specific explanation.

Conclusions

Thermal inactivation of viable aerosolized *B. subtilis* spores due to short-term exposure to an axially-heated airflow was studies. While at some location of the test chamber air was heated to temperatures above 1000°C, the characteristic exposure temperature conservatively defined here for assessing the spore inactivation did not extend beyond 450°C. The reported *IF*-values serve as the lower approximation of the actual inactivation. For both air flow rates representing different exposure conditions, the spore viability was barely affected by the heat at T_e below ~200°C for Q=18 L min^{-1} and T_e below ~250°C for Q=36 L min^{-1}. This demonstrates that airborne *B. subtilis* spores are resistant to a dry heat exposure occurring over a fraction of a second. Once the temperature exceeded the respective levels, *IF* began increasing turning into an exponential function of T_e. Depending on the flow rate, *IF* exceeded ~10^4 at T_e >320°C (Q=18 L min^{-1}) or T_e >360°C (Q=36 L min^{-1}). At T_e ≈375 – 400°C, the spore inactivation obtained at both flow rates reached the limit of quantification established in this study protocol, which translates to approximately 99.999% viability loss. This "critical" temperature was not flow rate dependent. This suggests that a biological phenomenon behind spore killing is characterized primarily by the exposure temperature rather than by the time of exposure.

The findings were attributed primarily to the heat-induced damage of DNA and denaturation of essential proteins. Another heat-associated mechanism – increase of inner pressure applied to the spore wall – is unlikely to break the coat layers of *B. subtilis* spores under the test conditions of this study [as we concluded based on the review of scanning electron micrographs published by Jung *et al*. (2009b)]. Up to a certain level of thermal exposure, the DNA damage and protein denaturation are repairable; however, the self-repair capability diminishes as heat rises further and – at a certain temperature – the damage become irreversible.

The data generated in this study provide an important reference point for thermal inactivation of stress-resistant bacterial spores in various biodefense/counterterrorism and air quality control applications.

Chapter 3. Inactivation of aerosolized viruses in continuous air flow with axial heating

Paper published: Grinshpun, S.A., Adhikari, A., Li C., Yermakov, M., Reponen, L., Johansson, E., and Trunov M. (2010) Inactivation of Aerosolized Viruses in Continuous Air Flow with Axial Heating, *Aerosol Science and Technology*, 44(11):1042-1048.

Introduction

Different methods are available for protecting air environments from bioaerosol hazards including, but not limited to, pathogenic aerosol agents. While some methods achieve this goal by reducing the total aerosol concentration, others specifically target viable bioaerosol particles. Heat treatment has been found efficient for inactivating viable bacteria (Northrop and Slepecky 1967; Setlow 1995; Setlow and Setlow 1995; Stumbo 1973) and viruses (Johnson *et al*. 2007; Stonehouse and Stockley 1993). However, most of the previous studies have been primarily motivated by "non-aerosol" applications, such as the sterilization of food products, water purification, and surface decontamination. Consequently, these studies involved microorganisms in aqueous media or on solid surfaces. Few investigations on heat-induced microbial inactivation have dealt with aerosolized biological particles – bacterial spores (Grinshpun *et al*. 2010a; Mullican *et al*. 1971), vegetative cells (Jung *et al*. 2009b; Lee and Lee 2006), or fungal spores (Jung *et al*. 2009c). To our knowledge, no data are currently available on the inactivation of *aerosolized* viruses by their exposure to hot air flow.

It is anticipated that aerosolized microorganisms exhibit different responses to heat stress than those suspended in liquid or attached to solid surfaces (Nicholson *et al*. 2000). One parameter that promotes the crucial difference in stress responses is the time of exposure because viruses in aerosol phase may be exposed to heat over relatively short period of time as compared to those subjected to the heat treatment in liquids or on surfaces.

The quantification of the thermal inactivation of airborne virions is particularly important for situations when the exposure time is as short as ~0.1 s (or even shorter) and the air temperature ranges from ~100ºC to ~1000ºC. Bio-defense applications serve as a good example of such bioaerosol exposure. It is presently unknown whether viral warfare agents aerosolized under high-temperature conditions (e.g., in a bio-agent defeat scenario) are likely to lose 100% of their infectivity during a short-term exposure to dry heat. Should some virions survive the exposure, their presence in the atmosphere may pose a serious public health threat. Inactivation of airborne virions in an air flow drawn through a heating unit is also relevant to indoor air quality. Heat treatment is believed to be an effective, safe and environmentally-friendly method for purifying air contaminated with bioaerosol particles in continuous-flow settings, e.g., heating, ventilation and air-conditioning systems (Jung *et al*. 2009b, 2009c).

In this study, we investigated inactivation of aerosolized MS2 virions in a continuous air flow with axial heating. In the absence of moisture, the dry heat induced inactivation was evaluated for the characteristic air temperatures ranging from <50°C to > 300°C and exposure time intervals of ~10^{-1} – 10^{0} s. MS2 bacteriophage, approx. 0.03 μm tailless non-enveloped icosahedral RNA-coliphage, is relatively stable against environmental stress, and has been used in the past as a simulant of mammalian and other viruses (Jones *et al*. 1991; Verreault *et al*. 2008). It is also known as an indicator for enteric viruses (Havelaar *et al*. 1993).

Materials and Methods

Preparation of viral suspension and experimental protocol.

Stock suspension of MS2 virus was prepared as described in our previous publication (Balazy *et al*. 2006). In brief, a volume of 9 mL of Tryptone Yeast extract Glucose (TYG) broth with ultrafiltered water was added to a freeze-dried bacteriophage MS2 vial (ATCC 15597-B1) obtained from the American Type Culture Collection (ATCC, Manassas, VA,

USA). The aliquot was filtered and serially diluted to achieve 10^8–10^9 PFU (plaque forming units) per mL of the suspension. The titer was determined with a modified plaque assay (ISO 2000) using the *Escherichia coli* (ATCC 15597, strain C3000) as the host organism.

While the airborne stability of bacteriophages depends on multiple factors (Dubovi and Akers 1970; de Jong *et al*. 1975), MS2 virus has been shown to maintain its infectivity in a nebulizer suspension and in aerosol phase with variability <25% for at least 90 min (Tseng and Li 2005). More recent study conducted with MS2 virions dispersed in a large chamber at air temperatures 24–26 ºC and relative humidity of 21–30% revealed that the aerosol concentration of active virions remains stable (within 20% tolerance) over 60 min (Grinshpun *et al*. 2007). The virion can also maintain its infectivity for long time after it is collected on conventional filters (Rengasamy *et al*. 2010).

The experimental facility and test design were described in detail in our earlier papers (Grinshpun *et al*., 2010a,b). The setup was operated inside a class II biosafety cabinet (Model 6TX, Baker Co., Inc., Sanford, ME, USA). Figure 1 provides the general schematics of the setup. MS2 virions were aerosolized by a Collison nebulizer (BGI Inc., Waltham, MA, USA) operated at 6 L/min. Dry dilution air was supplied through a HEPA-filter at two flow rates of 12 and 30 L/min producing the total flows of Q=18 L/min and Q=36 L/min, respectively, which represented two different thermal flow regimes and exposure times. The bioaerosol was charge-equilibrated by passing through a channel containing a 10 mCi ^{85}Kr source (model 3012, TSI Inc., St. Paul, MN, USA). Subsequently, the bioaerosol was dispersed in a vertically oriented, cylindrical test chamber of 50 mm in inner diameter and 320 mm in height. The chamber as well as other sections of the experimental setup was made of stainless steel. A cylindrical electric heating element (Mighty-Watt Heater, Gordo Sales, Inc., Layton, UT, USA) of 10 mm in diameter and 230 mm in height was installed in the test chamber along its axis on a flat holder 16 mm above the chamber entrance. The axial air flow heating design was utilized due to its relevance to another laboratory study conducted in parallel to investigate the selected bio-agent defeat during explosion and combustion. This configuration is also being explored for thermal air

purification of biocontaminated indoor air (Jung *et al*. 2009b, 2009c; Lee and Lee 2006). Connected to a variable voltage source (Staco Energy Products, Co., Dayton, OH, USA) through a general purpose transformer (Acme Electric Corp., Lumberton, NC, USA), the heating element was operated at voltages of 50 to 160 V, producing a wide range of temperatures T_{heater} . Depending on the voltage applied to the heating element and the air flow rate, it took approximately 30 – 60 min to achieve a stable thermal condition represented by a specific target temperature of the test chamber wall, T_{wall}, which was measured using thermocouple probes (Model 5TC-GG-20, Omega Engineering, Inc., Stamford, CT, USA) with a digital thermometer (Model HH12A, Omega Engineering, Inc., Stamford, CT, USA).

After passing through the test chamber and a 500-mm long transportation line, the aerosol was isoaxially sampled into three identical probes and transported through a cooling system that cooled the air down to room temperature. The viruses were collected from each probe downstream of the cooling system on a sterile 25-mm diameter gelatin filter (SKC Inc., Eighty Four, PA, USA). Gelatin filters are appropriate for collecting airborne viruses as viral infectivity is not critically impacted during collection (Verreault *et al*. 2008). The sampling was conducted at a flow rate of 5 L/min over a period of 1 min. The filters were subsequently removed, dissolved in sterile, filtered deionized water, and analyzed using a modified plaque assay (ISO 2000). The PFU count was performed on TYG agar plates from 1 mL aliquots of the original or diluted filter extracts. Dilution ratios of 10^1, 10^2, 10^3, and 10^4 were used. The concentration of plaque forming viruses was determined as an average from the three filter samples obtained in each trial. At least two trials were conducted for each set of conditions. The lowest countable number was 1 PFU per plate. Some plates (representing the samples obtained under high thermal exposure conditions) showed zero count. For those, we assigned a value of 0.5 PFU that was input when determining an average count from several replicates – the approach conventionally used in other studies (Heinrich *et al*. 2003). The limit of detection (LOD) was calculated using 1 PFU per sample and a total sample volume of 1 mL. Available analytical guidelines recommend using the Practical Quantification Limit (PQL), which is 5-fold greater than LOD. It represents the lowest level that can be reliably achieved within specific precision

and accuracy limitations provided by routine laboratory operating conditions (Benjamin and Belluck 2001; McBean and Rovers 1998; Wayman *et al*. 1999). Following these guidelines, we adopted PQL=5×LOD as the quantification limit for our analysis. We acknowledge that in quantitative microbiology credible estimates are usually based on colony/plaque counts higher than 5 CFU or PFU; however, as this test protocol aimed at achieving conditions causing the maximum possible inactivation, we accepted 5 PFU as a reasonable limit.

The experiments were conducted with no voltage applied to the heating element, i.e., at a room temperature, T_0=20°C (regarded as control), and at various voltages representing specific thermal conditions to which the virions were exposed in the chamber (temperature T). The inactivation factor (IF) can be quantified through the test-control comparison as follows:

$$IF = \frac{C_{PFU}(T_0)}{C_{PFU}(T)} \qquad (3.1)^1$$

Here $C_{PFU}(T_0)$ and $C_{PFU}(T)$ are the concentrations of active plaque forming virions (PFU/m^3) collected after they passed the test chamber with no heating and with heating, respectively. The above definition assumes that all the viruses were exposed to the same air temperature during the same time interval, which is not the case in the presence of gradients of air temperature and velocity – longitudinally (y) and radially (x), see Fig. 3.1. Unlike the confined thermal systems used for sterilizing food and liquids, a continuously heated air flow system cannot, in principle, maintain a single temperature because of continuous energy transfer (Grinshpun *et al*. 2010a; Jung *et al*. 2009c). Consequently, an aerosol particle passing through the chamber is exposed to different temperatures along its trajectory. In an axially heated flow, the radial (cross-sectional) gradient of air temperature is relatively high in a close proximity to the heater; it essentially diminishes as the distance to the heater increases (Grinshpun *et al*. 2010b). The virions moving close to the heater are expected to be inactivated much more efficiently than those moving further from the heater and closer to the wall. Thus, the experimentally determined inactivation factor should

[1] It is common in microbiology to use the "*log* inactivation" by quantifying log_{10}(IF).

represent some integral value accounting for air temperatures at different distances from the heater. Based on the measured longitudinal and radial air temperature profiles (see below), we defined the characteristic temperature and introduced an appropriate correction for the experimentally determined *IF*, which established a conservative estimate of the viral thermal inactivation as explained below.

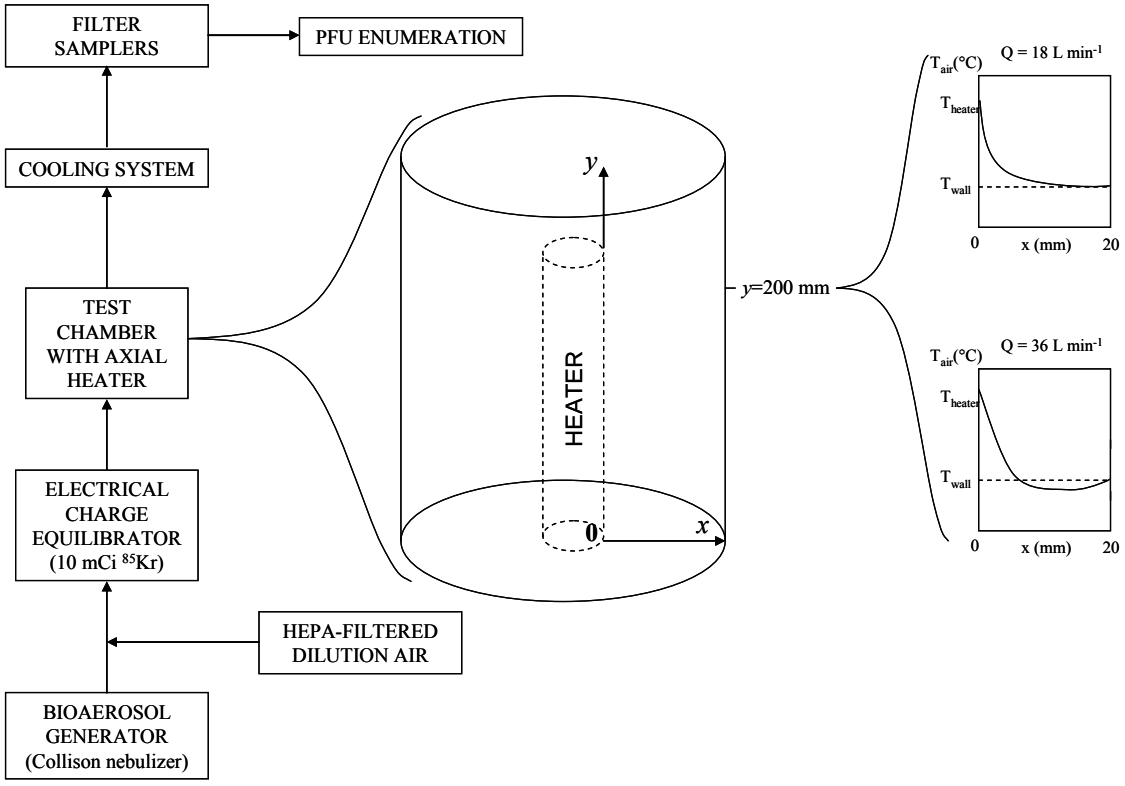

Figure 3.1. Schematic representation of the experimental set-up and temperature profiles.

Characteristic exposure temperature and conservative estimate of thermal inactivation in axially heated air flow.

In accordance to the approach developed in our earlier study (Grinshpun *et al*. 2010a), the characteristic exposure temperature was defined based on the following considerations:

1. The longitudinal air temperature profile is non-monotonic. For any specific flow streamline (x=const), the air temperature T_{air} increases as the air moves along the heater and then decreases. Based on our previous measurements, depending on the target temperature and the radial coordinate, the peak ($T_{y,\max}^{x=const}$) occurs at different points, mostly around y=200 mm. For a specific particle trajectory, the peak temperature largely determines the airborne virus inactivation.
2. While being very high for the air streamlines near the heater (small x), the peak values of air temperature are much lower for streamlines near the wall (large x). $T_{y,\max}$ decreases radially following a monotonic pattern (mostly for lower flow rates) or a non-monotonic pattern (for higher flow rates), see Fig. 3.1. The difference is associated with the thermal development of the air flow (Holman, 2002, Thomas, 1992). At any flow rate, an annular area can be identified between x=x^* and x=20 mm (wall), in which the air flow is heated the least. In our earlier study involving the same experimental set-up, the entire cross-section was divided in four annuli, x=0–5 mm, x=5–10 mm, x=10–15 mm, and x=15–20 mm, and the "low-heat zone" was identified as the last two annuli (Grinshpun *et al*. 2010a). It was postulated that if the microorganisms moving through this zone did not survive, those moving through a hotter area (closer to the heater) would not survive either. According to this conservative approach, the zone of $x > x^*$ was selected for characterizing the exposure causing inactivation, and the maximum integral temperature achieved in this zone was regarded as the characteristic air temperature, $\overline{T}_{air}$.
3. There is a certain time needed for an aerosol particle to get adjusted to a specific surrounding air temperature. Thus, in an air flow with constantly changing T_{air}, the particle temperature at a point (x, y) may differ from the air temperature measured at the same point. However, for the test conditions of this study, the thermal equilibration time for particles as small as MS2 virions is estimated to fall below 1 millisecond, based on the assessment provided in Grinshpun *et al*. (2010a). This suggests that the airborne virions adapted the air temperature practically instantly, i.e., the characteristic air temperature defines the characteristic virion exposure temperature: $\overline{T}_{air} = T_e$.

Similar to our previous investigation (Grinshpun *et al*. 2010), the air temperature profiles inside the test chamber were determined with non-sheathed thermocouple probes (Type J, Model TJ36-ICIN-116, Omega Engineering Inc.,Stamford, CT, USA) positioned at a specific points (x, y); all thermocouple-measured air temperature values were subjected to correction for radiation. In the previous study, the measurement precision was $\Delta T = \pm 15°C$, representing variations associated with positioning the thermocouple inside the chamber. In this study, we improved the spatial resolution as compared to the earlier measurements by decreasing the radial increment from Δx=5 mm to Δx=1 mm. The air temperatures determined at x=1, 2, 3, …, 19 mm from the heater were combined with the surface temperature data assuming $T_{air}^{x=0} = T_{heater}$ and $T_{air}^{x=20\,mm} = T_{wall}$. For each of the four 5-mm thick annuli, the average temperature value was calculated by integrating over the corresponding cross-section. The average air temperature values of adjacent annuli were compared. If the difference fell below 30°C (twice the precision-based uncertainty, ΔT=15°C), no differentiation was made between the annuli with respect to the heat exposure. These annuli were combined to establish the characteristic exposure zone (x^* to 20 mm) for the conservative determination of the heat-induced viral inactivation. The interval of air temperatures, $\widetilde{T}_{air}$, measured across this zone with a 1-mm increment and the average value, $\overline{T}_{air}$, calculated by integrating over the zone's cross-section, was recorded. The former represented the temperature variation within the characteristic exposure zone, and the latter allowed assigning a single characteristic exposure temperature for which the *IF*-value was experimentally determined.

The control sample accounted for all viable virions arrived from the test chamber, i.e., those which moved through the entire cross-section (x=0 to 20 mm). As explained above, the test sample accounted for the surviving virions arrived from the characteristic exposure zone (x=x* to 20 mm), because others were postulated to be 100% inactivated by the more intense heat. The relative difference between the corresponding cross-sectional areas, expressed as

$$S = \frac{25^2 - (5 + x^*)^2}{25^2 - 5^2} = 1 - \frac{x^*(10 + x^*)}{600} \quad (x^* \text{ is in mm}) \tag{3.2}$$

was applied as the correction factor to the measured *IF*-values:

$$IF_{corrected} = S \times IF_{measured} \tag{3.3}$$

The above modeling is valid under laminar flow conditions in the test chamber along the heating element. The flow rate and flow dimensions tested in this study yield the Reynolds number below 1000, which supports the laminar flow assumption. The corrected *IF* represents the lowest boundary for the heat-induced inactivation of aerosolized virions, or its conservative estimate. The actual inactivation is believed to be in the range between $IF_{corrected}$ and $IF_{measured}$.

Data analysis

The mean *IF*-value and the geometric standard deviation were calculated for every test. The upper limit of the reportable *IF* was derived from PQL=5×LOD and referred to as the highest practical quantification limit (HPQL).

Results

According to the criteria presented in the Materials and Methods section, the combination of the third (x=10 – 15 mm) and the fourth (x=15 – 20 mm) annuli was established as the characteristic exposure zone for determining the inactivation factor. Figure 3.2 presents $IF_{corrected}$=0.667×$IF_{measured}$ plotted against the characteristic exposure temperature for two exposure/flow conditions: Q=18 and 36 L min^{-1}. The horizontal bars represent the above-defined range of temperatures $\widetilde{T}_{air}$. The vertical error bars represent the geometric standard deviations (GSD) for the corrected values of the inactivation factor.

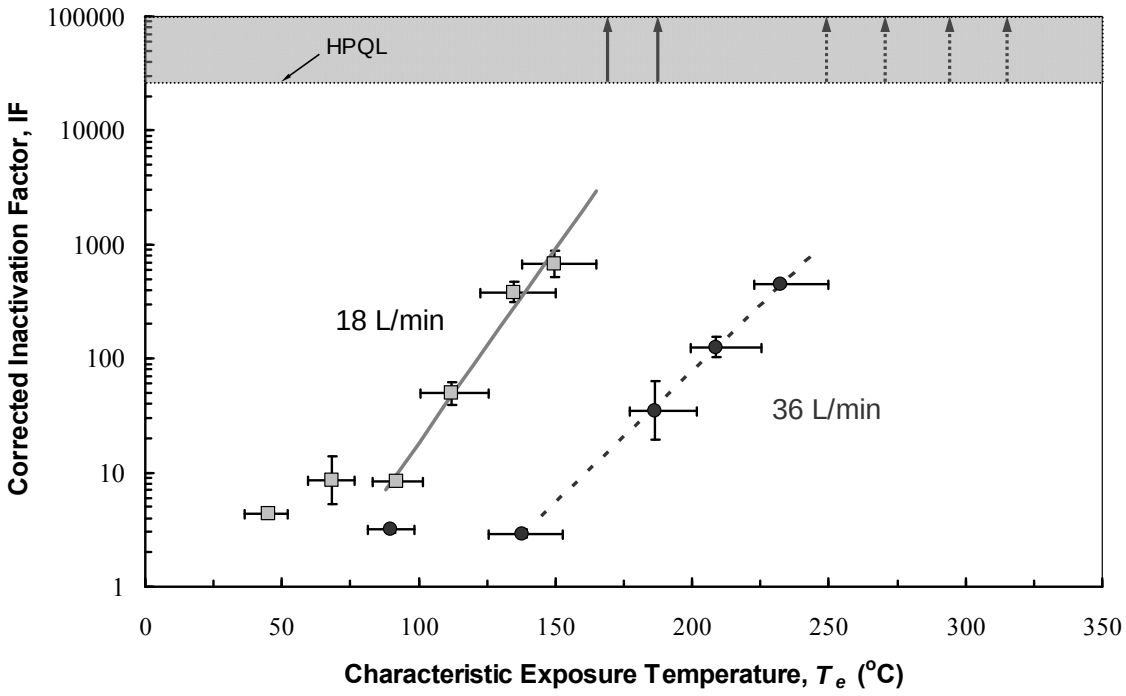

Figure 3.2. Effect of the characteristic exposure temperature and the air flow rate through the test chamber on the inactivation of aerosolized MS2 virions. Points: experimentally obtained values of $IF_{corrected}(T_e)$; horizontal bars: range of $\widetilde{T}_{air}$; vertical bars: GSD of $IF_{corrected}$. HPQL = Highest Practical Quantification Limit.

It is seen that a short-term exposure to temperatures of up to ~90°C (Q=18 L min^{-1}) or up to ~140°C (Q=36 L min^{-1}) produced a steady MS2 virus inactivation at relatively modest levels of IF~10 or lower. Further increase in T_e resulted in a rapid infectivity decline demonstrated by an exponential increase of the inactivation factor. The latter reached ~10^3 (~99.9% viruses killed) at T_e ~ 150°C as a result of a longer exposure (Q=18 L min^{-1}) or at T_e ~ 230°C after shorter exposure (Q=36 L min^{-1}). Further – even moderate – increase of T_e beyond the above-indicated values generated a rapid jump of the efficiency of MS2 inactivation with IF exceeding HPQL. This was confirmed by multiple measurements performed at T_e >170°C (Q=18 L min^{-1}) and T_e >250°C (Q=36 L min^{-1}), as shown in Fig. 3.2 by vertical arrows at specific temperatures corresponding to counts of zero or few PFUs per sample that produced IF>HPQL. These IF levels translate into a virus inactivation rate of ~99.996% or greater.

Discussion

The time of a specific thermal exposure was not explicitly defined by this study protocol because a virion moving along a specific trajectory was exposed to different air temperatures at different points between the entrance and the exit of the test chamber. Thus, in spite of experimental advantages and practical relevance, the axial design presents a clear limitation for establishing relationship between the exposure temperature and exposure time. In this context, a more accurate characterization of thermal inactivation of bioaerosol particles in air flows may require a more pertinent experimental system. Nonetheless, the exposure time was estimated by applying the time-of-flight concept to a distance hypothetically characterized by a constant temperature $\widetilde{T}_{air}$. Based on the review of the longitudinal air temperature profiles, we estimated this distance to be approximately one quarter of the heater's length. Consequently, the time of flight along this distance (i.e., 230/4=57.5 mm) was assigned as a reasonable estimate of the characteristic exposure time. Accounting for the dependence of air velocity on air temperature (through its effect on the air density), the estimated characteristic exposure time ranged approximately from 0.10 to 0.15 s at Q=36 L min^{-1} (calculated for the tested range of T_e=90–250°C; the higher temperature corresponds to the shorter exposure time). At 18 L/min, it ranged from 0.24 to 0.33 s (calculated for the tested T_e=45–170°C).

For each flow rate, the results show that the initial temperature increase caused only a moderate inactivation with *IF* exhibiting a weak or no dependence on T_e. This is due to insufficient exposure to heat that resulted in relatively low heat energy transfer. Generally, thermal inactivation is quantitatively characterized by the probability of the virus colliding with a molecule of sufficient energy to cause lethal damage or a number of such collisions. With further increase in T_e , this probability is expected to increase exponentially (Hiatt 1964), which is evident from the experimentally determined exponential increase of the inactivation factor from ~10^1 to ~10^3 (Fig. 3.2). The final phase is portrayed by a sudden boost in *IF* above the reportable limit of the study protocol as the temperature further

increased by a small margin. This may possibly indicate that a different, or an additional, mechanism is responsible for inactivation at extreme temperatures.

The data sets obtained at the two flow rates show the same trends but quantitatively are remarkably different. The 2-fold difference between the tested flow rates (corresponding to a relatively modest difference in exposure time) produced a sizable change in the virus inactivation. The assessment described in the Supplemental Information section below demonstrates that it is possible.

Little is known about physicochemical and biochemical mechanisms that lead to thermal inactivation of *aerosolized* viruses. However, some information generated in studies with thermal inactivation of the MS2 bacteriophage in liquids seems relevant and is utilized in the discussion below.

The full virion of MS2 consists of a non-enveloped icosahedral protein capsid surrounding an RNA genome. The protein coat is formed from 180 identical subunits through self-assembly. In addition, this bacteriophage features the assembly protein A, which is an important component required for the phage attachment to the side of the pilus of the host bacterium containing the F plasmid (F+ or male *E. coli*) (Brock *et al*. 1964). Although the location of protein A in the MS2 protein shell structure is not well characterized (e.g., it has not yet been resolved by the three-dimensional X-ray crystallographic analysis), chemical labeling and antibody-binding experiments suggest that protein A is at least partially exposed on the capsid surface (Curtiss and Krueger 1974; O'Callaghan *et al*. 1973). Thus, heat treatment may damage not only the coat protein but potentially also protein A. Heat may also damage the single-stranded RNA inside the capsid. This damage is represented by effects such as denaturation, mutation, and strand breaks, or their combination. Each of the effects or all of them combined can inactivate an MS2 virion and make it non-infectious to the host bacterium, which ultimately reduces the fraction of viruses forming plaques. While the exponential decrease in infectivity with the temperature observed in our experiments is consistent with the conventionally accepted first-order concept (Hiatt 1964), the same concept does not explain the rapid enhancement of viral inactivation observed at

T_e ~170°C for Q=18 L min^{-1} and at ~250°C for Q=36 L min^{-1}. Additional experiments are needed to identify possible mechanisms associated with the final abrupt drop in the phage survival.

Stonehouse and Stockley (1993) investigated the damage of MS2 coat protein by exposing aliquots of assembled coat protein (from empty capsid lacking RNA) to specific temperatures for a 10-min period. Once heated to 70.5°C (in liquid), reassembly of coat proteins was found no longer possible. Johnson *et al*. (2007) compared the recovery of the capsid proteins after heating for 2 h using sodium dodecyl sulfate polyacrylamide gel electrophoresis (SDS–PAGE) and reported that no capsids were recovered at temperatures above 70°C due to precipitation of the denatured protein. It is acknowledged that the temperature and exposure time in the above-quoted studies were different than in ours and, therefore, the results may not be directly comparable. Nevertheless, these studies provide evidence that disassembly and reassembly of capsid proteins may take place until a certain "threshold" temperature is reached, which makes the disassembly of coat proteins irreversible.

From the practical perspective, it seems meaningful to define the "threshold" exposure temperature which inflicts irreparable damage to all viruses within the quantification limit of the test method. Figure 3.3 schematically demonstrates this "threshold" plotted against the thermal exposure time.

The left part of the scale represents short-term treatments, which typically take place in aerosol systems, while the right part features much longer thermal exposures occurring in liquid suspensions. In this figure, we plotted the actual experimental data obtained in the present study with aerosolized MS2 virions (red circles) as well as the data reported by Stonehouse and Stockley (1993) and Johnson *et al*. (2007) from their tests on the inactivation of MS2 bacteriophage in liquid (blue triangle and blue diamond).[2] For longer exposures, the threshold temperature corresponding to the virus irreparable damage is not expected to show an appreciable dependence on time.

[2] Straight lines in Fig. 3.3 are drawn through the data points and do not aim at representing specific linear trends.

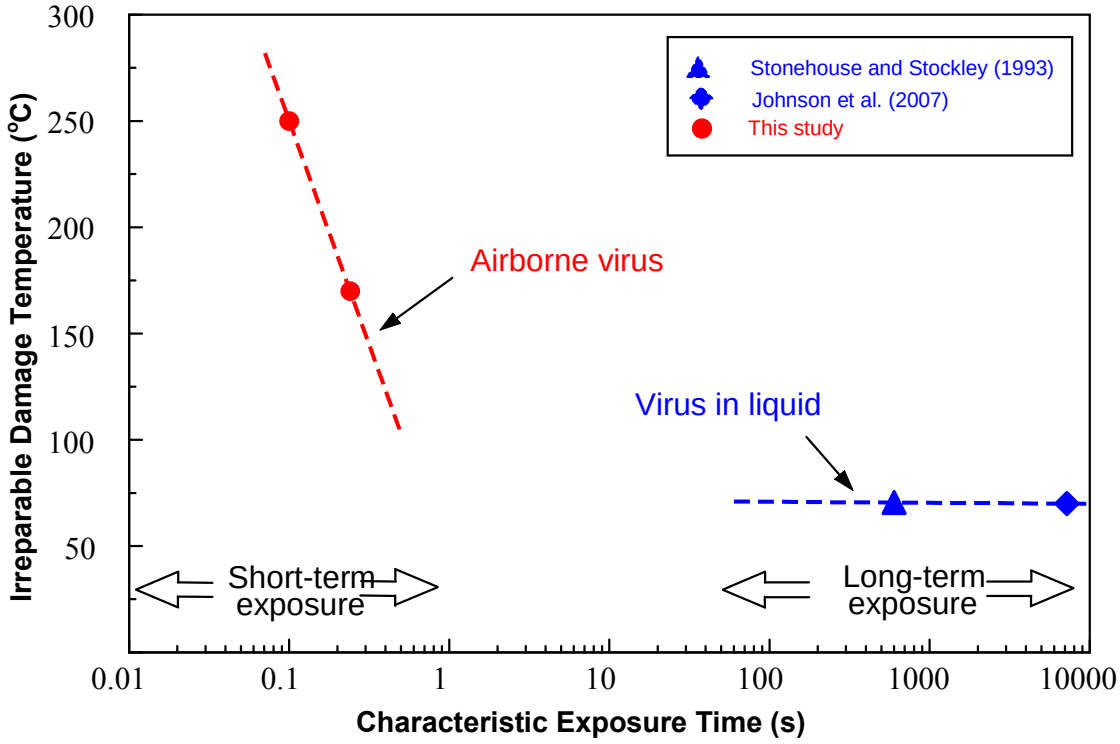

Figure 3.3. Effect of exposure time on the "threshold" exposure temperature corresponding to irreparable damage of all viruses within the quantification limits of the test protocols.

In contrast, manifestation of the temperature-time dependence is anticipated when virions are exposed to heat over sub-second time intervals, which is sufficient for adopting the surrounding air temperature but may fall short of providing sufficient time for the expected lethal response. Thus, the airborne virions exposed to hot air for less than one second may survive much higher temperatures than those suspended in hot liquid media for minutes or hours. In addition, the data points representing viruses in liquid may signify individual dispersed MS2 virions. In contrast, the MS2 aerosols generated by the Collison nebulizer are likely contained aggregates and/or particles covered by residue from the nebulization suspension (Eninger *et al*., 2009; Hogan *et al*., 2005; Riemenschneider *et al*., 2010). These factors, in principle, can enhance resistance of aerosolized viruses to environmental stress, including heat. Consequently, irreparable damage may occur at higher temperatures.

Conclusions

A short-term (~10^{-1} – 10^{0} s) thermal inactivation of aerosolized MS2 virions began at a certain level of heat exposure and continued gradually as T_e increased from ~90°C to ~160°C (for Q=18 L min^{-1}) or ~140°C to ~230°C (for Q=36 L min^{-1}) exhibiting an exponential pattern. Longer thermal exposure produced greater inactivation. Under certain conditions (T_e ~170°C for Q=18 L min^{-1} and ~250°C for Q=36 L min^{-1}), the experimentally determined *IF*-values exceeded ~2.4×10^{4}, indicating that over 99.996% of viable virions lost their infectivity – the maximum fraction quantifiable by this study protocol. The reported *IF* represents the lower (i.e., conservative) approximation of the actual inactivation. It was found that airborne MS2 virions exposed to hot air for sub-second time intervals may survive much higher temperatures than those subjected to thermal treatment in liquid suspensions for minutes or hours. We postulate that the findings may be attributed to effects such as denaturation of coat proteins and protein A, mutation, and strand breaks, or their combination. Further studies are necessary to identify the mechanisms of inactivation.

Supplemental Information

Based on the first order kinetic reaction model (Hiatt 1964), the virus infectivity decay from N_0 (PFU m^{-3}) to N (PFU m^{-3}) cover time t can be described as

$$N = N_0 e^{-kt} \tag{3.4}$$

Where

$$k = k(T_e, E_a) \tag{3.5}$$

E_a is the inactivation energy that indicates the extent of the inactivation dependence on the virion exposure temperature (T_e) at a given set of conditions, including the species-specific stress-resistance characteristics, relative humidity, and other factors. Accordingly

$$IF = \frac{N_0}{N} = e^{kt_e} \tag{3.6}$$

Thus, for two tests, in which identical aerosolized virions were exposed to dry heat during time intervals of t_{e1} and t_{e2} , the inactivation factors can be expressed as

$$IF_{e1} = e^{k_1 t_{e1}} \tag{3.7}$$

$$IF_{e2} = e^{k_2 t_{e2}} \tag{3.8}$$

respectively, i.e.,

$$\frac{IF_{e2}}{IF_{e1}} = e^{k_2 t_{e2} - k_1 t_{e1}} \tag{3.9}$$

Assuming in the first approximation, that kinetics of inactivation is the same in the two tests, equation (9) yields

$$\frac{IF_{e2}}{IF_{e1}} = e^{k(t_{e2} - t_{e1})} \tag{3.10}$$

If the two tests differ solely by the air flow rate through the chamber, specifically $Q_1=2Q_2$ (i.e., 36 L min^{-1} vs. 18 L min^{-1} representing the experimental conditions of this study), then

$$t_{e2} = 2t_{e1} \tag{3.11}$$

and

$$\frac{IF_{e2}}{IF_{e1}} = e^{kt_{e1}} = IF_{e1} \tag{3.12}$$

from which we derive a quadratic relationship:

$$IF_{e2} = IF_{e1}^2 \tag{3.13}$$

The second (more realistic) approximation accounting for cumulative thermal exposure suggests that

$$k_2(T_e, E_{a2}) > k_1(T_e, E_{a1}) \tag{3.14}$$

which translates into

$$IF_{e2} > IF_{e1}^2 \tag{3.15}$$

The difference is expected to amplify as T_e rises. Thus, a relatively modest increase in the exposure time may cause a very sizable increase in inactivation of airborne virions that was indeed observed in our tests. For instance, at $T_e \sim 150°C$, IF was ~5 at Q=36 L min^{-1} and ~10^3 at Q=18 L min^{-1}, which suggests a stronger than square relationship.

Chapter 4. Association between increased DNA mutational frequency and thermal inactivation of aerosolized *Bacillus* spores exposed to dry heat

Paper published: Johansson, E., Adhikari, A., Reponen, T., Yermakov, M., and Grinshpun, S.A. (2011) Association between Increased DNA Mutational Frequency and Thermal Inactivation of Aerosolized *Bacillus* Spores Exposed to Dry Heat, *Aerosol Science and Technology*, 45:376-381.

Introduction

Inactivation (neutralization) of viable bioaerosol particles has several potential applications. For instance, effective destruction of aerosolized biological agents (primarily bacterial spores) over a relatively short time is a prominent part of defense research programs in the US (Henderson, 2004; Hitchcock *et al*., 2006; Koch, 2006) and abroad (Tan *et al*., 2006; Nadasi *et al*., 2007). If a bio-agent aerosolized from a bio-weapon facility in an explosion or fire remains pathogenic, it can contaminate large areas, thus posing a major threat (Nelson, 2004). Inactivation of viable airborne microorganisms has also been explored in applications related to indoor air quality control. Methods such as germicidal ultraviolet (UV) radiation, ion emission, and thermal treatment have been studied with respect to their biocidal effects against bacterial spores (Luna *et al*. 2008; Lin and Li (2002); Jung *et al*. 2009b; Grinshpun *et al*. 2005, 2007, 2010a).

Bacterial spores are among the hardiest microorganisms on earth, and dormant spores can remain viable under unfavorable environmental conditions for extremely long periods of time. The factors causing this resistance include a very thick spore coat surrounding the outer spore membrane, low core water content, high core mineral content, and a group of DNA-stabilizing proteins called α/β-type small acid soluble spore proteins (SASPs) (Nicholson *et al*. 2000). Most of what is known about the factors that determine the remarkable stability of bacterial spores and the mechanisms involved in their inactivation come from studies utilizing *Bacillus* species as model organisms, with *Bacillus subtilis*

being the most commonly used because it is readily manipulated genetically (Setlow 2006). Spores can be inactivated by various stress-inducing factors, including wet and dry heat, UV radiation, γ-radiation, alkylating agents, oxidizing agents, acids, and extreme desiccation. DNA damage of various kinds has been shown to be a major cause of the spore inactivation by most of these factors (Setlow 2006; Roth *et al*. 2009). Conversely, DNA-stabilizing α/β-type SASPs have a key role in spore resistance, and although wet heat appear to inactivate wild-type spores by a DNA-independent mechanism, $\alpha^{-}\beta^{-}$ spores, which lack α/β-type SASPs, are significantly more sensitive to wet heat treatment and appear to be killed in part by DNA damage (Fairhead *et al*. 1993). Previous studies have demonstrated that dry heat treatment of lyophilized (non-aerosolized) spores at temperatures <155°C for time periods from five minutes to several hours is associated with increases in mutational frequency (Zamenhof 1960; Northrop and Slepecky 1967; Setlow and Setlow 1995; del Carmen Huesca Espitia *et al*. 2002). A recent interesting study by Jung *et al*. (2009b) addressed cellular processes that may potentially be involved in a short-term thermal inactivation of vegetative cells of *airborne* bacteria. To our knowledge, no previous studies have identified the mechanism(s) of inactivation of *aerosolized bacterial spores* exposed to dry heat.

In the frameworks of this grant, we has studied the short-term (sub-second) thermal inactivation of aerosolized *Bacillus* endospores in a controlled heated air flow at characteristic exposure temperatures ranging approximately from 150°C and 400°C (Grinshpun *et al*. 2010a). The conditions (in terms of air temperature and exposure time) causing effective heat-induced inactivation, were determined experimentally by quantifying the spore culturability loss. It was found that the thermal exposure produced no effect or only a moderate inactivation when the characteristic exposure temperature remained below ~200°C for a tested air flow rate of 18 $Lmin^{-1}$ and ~250°C for 36 L min^{-1}; however, inactivation rapidly increased with the exposure temperature once the above values were exceeded. Although some speculations about causative mechanisms of the inactivation of airborne spores were shared in that paper as a part of data interpretation, the investigation of these mechanisms was beyond the scope of the quoted study.

We hypothesized that the thermal inactivation of aerosolized *Bacillus* endospores exposed to dry heat over sub-second time intervals is associated with DNA mutation damage. The present investigation was initiated to test this hypothesis under experimental conditions when significant inactivation emerges from increase of air temperature. The relative mutational frequency, which served as a quantitative measure of the mutational damage, was determined by culturing exposed spores on Trypticase Soy agar (TSA), as well as on TSA containing the antibiotic nalidixic acid. The latter allowed detecting mutations producing nalidixic acid resistance. To our knowledge, this is the first study focused on the mechanism governing inactivation of *aerosolized* bacterial spores exposed to dry heat.

Materials and methods

Challenge bioaerosol

B. atrophaeus (also known as *B. subtilis* var. *niger* and *B. globigii* [BG]) was chosen as the challenge microorganism for this study because it is well-characterized and has been extensively used as a stimulant of biological warfare agents, including *B. anthracis* (Johnson *et al*. 1994; Franz *et al*. 1997; Hill *et al*. 1999; Helfinstine *et al*. 2005; Luna *et al*. 2008). As a genus-level representative, *B. atrophaeus* has been utilized to evaluate inactivation techniques such as UV radiation (Shafaat and Ponce 2006), plasma sterilization (Muranyi *et al*. 2007) and thermal sterilization (Kempf *et al*. 2008). *B. atropheus* is not identical with, but closely related to *B. subtilis*.

B. atrophaeus endospores were aerosolized from liquid suspension using a six-jet Collison nebulizer (BGI Inc., Waltham, MA, USA). For the preparation of the aqueous spore suspension, freeze-dried spores were suspended in sterile deionized water, vortexed to remove clumps, and centrifuged at approximately 6,300×g for 7 minutes. The spores were washed twice with sterile water by vortexing and centrifugation, and resuspended in sterile water to a concentration of approximately $(1 – 2)\times10^9$ colony forming units (CFU) per mL.

Spore concentrations were determined by making serial dilutions in sterile water and cultivating aliquots on TSA (BD, Franklin Lakes, NJ, USA) at 37°C for 24 hours.

Exposure of spores to dry heat

The experimental method and setup for exposing bioaerosol particles to a continuous heated air flow have been described in detail in Grinshpun *et al*. (2010a,b). Briefly, a cylindrical electric heating element (Mighty Watt Heater, Gordo Sales, Inc., Layton, UT, USA) installed along the axis of a cylindrical continuous-flow exposure chamber was operated at voltages ranging approximately from 50 to 200 V, producing different heating conditions in the chamber. The axial geometry was chosen because it is relevant to a simultaneously performed laboratory study on the bio-agent defeat during explosion and combustion. Also, the continuous flow design is considered feasible for the development of air purifiers utilizing thermal energy (Jung *et al*., 2009b). The air temperature profiles inside the chamber were determined for each set temperature and air flow rate using thermocouple probes (Type J, Model 5J36-ICIN-116, Omega Engineering, Inc., Stamford, CT, USA). The characteristic exposure temperature ($T_{exposure}$) was estimated based on the measured air temperature profiles and corrections made for heat radiation (Grinshpun *et al*. 2010a). The nebulizer-generated *B. atrophaeus* aerosol flow (6 L min^{-1}) was diluted with HEPA-filtered air at two flow rates of 12 and 30 L min^{-1} producing the total flows of Q=18 L min^{-1} and Q=36 L/min, respectively, which represented two different thermal flow regimes and exposure times, as explained below. The aerosol was passed through a 10-mCi 85Kr charge equilibrator (model 3012, TSI Inc., St. Paul, MN, USA) and then entered the exposure chamber. The setup was housed in a Class II biosafety cabinet (Model 6TX, Baker Co., Inc., Sanford, ME, USA).

The aerosol concentration and particle size distribution were measured in real time at the inlet and outlet of the exposure chamber using an optical particle size spectrometer (Model 1.108, Grimm Technologies, Inc., Douglasville, GA, USA). After exposure, the aerosol was sampled into three identical probes at 5 L min^{-1} and collected on three sterile 25-mm

filter cassettes (SKC Inc., Eighty Four, PA, USA) equipped with 25-mm polycarbonate filters (Millipore Corp., Billerica, MA) (pore size=0.4 μm). The sampling time was 10 min. In a control experiment, endospores were passed through the system with the heating element turned off, i.e. at room temperature ($T_{control}$). Immediately after collection, the filters were removed. Each filter was submerged in 1 mL sterile de-ionized water and vortexed for 2 min to extract the spores. Cultivation of surviving spores was carried out as described below.

Sample analysis for quantifying the spore inactivation

Fifty μL of the spore suspension obtained after exposure was serially diluted with sterile water and 100-μL aliquots were spread on TSA. Cultures were incubated 24 h at 37°C, after which colonies were enumerated to obtain CFU_{TSA}. An average CFU value was determined from three separate counts on three replicate agar plates.

The culturable counts were compared for each test-control combination to determine the loss in spore culturability as a result of a specific thermal exposure. The loss in culturability served as a surrogate for the viability loss. Although culturable count may be lower than the viable count, culturability is widely used as a measure of viability, which is relevant to pathogenic species given that their hazard level is usually associated with the ability to multiply. Thus, the inactivation factor, *IF*, was defined as the control-to-test ratio of culturable spores, as described in Chapters 1-2:

$$IF = \frac{CFU_{TSA}(T_{control})}{CFU_{TSA}(T_{exposure})} \tag{4.1}$$

Experimentally determined inactivation factors calculated by Eq. (4.1) were corrected by multiplying by 0.667 to account for temperature profiles in the axially heated air flow This

correction, introduced in Grinshpun *et al*. (2010a), reflects the fraction of the annular flow cross-section (50% pre-wall by the axial flow dimension), for which the characteristic exposure temperature was designated. The corrected *IF*-values serve as the lower approximation of the actual inactivation (Grinshpun *et al*., 2010a).

Sample analysis for quantification of DNA mutational damage

The remaining spore suspension from each filter was centrifuged for 2 min at 5,200×g and resuspended in 100 µL of sterile water. Mutational damage in *Bacillus* endospores results in nalidixic acid-resistance (nal^r) in a portion of exposed cells through specific mutations in the *GyrA* gene (Munakata *et al*. 1994; del Carmen Huesca Espitia *et al*. 2002). To quantify mutational damage we used an assay that involves the detection of resistant colonies formed on solid medium containing the antibiotic nalidixic acid (del Carmen Huesca Espitia *et al*. 2002). The frequency of nal^r mutations in the spore is assumed to be proportional to the total number of mutations in the genome. Although most mutations are unlikely to completely inactivate the spore, any mutation that causes the loss of expression or function of an essential gene product will lead to loss of viability.

To determine the frequency of mutations producing nal^r, the resuspended endospores were spread on TSA containing 20 µg nalidixic acid (Sigma-Aldrich, St. Louis, MO, USA) per liter. Only spores that carry nal^r-inducing mutations are able to form colonies on this medium. Because the number of mutant spores in these experiments was always low, the entire aliquot from each filter was spread on one plate to increase the limit of detection. After incubation at 37°C for 48 h, nal^r colonies (CFU_{nal^r}) were enumerated. The mutational frequency (MF) for each filter was obtained by relating the colony counts on TSA without nalidixic acid and TSA containing nalidixic acid:

$$MF = \frac{CFU_{nal^r}}{CFU_{TSA}} \tag{4.2}$$

For each characteristic exposure temperature, we related the MF-values obtained for spores exposed and non-exposed (control) to heat. This was quantified by the mutational frequency ratio (*MFR*) defined as:

$$MFR = \frac{MF(T_{exposure})}{MF(T_{control})} \tag{4.3}$$

Experimental conditions

In accordance with the hypothesis of this study, the test conditions were chosen to examine the relationship between DNA mutational damage and heat-induced inactivation of endospores. The test temperatures were selected to cover the range in which *IF* rapidly changes from 1 (no effect) to ~10^2. We anticipated that the endospore inactivation of higher levels (several $\log_{10}$ reduction) may become too complex to be described by a single mechanism or a simple kinetics relationship. Ababouch *et al*. (1995) suggested that multiple mechanisms may be involved in injury and repair of *B. subtilis* spores and that spores may become more resistant during heating at relatively high levels. Based on our previous findings, the chosen *IF*-range (1–100) corresponds to the following ranges of the estimated characteristic exposure temperature: $T_{exposure}$ ~ 160°C to 240°C for Q=18 L min^{-1} and $T_{exposure}$ ~ 190°C to 300°C for Q=36 L min^{-1} (Grinshpun *et al*., 2010a). These ranges translate to the following chamber wall temperatures, which served in the experiments as the set conditions: 150°C–225°C for 18 L min^{-1} and 200°C–325°C for 36 L min^{-1}. The above-referred estimate of the characteristic exposure temperature was made with an uncertainty of 21°C to 26°C, depending on Q and $T_{exposure}$.

Although the time of heat exposure was not clearly defined by this study design because the spores were exposed to different temperatures while moving in the flow, the characteristic exposure time was always below 1 s. For example, based on our earlier estimates

(Grinshpun *et al*. 2010a,b), it is approximately 0.24 s at Q=18 L min^{-1} and $T_{exposure}$=170°C and approximately 0.10 s at Q=36 L min^{-1} and $T_{exposure}$=250°C.

It should be noted that this study targeted temperatures in excess of those used in previous investigations addressing the spore inactivation mechanism (e.g., 155°C in Setlow and Setlow 1995). At the same time, we used much shorter duration for the thermal exposure than the quoted research.

Statistical methods

For each test temperature, the average values and the standard deviations of *IF* and *MFR* were calculated for 3-8 filter samples, each of which generated three replica plate counts. A One Way Analysis of Variance (ANOVA) was used to test the differences in *IF* and *MFR* at different $T_{exposure}$. The Pearson product moment correlation analysis was applied to test the relationship between the spore thermal inactivation and the DNA mutational frequency. The linear regression analysis was used to relate the natural logarithm of *IF* to *MFR*.

Results and discussion

Following a 10-min nebulization period, a stable concentration of the challenge aerosol was achieved upstream and downstream of the exposure chamber. The optical particle size distribution exhibited a peak at 0.7 – 0.8 μm, which corresponds to intact *B. atrophaeus* endospores (An *et al*. 2004). The distribution remained the same at both air flow rates tested in this study. Furthermore, axial heating did not affect the size distribution of the test aerosol (within the tested temperature range). These findings suggest that (i) the physical characteristics of the challenge bioaerosol used in this study were consistent in all the tests, (ii) the particle losses in the system were negligible, and (iii) the challenge aerosol is represented primarily by single spores. Testing with single spores (as opposite to spore agglomerates) is advantageous because it eliminates undesirable effects such as shielding and uneven heat transfer to the spore, which can potentially complicate the data interpretation.

Table 4.1 presents *IF* and *MFR* as functions of $T_{exposure}$ for each of the tested flow rates. As expected, increase in the characteristic exposure temperature resulted in increase in *IF*. For both flow rates, the *IF* data agreed with the results reported in Grinshpun *et al*. (2010a). The more important finding was that *MFR* also increased with increase of the temperature.

Table 4.1. The inactivation factor (*IF*, corrected) and the mutational frequency ratio (*MFR*) for aerosolized *Bacillus subtilis* var. *niger* endospores exposed to dry heat at different characteristic exposure temperatures and air flow rates. Each value represents an average or standard deviation (SD) of n=3–7 filter samples, each of which generally generated three replica plate counts.

Flow rate, L min^{-1}	$T_{exposure}$, ^{o}C	Uncertainty in estimating $T_{exposure}$, ^{o}C	*IF*		*MFR*	
			Average	SD	Average	SD
18	164	25	1.07	0.20	3.60	0.89
	188	26	2.15	0.35	8.59	0.63
	212	26	10.8	6.53	20.7	11.3
36	191	18	1.69	0.60	2.50	0.72
	228	20	3.72	1.75	7.91	2.90
	255	21	13.0	6.57	22.2	8.65
	277	22	86.0	24.9	33.0	2.71

For example, at Q=18 L min^{-1}, the average *MFR* increased from approximately 3.6 at $T_{exposure}$ ~ 164°C to 20.7 at $T_{exposure}$ ~ 212°C. At Q=36 L min^{-1}, it increased from 2.5 at $T_{exposure}$ ~ 191°C to 33 at $T_{exposure}$ ~ 277°C. Thus, differences in each of the two outcomes – the loss of spore viability (represented by *IF*) and the change in frequency of DNA mutation (represented by *MFR*) – were associated with the differences in exposure temperature (ANOVA, $p < 0.001$).

In a single mechanism model, the inactivation should follow the first-order kinetics, i.e.

$$IF \propto e^{kE_a} \tag{4.4}$$

where E_a is the activation energy. Previous investigators who tested UV and heavy ion radiation of *Bacillus* spores reported a linear relationship between mutational frequency and radiation dose (Tanooka *et al*. 1978; Baltschukat and Horneck 1991). It seems reasonable to assume the same type of linear relationship for mutations caused by other types of energy transfer. Consequently, if mutational damage is the main cause of spore inactivation, *IF* must be described by an exponential function of *MFR*:

$$IF \propto e^{k_1 MFR} \tag{4.5}$$

Here k and k_1 are proportionality constants, which are generally dependent of the exposure time and other parameters. Eq. (4.5) yields a linear relationship between ln*(IF)* and *MFR*.

To quantitatively characterize the relationship between the *IF* and *MFR* experimentally obtained for the same heat exposure, their measures were plotted against each other as

$$\ln(IF) = f(MFR) \tag{4.6}$$

and tested for linearity. When the data points obtained in the study were averaged [as ln(*IF*) and MFR for $T_{exposure}$=const, Q=18 and 36 L min^{-1}] and subjected to a linear regression analysis, the calculated R^2 value was as high as 0.951 ($p<0.001$), see Fig. 4.1.

The Pearson product moment correlation analysis indicates that the spore thermal inactivation in these tests can be attributed almost entirely to increased mutational frequency, at least for *IF* below ~10^2. It is anticipated that a single (or dominant) mechanism may govern the spore inactivation process up to a certain level; at higher levels, more mechanisms or more complex kinetics may be involved.

Higher inactivation levels corresponds to greater E_a values which may affect the kinetics of the process, e.g., by suppressing linearity of $MFR=f(E_a)$. More research is needed to quantify the boundaries of the first-order kinetics and potentially develop a predictive model for the process.

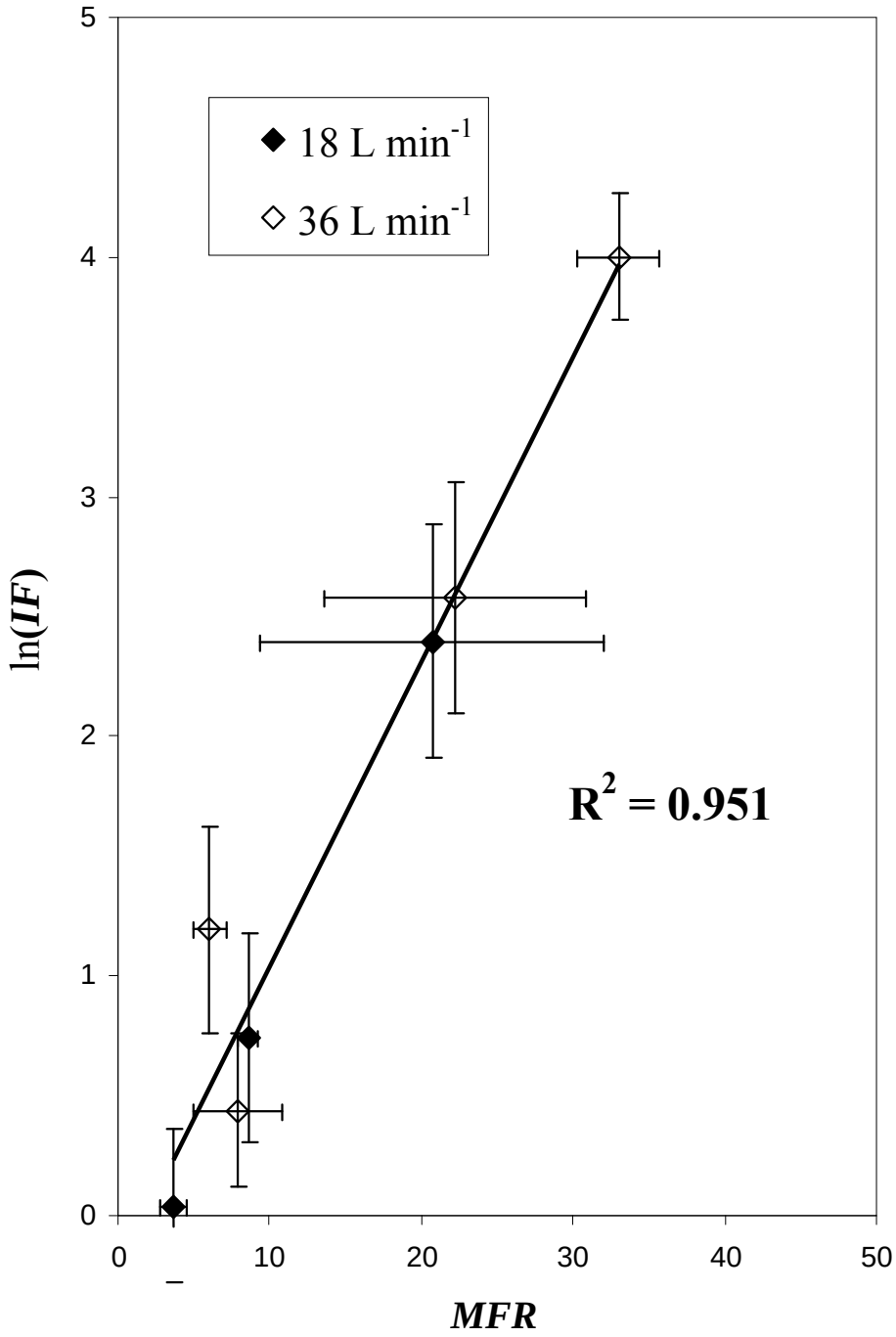

Figure 4.1. Relationship between the inactivation factor (*IF*, corrected) and the mutational frequency ratio (*MFR*) for aerosolized *Bacillus subtilis* var. *niger* endospores exposed to dry heat. Each data point represents an average value for n=3–7 filter samples, each of which generally generated three replica plate counts. Each bar represents the standard deviation. The line represents the linear regression.

It is notable that the relationships obtained at two different flow rates (corresponding to different exposure times) were essentially identical. The strong correlation between inactivation and mutational frequency suggests that mutational damage is causally linked to viability loss for aerosolized endospores exposed to dry heat for sub-second time periods. It does not, however, prove direct causality. The precise mechanism by which dry heat causes mutations, or the nature of the lesions, will be explored in a follow-up study.

Cell death may occur as a direct result of mutations in, and inactivation of, essential genes, or it may be caused by failure to repair DNA lesions during germination. Loss of, or disrupted binding by, SASPs would also be expected to increase the sensitivity of DNA to mutational damage Previous studies have indicated that dry heat generates abasic sites in DNA at least in part through depurination, which SASPs protects against, and $\alpha^{-}\beta^{-}$ spores are less resistant to dry heat than wildtype spores (Setlow and Setlow, 1995). A recent study by Barraza-Salas *et al*. (2010) showed that over-expression of the endogenous endonuclease Nfo enzyme, which repairs apurinic-apyridinic DNA damage, accumulated in dormant or germinating spores, increases the resistance of *Bacillus* spores to dry heat. Interestingly, the protective effect was much smaller in wildtype spores than in spores lacking SASPs suggesting that the efficiency with which SASPs protects DNA against apurinic damage makes repair enzymes such as Nfo in part dispensable. Although associations between dry heat inactivation of *Bacillus* spores and mutational damage have been reported earlier (Setlow and Setlow, 1995; del Carmen Huesca Espitia *et al*., 2002) these studies addressed a different type of exposure situation: much longer exposure periods (up to several hours) and lower temperatures (90°C–155°C). Furthermore, previous studies made use of lyophilized spores on solid support sealed under vacuum, whereas we investigated *aerosolized* spores. Given the differences in heat transfer for aerosolized and non-aerosolized spores exposed to heat, the similarity in mechanisms governing their inactivation is remarkable.

The present investigation has limitations. One comes from a less than straight-forward definition of the characteristic exposure temperature, which attempts to integrate the non-uniformities of air temperature produced by the continuous flow design, but causes uncertainties leading to fairly large coefficients of variation for *IF* and *MFR*. The same constraints of the continuous flow design limited our ability to quantify the time of exposure to a specific temperature in a more definitive way as compared to the approximation offered in this study.

Conclusion

A significant association was established between short-term thermal inactivation of aerosolized endospores of *B. atrophaeus* and the spore DNA mutation. Both the inactivation factor and the mutational frequency ratio increased as the exposure temperature increased. The strong correlation between *IF* and *MFR* appeared to be independent of the flow rate in the test system, which is linked to the exposure time (sub-second time periods were tested). The experimental findings are in agreement with the first-order kinetics of the inactivation process up to the inactivation factor of 100. Although similar associations have been reported for non-aerosol applications, long-term exposures and moderate heating temperature, this study is the first one providing strong evidence that short-term heat-induced inactivation of *aerosolized* endospores is causally associated with DNA mutational damage. Other mechanisms, e.g. associated with protein changes, should be investigated in future studies.

Chapter 5. Mechanically alloyed Al-I composite materials

Paper published: Zhang S., Schoenitz, M., and Dreizin, E.L. (2010) Mechanically Alloyed Al–I Composite Materials. *Journal of Physics and Chemistry of Solids*, 71: 1213-1220.

Introduction

In recent decades, mechanical alloying was used to prepare a wide variety of unique compounds for multiple applications (Suryanarayana, 2001, 2008). One type of potential application for mechanically alloyed materials includes the use as metallic fuel additives for propellants, explosives, and pyrotechnics (Schoenitz and Dreizin, 2003, 2004, 2006; Shoshin *et al*., 2006; Zhu *et al*., 2006; Chen *et al*., 2006; Zhu *et al*., 2007). Such materials are being developed to tailor the rates of energy release from the burning metal and thus improve performance of various energetic formulations. In applications for explosives designed to defeat stockpiles of chemical and biological weapons, it is desirable that in addition to the generated temperature and pressure pulses, biocidal combustion products are released. It is further desired to combine the capability to produce biocidal compounds with an optimized combustion behavior. Halogens are well known to form a variety of biocidal species. However, from the point of view of energetic ingredients, halogens form either stable ionic compounds limiting the energy available for combustion, or compounds that are relatively unstable, hard to handle, and subject to rapid aging. Therefore, directly adding halogens to energetic formulations appears to be impractical. Instead, metal-based composites containing elemental (or loosely bound) halogens stabilized at room temperature are of interest. Such fuels are expected to increase the volumetric reaction enthalpy of energetic formulations, as do conventional metal fuel additives; they also will help producing biocidal combustion products upon ignition. This paper presents an effort to develop such a fuel additive based on aluminum, the most widely used metal additive to all types of energetic formulations. In this work, it is proposed that stabilized Al-halogen composites can be prepared by mechanical alloying, so that biocidal halogenated combustion products are released upon combustion. Iodine, which is solid at room

temperature and is more readily available and simpler to handle than other halogens, was selected for this effort.

The objective of this work was to prepare powder-like Al-I composites which can be easily handled at normal conditions. Such materials are expected to burn similar to unmodified aluminum and produce iodine-containing biocidal combustion products. The capability of such powders to capture and retain iodine until they are heated to high temperatures is of critical importance. In order to produce a material for which combustion and biocidal characteristics can be readily determined in laboratory experiments, it is desired to produce equiaxial particles in the size range of 10-100 μm. Particles that are much coarser, much finer, or flake-shaped could be of interest to practical applications, but are difficult to characterize using established laboratory ignition and combustion measurement techniques developed for micron-sized metal powders.

Material and methods

The Al-I composites were prepared by ball-milling elemental aluminum and iodine under various conditions. The initial mixture loaded into the ball mill was a blend of aluminum powder and iodine chips. Aluminum powder, -325 mesh size (< 45 μm), 99.5% pure was provided by Atlantic Equipment Engineers. Iodine chips, 99% pure, were provided by Sigma Aldrich. In one experiment, the starting mixture comprised aluminum powder mixed with a powder of aluminum iodide, 99.99+% (metals basis).

Ball milling equipment and parameters

Most of the samples were prepared using a model 01HD attritor mill by Union Process. The mill includes a stationary milling vial inside a cooling jacket. The balls are agitated by a rotating impeller. Two types of milling vial lids provided by Union Process were used: one designed for experiments in controlled gas environments, and the other, designed for milling in liquid nitrogen. In all experiments, the impeller rotation rate was set to 400 rpm. The main process variables were the milling environment inside the milling vial and the cooling

agent circulating through the cooling jacket surrounding the milling vial. Powders were loaded at room temperature in air; milling balls were added after the starting materials. Nitrogen was flushed through the charge to prevent oxidation during the milling process. Room temperature milling runs used running water in the cooling jacket and nitrogen gas fed through the milling vial at a flow rate of about 2 CFM (0.94 L s^{-1}). In initial experiments, the flow rate was not closely monitored, but it was noticed that a higher nitrogen flow rate results in a lower average amount of iodine retained in the mechanically alloyed powders. Cryogenic milling runs used two configurations, in both cases the cooling jacket was filled with liquid nitrogen. In one setup, gaseous nitrogen was continuously fed through the milling vial, and in the other, the milling vial was also filled with liquid nitrogen.

The total mass of milling balls was fixed at 1.8 kg. Different aluminum-to-iodine mass ratios were used to prepare materials with different compositions. Milling ball sizes and ball-to-powder mass ratios (BPR) were also varied. The bulk of the material was recovered after completion of a run lasting typically 6 hours. In addition, small samples of materials were recovered from the vial at intermediate milling times to observe the particle evolution. In one run, the milling time was extended to 24 hours. No process control agent was added to the material being milled. In one test, the product powder obtained by ball-milling under specified conditions was used as a starting material for the second ball-milling run.

Table 1 shows a summary of the milling conditions representing samples prepared in the attritor mill.

A shaker mill (SPEX Certiprep, 8000 series) was also used to prepare Al-I composites. In addition to using elemental Al and I as starting materials, in one shaker mill experiment, elemental Al was mixed with AlI_3 to obtain an equivalent Al/I=90/10 composition. In the shaker mill the milling vial is cooled by a flow of room temperature air. Milling time for all shaker mill runs was set to 10 hours. Powders were loaded in argon gas. Material compositions, ball sizes, and ball-to-powder mass ratios were varied, as shown in Table 5.2.

Table 5.1. Samples prepared in attritor mill.

Sample ID	Ball Size, inch	Mass load ratio (Al/I)	BPR	Milling time, h	Cooling agent	Milling environment
1-1	3/8	95/5	36	6	Liquid N_2	Gas N_2
1-2	3/8	90/10	36	6	Liquid N_2	Gas N_2
1-3	3/8	80/20	36	6	Liquid N_2	Gas N_2
2-1	3/8	95/5	36	6	Water	Gas N_2
2-2	3/8	90/10	36	6	Water	Gas N_2
2-3	3/8	80/20	36	6	Water	Gas N_2
2-4	3/8	90/10	36	24	Water	Gas N_2
3-1	3/16	95/5	18	6	Liquid N_2	Gas N_2
3-2	3/16	90/10	36	6	Water	Gas N_2
4-1	3/8	95/5	36	6	Liquid N_2	Liquid N_2
4-2	3/16	90/10	36	6	Liquid N_2	Liquid N_2
5-1*	3/16	90/10	36	3.5	Liquid N_2	Liquid N_2

*Note: sample 5-1 used sample 3-2 as a starting material;

Table 5.2. Samples prepared in shaker mill

Sample ID	Starting materials	Ball size, inch	Mass load ratio (Al/I)	BPR
s-1	Al, AlI_3	3/8	90/10	10
s-2	Al, I	3/8	90/10	10
s-3	Al, I	3/8	95/5	10
s-4	Al, I	3/16	95/5	5

Characterization of the Al-I composites

The powders were characterized using scanning electron microscopy (SEM). For SEM analyses, a Phenom Tabletop Microscope by FEI Technologies Inc. was employed. Back-scattered electrons were used to obtain images showing the phase contrast between the materials. X-ray diffraction (XRD) was used to determine phase composition for each

sample. The XRD was performed on a Philips X'pert MRD powder diffractometer operated at 45 kV and 40 mA using unfiltered Cu K_α radiation (λ=1.5438 Å). Scan angle was in the range of 10-70 degrees. Two sample holders were used for XRD measurements. The standard sample holder has 20 mm length, 15 mm width and 2 mm depth. It was used for samples available in relatively large quantities. When only small amounts of powders were available, as was the case for samples recovered from intermediate milling times, or for samples pre-heated to and cooled from a specific temperature, a smaller quartz sample holder was used with the diameter of the sample area of about 8 mm. Selected XRD traces were processed for the purpose of quantitative phase analysis by whole-pattern refinement using the GSAS software package (Larson and Von Dreele, 2004). The choice of sample holder influenced these results. The smaller quartz sample holder uses very small amounts of material, and therefore systematically underrepresents the diffracted intensities at lower diffraction angles. In most product samples AlI_3 was present, although only its main peaks at relatively low diffraction angles could be clearly distinguished. This caused the estimated concentration of AlI_3 to be systematically lower when the quartz sample holder was used compared to when the larger standard sample holder was used. The amount of iodine captured in the materials and its release upon heating were more directly determined from thermogravimetric (TG) traces. A TA Instruments model Q5000IR thermogravimetric analyzer was used in this project. Samples were loaded into an alumina crucible. The mass of material used in each test varied in the range of 5-35 mg. The balance and the furnace were purged with argon at 10 and 25 mL min^{-1}, respectively. The heating rate used for all experiments was set at 5 K/min and the maximum temperature was limited to 1000ºC (1273K).

Results

Particle shapes and dimensions

Characteristic SEM images of the materials prepared under different conditions are shown in Fig. 5.1. For 6-hour long milling runs, flake-like particles were formed under all milling conditions, except for the case when liquid nitrogen was used both inside the milling vial

and in the cooling jacket. In the latter case, the particles were roughly equiaxial. In addition, particles with equiaxial shapes were obtained in run 2-4, when milling time was increased to 24 hours. As illustrated in Fig. 5.1, cryomilling generally produced smaller particles than milling at room temperature. Images shown in Fig. 5.1 used backscattered electrons, and iodine-rich areas appear brighter. In Fig. 5.1A, at low magnification the scale of mixing between aluminum and iodine appears quite coarse. For samples appearing homogeneous, the scale of mixing is below the resolution of the images.

Particle sizes are observed to decrease with increasing iodine concentration. In general, particle sizes and shapes for powders prepared in the shaker mill were similar to those of powders prepared in the attritor mill at room temperature.

Iodine content and its release upon heating

For direct reference, mass reduction upon heating for both pure iodine and AlI_3 were characterized by TG; the results are shown in Fig. 5.2 where a TG trace for one of the mechanically alloyed samples is also shown. The pure iodine sample evaporates completely before it reaches 200°C. AlI_3 starts decomposing from room temperature, the decomposition rate increases at around 200°C when AlI_3 melts, and most of the decomposition ends before the sample reaches 400°C. The TG trace for the material mechanically alloyed in the shaker mill, sample s-3, shows a very small mass loss up until the temperature reaches about 440°C. The mass loss occurring at higher temperatures accelerates near the aluminum melting point. As discussed below, this behavior was generally observed for all mechanically alloyed samples, except for those milled in liquid nitrogen.

Sets of TG traces for the materials series 1 and 2 (see Table 5.1) are shown in Fig. 5.3. As expected, the overall mass loss at 1000ºC is greater for greater nominal iodine contents of the composite. This is true for both, samples milled at room temperature and at cryogenic temperature. Further, iodine release occurs in several steps, which are more or less clearly distinguished, depending on the sample.

For all samples the mass loss rate increases around 100 ºC, and decreases again by about 350ºC. Fig. 5.3 shows the mass loss for samples milled in N_2 gas. For samples milled in liquid N_2 the overall mass loss was substantially smaller. At temperatures between 100 and 350ºC, samples milled in liquid N_2 (samples 4-1 and 4-2 in Table 5.1) behaved similarly to the other materials. However, almost no mass loss was detected for those materials at higher temperatures. Therefore, the following discussion is focused on the materials milled in N_2 gas.

For both, cryomilled and room-temperature milled samples, for compositions with less than 10% of iodine, only minor mass loss is observed at temperatures between 100 and 350ºC. It is noticeable, however, that for this temperature range samples milled at room temperature (series 2) lose more mass than respective samples with nominally identical compositions milled at cryogenic temperature (series 1). Starting at about 400ºC, the second broad mass loss step continues up to the melting point of Al. A sharp mass loss step is associated with Al melting. It is followed by additional slight and gradual mass loss.

The pattern observed for the samples nominally containing 20% iodine is qualitatively different and primarily consists of two mass loss steps spread over broad temperature ranges.

The first step begins at about 100ºC, as for all other samples, but is much stronger than for samples with lower nominal iodine content. It is followed by a second gradual mass loss step beginning at about 400ºC. For the cryomilled sample, the first step ends at about 350ºC, while for the sample milled at room temperature, the first step effectively overlaps with the second one. This second step continues until the sample reaches the aluminum melting point, and it is apparent that nearly all iodine captured in the material is released by that time. Thus, only minor iodine release occurs upon Al melting, while a slow mass loss continues as the sample is heated to higher temperatures.

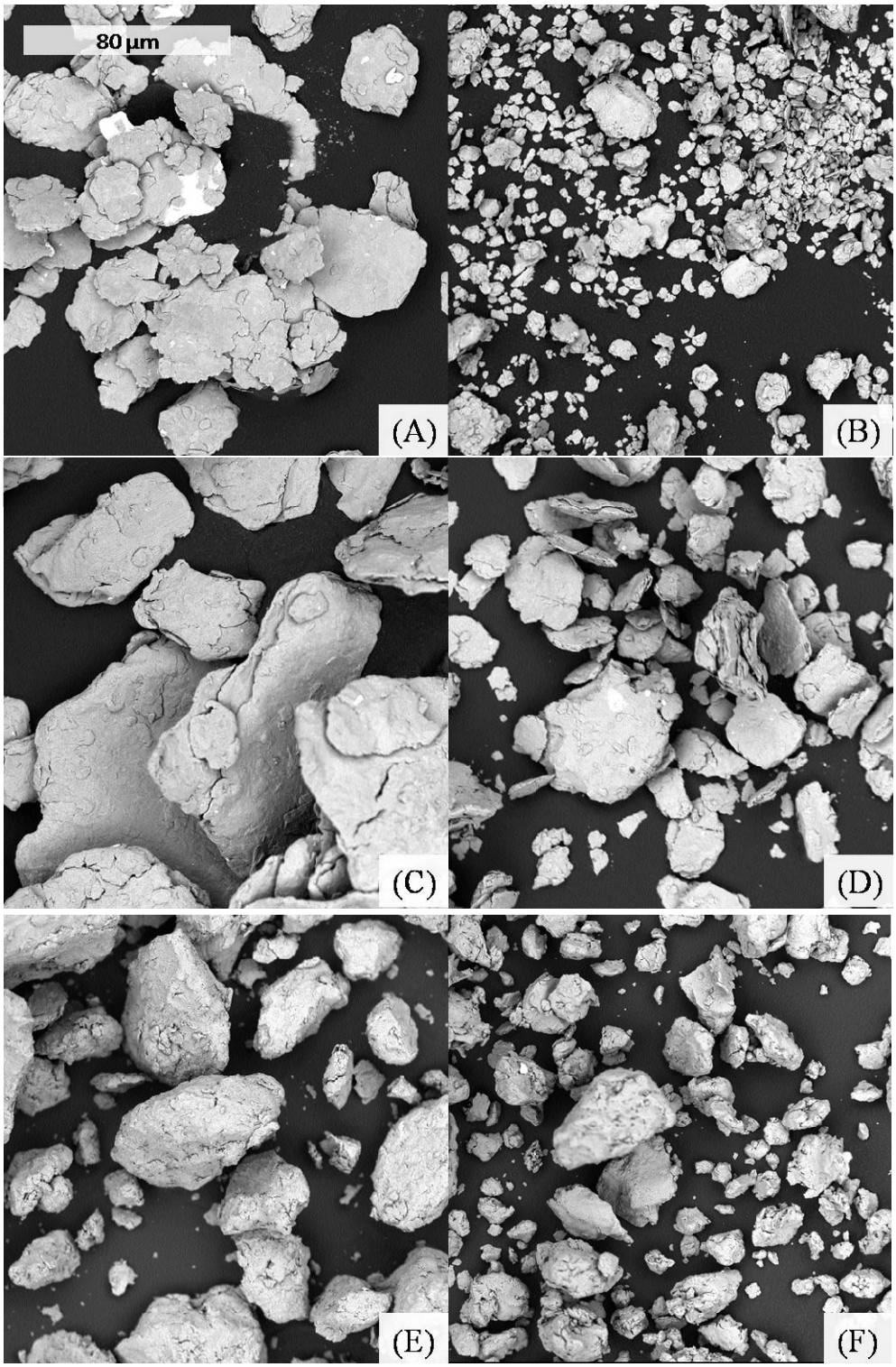

Fig. 5.1. SEM images of samples; magnification is the same for all images. Samples have nominal iodine concentrations of 5% on the left and 10 % on the right. Samples in the first row were cryomilled in N_2 gas, samples in the middle row were milled at room temperature in N_2 gas, and samples in the bottom row were cryomilled in liquid nitrogen. (A: 1-1, B: 1-2, C: 2-1, D: 2-2, E: 4-1, F: 4-2.)

TG traces for samples recovered at different milling times are shown in Fig. 5.4. For both, cryomilled and materials milled at room temperature the amount of iodine released at high temperatures increases with longer milling times. It is also noted that the total amount of iodine released upon heating to 1000ºC slowly decreases for longer milling times, indicating iodine loss during milling. This effect is stronger for material milled at room temperature.

Each of the two broad mass reduction steps between 100 and 350ºC and between 400ºC and the aluminum melting point consists of sub-steps, as is evident from the *dm/dT* signals. These sub-steps are better distinguished for the low-temperature (100–350ºC) mass loss for samples milled at room temperature, for which the mass loss at lower temperatures is greater. Conversely, for the cryomilled sample a more significant mass loss occurs between 400ºC and the aluminum melting point, and the respective mass loss sub-steps are distinguished better.

For all individual *dm/dT* peaks, except for the sharp peak associated with the aluminum melting, the peak positions shift to lower temperatures as the milling time increases. For the sample milled for 24 hours (not shown for brevity), the overall shape of the TG curve does not differ substantially from that shown in Fig. 5.4 for the sample milled for 6 hours. However, the strongest peak in the *dm/dT* trace shifts to higher temperatures, nearly coinciding with the sharp peak associated with aluminum melting.

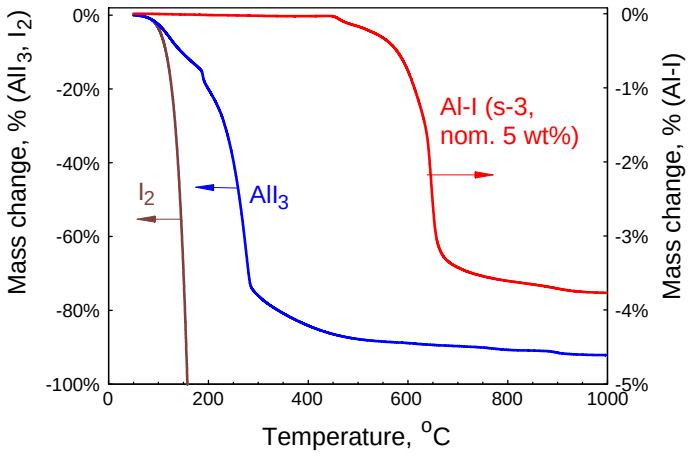

Fig. 5.2. TG decomposition traces of pure AlI_3, I_2 and sample s-3

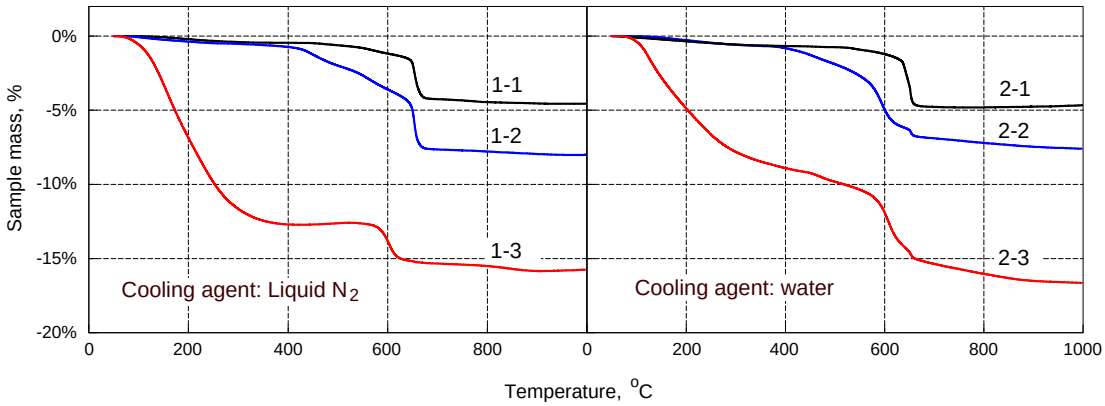

Fig. 5.3. TG traces of samples 1-1, 1-2, 1-3 and 2-1, 2-2 and 2-3

TG measurements were also performed for the samples prepared in the shaker mill. As illustrated in Fig. 5.2 (see also Fig. 5.5), these samples decomposed in a sequence of steps similar to that described above for the samples milled in the attritor mill with water used as a cooling agent.

The effect of the starting material is illustrated in Fig. 5.5. The shapes of the TG trace for material prepared from Al and I_2 is substantially the same as the trace for material prepared from Al and AlI_3 with the same nominal bulk composition.

This suggests that regardless of the starting material, the distribution of the bulk of the iodine within the Al matrix is only affected by the milling process. The most noticeable difference is a small but relatively sharp mass loss step around 280ºC for the sample prepared with AlI_3 as a starting material. This step-wise mass loss correlates well with the major mass loss step observed for pure AlI_3 as shown in Fig. 5.2. This step was never observed for mechanically alloyed samples prepared using elemental iodine. The onset of the main mass loss sequence in samples prepared from elemental iodine occurs at slightly higher temperatures. This may indicate the possibility that some AlI_3 remains unaltered under the milling conditions used here if AlI_3 is used as starting material.

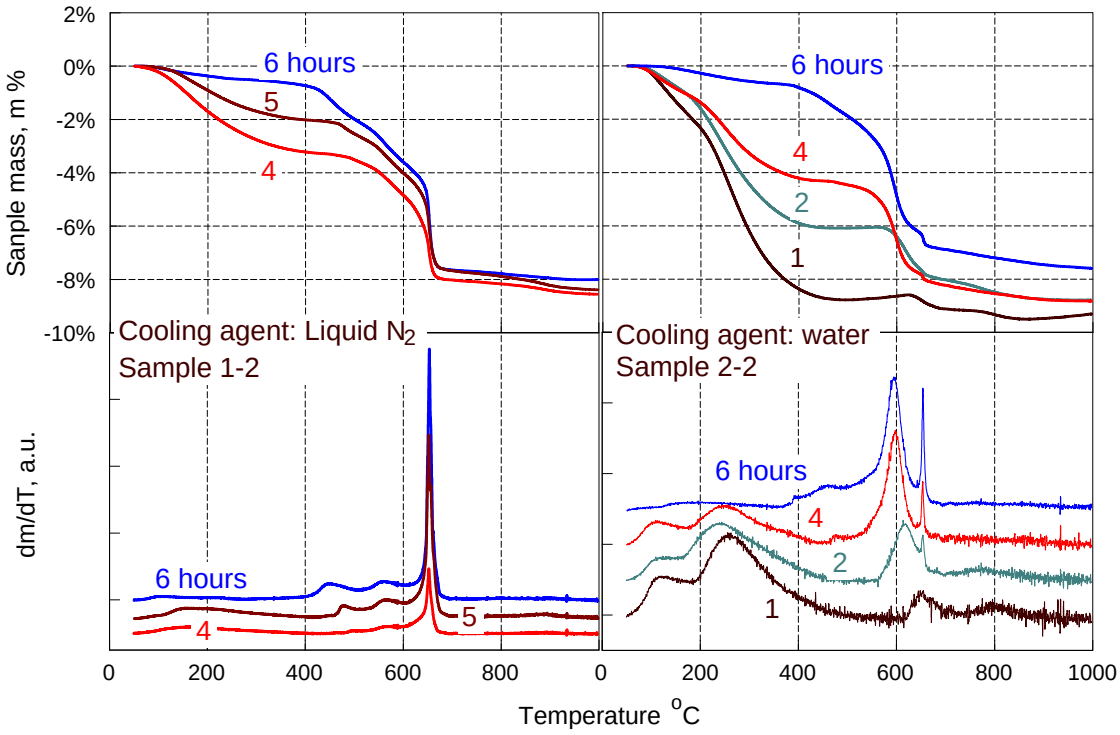

Fig. 5.4. TG traces and mass loss rates for samples recovered at different milling times.

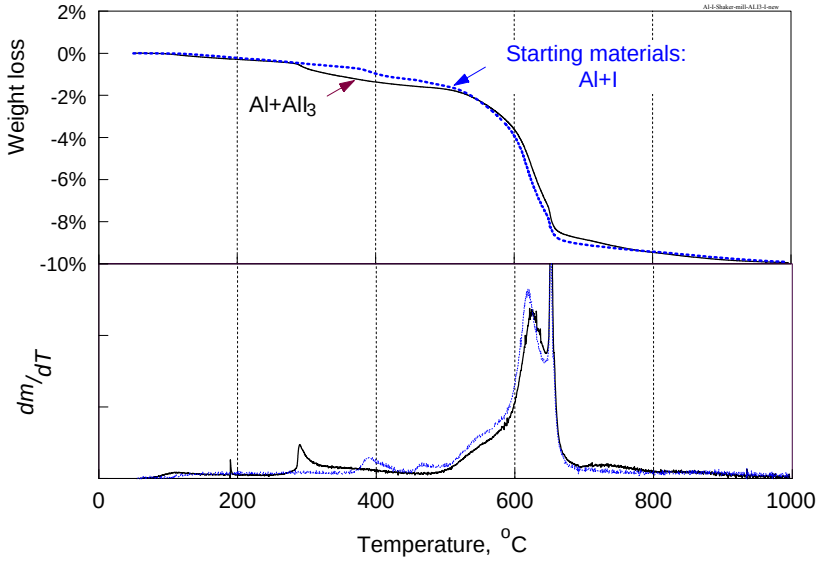

Fig. 5.5. TG traces and respective derivatives for samples s-1 (solid line) and s-2 (dashed line).

Material structure and composition

Characteristic XRD patterns collected for different samples with varying milling conditions are shown in Fig. 5.6. The peak pattern for Al and the strongest peak for AlI_3 (between 25 and 26º) were recognized for all samples. In some samples, additional AlI_3 peaks were identified. The peaks of AlI_3 are broad for most samples indicating that AlI_3 is not well crystallized. The strongest presence of AlI_3 occurs in the cryomilled sample 1-2. The XRD traces of series 1 and 2 show that cryomilled samples have sharper AlI_3 peaks, and thus a more ordered structure than the room temperature milled powders with the same nominal composition.

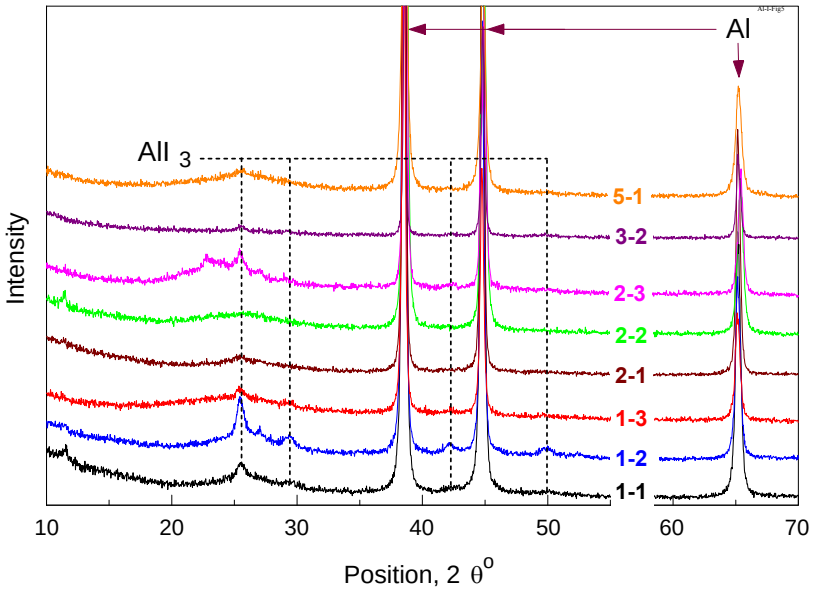

Fig. 5.6. XRD patterns for mechanically alloyed Al-I materials. A smaller quartz sample holder was used to characterize sample 3-2; other samples were placed into the standard sample holder.

Several peaks observed in the XRD patterns could not be identified. In particular, a peak around 27°C, most clearly observed for the samples 1-2 and 2-3 in Fig 5.5, was found in every pattern. It may not be clearly seen in some of the traces presented in Fig. 5.5; however, with whole pattern refinement (using GSAS (Larson and Von Dreele, 2004)) assuming the presence of Al and AlI_3, this peak was identified for all the patterns. Additional unrecognized peaks were observed in samples 1-2, 2-2 (at 11º) and 2-3 (at 23°).

Finally, XRD was used to examine samples heated to specific temperatures in the TG furnace. The patterns from sample 1-2 heated to and cooled from 400, 510, and 600 ºC, are shown in Fig. 5.7. The pattern for the as-prepared material, shown already in Fig. 5.6, is repeated in Fig. 5.7 for reference. The quartz sample holder was used to characterize the small batches of materials recovered after heating to intermediate temperatures. Upon heating, AlI_3 peaks become sharper but hardly decrease in intensity. The AlI_3 peaks remain clearly identifiable even for samples heated above the reported decomposition temperature of AlI_3 (~400ºC).

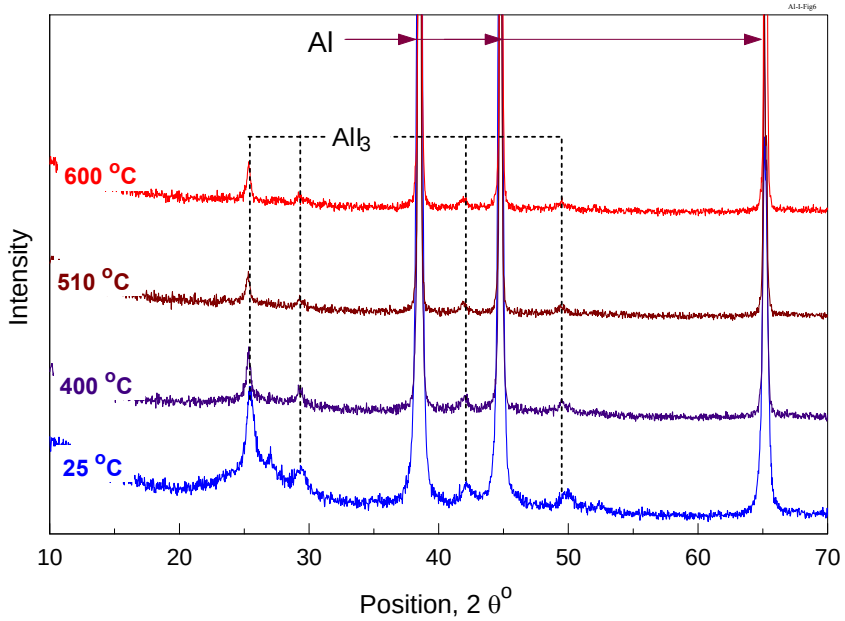

Fig. 5.7. XRD patterns of sample 1-2 heated to and cooled from different temperatures.

XRD results were analyzed by whole pattern refinement using the GSAS software package (Larson and Von Dreele, 2004). The measured patterns were fitted with calculated patterns assuming the composition to include only two components, Al and AlI_3.

Table 5.3 shows that substantial part of iodine incorporated into the mechanically alloyed materials, more than half for most samples, is not contained in the AlI_3 detectable by XRD. The relative amount of iodine unaccounted for by AlI_3 is smallest for the samples loaded with 10% of iodine.

Table 5.3. Iodine concentrations in the prepared materials estimated from TGA (I_{TG}) and from quantitative X-ray analysis (I_{AlI3}).

Sample ID	Wt. fraction of I loaded, I_0, %	Total TG mass loss, I_{TG}, %	XRD whole pattern processing: wt. fraction of I in AlI_3, I_{AlI3},%	Iodine balance (unaccounted for), $(I_{TG}-I_{AlI3},)/I_{TG}\cdot 100$ %
1-1	5	4.56	1.59	65.1
1-2	10	8.01	4.02	49.8
1-3	20	15.53	3.18	79.5
2-1	5	4.62	1.60	65.4
2-2	10	7.53	3.24	57.0
2-3	20	16.49	4.52	72.6
5-1	10	8.37	3.75	55.2

Quantitative X-ray analysis was also used to observe whether the iodine distribution within the sample changes upon heating. Respective results for sample 1-2 are shown in Table 5.4. For these measurements, the small sample holder was used consistently, and consequently the AlI_3 concentration shown for "as-prepared" material in Table 4 is lower than for the same material (1-2) shown in Table 5.3, for which the XRD data from the standard sample holder were used. Nevertheless, the results shown in Table 5.4 can be compared between themselves. The rate at which the overall weight loss is measured by TG exceeds slightly the relative rate of reduction in the AlI_3 concentration; respectively, the percentage of iodine that remains unaccounted for decreases slightly as the temperature to which the sample is heated increases. This is a somewhat unexpected result, considering that AlI_3 is reported to boil off at 382ºC (Gugelchuk, 2001) and is observed to decompose nearly completely by 400ºC in the TG measurements shown in Fig. 5.2.

Preparation of equiaxial powders with substantial iodine content

Examination of the samples prepared at different conditions showed that the most efficient particle size reduction and production of equiaxial particles occur when milling is performed with liquid nitrogen as a milling medium. However, based on the very low measured weight

loss in the TG experiments it was also observed that iodine is almost not retained in such powders. Therefore, additional experiments were performed in which material was initially prepared by room temperature milling and then size-reduced by milling in liquid nitrogen. Specifically, material 3-2 (see Table 5.1) was milled for 3.5 additional hours with liquid nitrogen in both the vial and cooling jacket (ID 5-1 in Table 5.1). Samples were recovered every 30 min from the mill, and substantial reduction of particle sizes and formation of equiaxial particles were observed after 3.5 hours, at which point the milling was stopped. The SEM images of samples 3-2 and 5-1 are shown in Fig. 5.8. Both, marked reduction in particle dimensions and change in the particle shapes are clearly observed. The TG traces for the prepared uniaxial powder (sample 5-1) and its parent material (sample 3-2) are shown in Fig.5.9. The traces are qualitatively similar; however, the overall iodine concentration retained in the material after milling in liquid nitrogen is reduced compared to the parent material. It is also noted that compared to the parent material, iodine release occurs at somewhat lower temperatures for the material milled in liquid nitrogen.

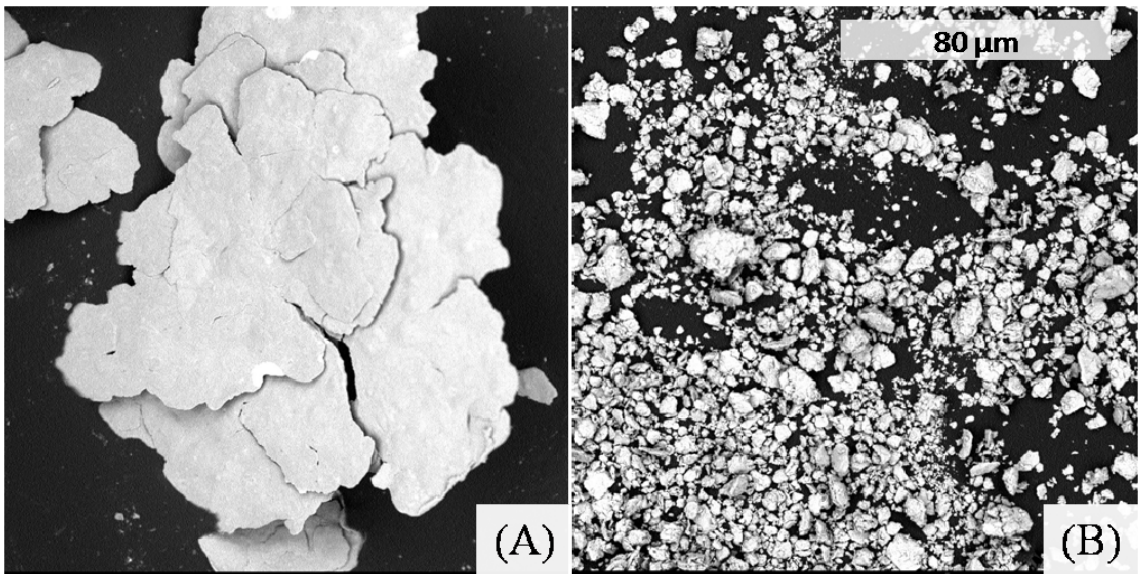

Fig. 5.8. SEM images comparison of sample 3-2 and sample 5-1; magnification is the same for both images. A: sample 3-2, B: sample 5-1.

Table 5.4. Iodine weight fractions estimated from TGA (I_{TG}) and from quantitative X-ray analysis (I_{AlI3}) for sample 1-2 quenched from elevated temperatures.

Temperature sample heated to, ºC	I_{TG}, wt %	I_{AlI3}, *wt %*	$(I_{TG}-I_{AlI3},)/I_{TG}\cdot 100$ %
As prepared	8.01	2.06	74.3
400	7.05	1.69	76.0
510	5.41	1.44	73.4
600	4.19	1.34	68.0

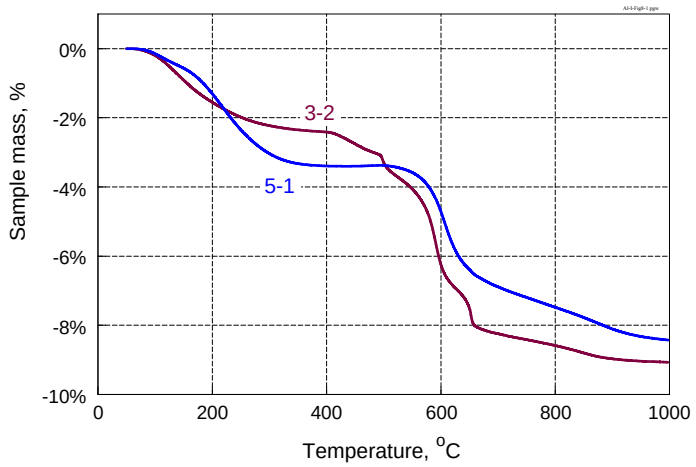

Fig. 5.9. TG traces of samples 3-2 and 5-1

Discussion

Synthesis of mechanically alloyed powders

Both, room temperature and cryogenic mechanical milling are suited to encapsulate iodine in aluminum. In both cases, iodine behaves as an effective milling process control agent resulting in flake-like particle shapes preserved for a relatively long time. Also, similar to the effect of conventional milling process control agents, an increase in the load of iodine results in a decrease in the product particle dimensions. The product particle sizes are also reduced by milling at liquid nitrogen temperature, presumably due to reduction in the

ductility of aluminum. Equiaxial particles are readily obtained by milling in liquid nitrogen as a milling medium; however, milling in liquid nitrogen results in a relatively rapid loss of iodine from the system. For milling in nitrogen gas, the loss of iodine is faster at higher nitrogen flow rate through the milling container. It is likely that the loss of iodine is directly correlated with the gas flow, which is substantially increased when the container is filled with boiling liquid nitrogen. When iodine loss is accelerated by a greater purging gas flow, its effect as a process control agent is also reduced, resulting in a more rapid formation of the mechanically alloyed composites between aluminum and the remaining iodine.

The difference in iodine release upon heating for the samples milled at different temperatures is relatively minor. At the same time, an improvement in stabilizing iodine in Al by cryogenic temperature milling compared to the room temperature milling is measurable. For both, room temperature and cryogenic milling, the amount of iodine released at higher temperatures increases with longer milling times. Comparison of samples milled for different times indicates that the 6-hr milling results in a stabilized material when the initial iodine concentration is 5 wt %. The material is also nearing its stabilized composition for the compositions with 10 wt % of iodine. For the compositions deemed stabilized, only about 10 % of the iodine retained in the material is released upon heating to 400ºC. Using longer milling times does not result in a substantial reduction of this relatively low-temperature iodine loss. Based on this assessment, the materials prepared at the liquid nitrogen temperature are closer to their stabilized state than similar materials prepared at room temperature. Further, materials with 20 wt % of initial iodine are far from their stabilized condition. Comparing their respective TG traces, it appears that a longer milling time would result in a further increase of iodine fraction retained in such materials; however, the very long milling times may be impractical especially considering the small but steady iodine loss due to the purging of the milling container. It is possible that the milling efficiency can be further improved by adjusting the ball sizes and speed of impeller (rpm), so that the times required to achieve a stabilized state are somewhat reduced. However, such optimization of the milling parameters was outside the scope of the present effort.

It is likely that the limit to the iodine concentration that can be retained in aluminum at elevated temperatures depends more on the specific milling conditions and less on the characteristics of aluminum and iodine themselves. More than 7 wt % of iodine was observed to be released above 400 ºC in this effort for a material prepared using elemental Al and I as starting materials in the attritor mill (cf. Figs. 5.3, 5.4); however, this concentration is not the limit for the material system. For the material prepared in the shaker mill, a greater overall percentage of iodine was captured in the material and more than 9 % of iodine was retained upon the material's heating to 400ºC (Fig. 5.5).

Aluminum-iodine compounds

Only a small portion of iodine contained in the mechanically alloyed material is similar to "free iodine" and thus released upon heating to 200ºC (cf. Fig. 5.1). Most of the retained iodine is either bonded to aluminum or at least effectively encapsulated, so that it remains in the material at elevated temperatures. It is also observed that AlI_3, the only reported stable aluminum iodide, may not be the only or even the primary compound formed. The formed AlI_3 is poorly crystalline and is likely embedded in an Al matrix. The latter assessments are based on both TG and XRD results. Based on TG measurements, pure AlI_3 decomposes nearly completely upon its heating to about 400ºC; however, less than 10 % of the entire iodine retained in stabilized mechanically alloyed powders is released upon heating to this same temperature (compare Fig. 5.1 vs. Figs. 5.3, 5.4). XRD also show that AlI_3 remains detectable as a stabilized phase in the material upon its heating up to 600 ºC, as shown in Table 5.4, while substantial loss of iodine content is observed from the TG measurements.

Release of iodine occurring in well-distinguishable steps preceding aluminum melting (see Fig. 5.4) indicates formation of several Al-I compounds. Identification of separate steps suggests that multiple distinct phases may be present in the material, or that some phases undergo transformations as the material is being heated. Indeed, formation of AlI and, possibly, other intermediate compounds was inferred by early work studying solubility of Al in AlI_3 (Corbett and Von Winbush, 1955). Mechanical alloying is known to effectively generate metastable alloys, similar to rapidly quenched melts (Suryanarayana, 2001), so the

formation of such compounds is not surprising. XRD was inefficient in resolving the structural differences between the formed compounds, indicating that they are either poorly crystalline or exist as very fine inclusions. However, the observation that decomposition steps shift to different temperatures (see Fig. 5.4) for materials milled for different times is consistent with the concept of iodine redistribution among several phases induced by mechanical milling. In the future, high resolution transmission electron microscopy studies could be useful in resolving such inclusions and identifying their compositions and structures.

Conclusions

Mechanical alloying is effective in preparation of Al-I compounds in which iodine is bonded to aluminum and is not released until the material is brought to high temperatures. Mechanical alloying at liquid nitrogen temperature is more effective in preparing stabilized Al-I compounds than milling at room temperature. An increase in the flow rate through the milling vial results in a higher rate of iodine loss during milling. Milling directly in liquid nitrogen does not allow preparation of the stabilized Al-I compounds; however, it results in the formation of relatively equiaxial particles as opposed to flake-like products obtained under other milling conditions. Therefore, milling directly in liquid nitrogen can be used as an additional milling step following the preparation of the stabilized material, when equiaxial and/or smaller particle sizes are desired.

Materials containing as much as 17 wt % of iodine were prepared. However, for such high iodine concentrations, a substantial fraction of the retained iodine was released when the material was heated to less than 400 ºC. In fully stabilized mechanically alloyed samples, containing more than 8 wt % of iodine, about 90 % of the entire iodine content was released after the material was heated above 400 ºC. In addition to poorly crystalline AlI_3, other iodine compounds were contained in the mechanically alloyed powders. In such compounds, iodine was bonded to aluminum stronger than in AlI_3, so that their thermal decomposition and respective iodine release occur at higher temperatures compared to decomposition and boiling of AlI_3.

Chapter 6. Iodine release, oxidation, and ignition of mechanically alloyed Al-I composites

Paper published: Zhang, S., Schoenitz, M., and Dreizin, E.L. (2010) Iodine Release, Oxidation, and Ignition of Mechanically Alloyed Al−I Composites. *Journal of Physical Chemistry C*, 114 (46): 19653-19659.

Introduction

Research is currently active on the development of multifunctional reactive materials. In particular, there has been interest in developing reactive compositions with biocidal combustion products (Johnson *et al*., 2008; Martirosyan *et al*., 2009; Farley and Pantoya, 2010; Sullivan *et al*. 2010; Amitai *et al*., 2010). Such materials are needed for munitions aimed to defeat stockpiles of biological weapons. The potentially harmful spores and bacteria should be inactivated before they are released to the environment, and various methods of increasing the rate of such inactivation are being explored. Halogenated compounds are known to be effective biocides (Russell, 2003) however, most such materials are unstable and difficult to handle. Therefore, it is of interest to generate such compounds in situ when biological agents are expected to be released. Aluminum powder is a common component of energetic formulations (Price, 1984) and it is added to conventional explosives to achieve greater reaction temperatures and to maximize the energy density of the payload (Vadhe, 2008). Recently, it was shown that mechanical milling can be used to prepare relatively stable aluminum-iodine (Al-I) composites (Zhang *et al*., 2010). These materials have a high combustion enthalpy, comparable to that of pure Al, and they also release iodine upon heating. Initial experiments showed that Al-I composites prepared by mechanical milling are more stable than conventional Al-I compounds, i.e., AlI_3 (Zhang *et al*., 2010; Gugelchuk, 2001). It was also shown that the properties of the prepared composites are not affected strongly by selection of the starting materials (e.g., elemental I or AlI_3 mixed with Al) used for mechanical alloying (Zhang *et al*., 2010). This study is aimed to further explore the Al-I composites prepared by mechanical milling; in particular, it is of interest to consider the kinetics of reactions

leading to iodine release at different temperatures. Furthermore, ignition and oxidation behaviors of the prepared materials will be investigated and correlations between different reactions will be considered.

Materials

Powders of Al-I composites were prepared by ball-milling elemental aluminum and iodine using a model 01HD attritor mill by Union Process. Starting materials were aluminum powder, -325 mesh (< 45 μm), 99.5%, by Atlantic Equipment Engineers and iodine chips, 99%, by Sigma Aldrich. 1.8 kg of hardened steel balls served as milling media. Liquid nitrogen was flushed through the cooling jacket of the milling vial and gaseous nitrogen was fed into the milling vial. Further details describing materials preparation are given elsewhere (Zhang *et al*., 2010). Two composite samples, referred to as samples A and B were prepared for this project. Sample A was continuously milled for 10 hours. The product powder was passed through a 170 mesh (88 μm opening size) sieve. Sample B was milled in two steps. The first step included milling for 6 hours as outlined above. The second step included 3.5 hour milling with liquid nitrogen fed into both cooling jacket and inside the milling vial. As described in ref. (Zhang *et al*., 2010), using liquid nitrogen inside the milling vial helps reducing the particle sizes of the prepared powders, but it also results in a less stable material for which greater iodine release occurs at low temperatures. Figure 6.1 shows the particle size distribution (PSD) and respective volume mean particle sizes of samples A and B. The abrupt drop of the volume fraction of particles coarser than about 60 μm for sample A is due to sieving prior to use in this project. Both samples consist of micron-sized particles. The morphology of particles is illustrated in SEM images shown in Fig. 6.2. Generally, both samples contain particles with equiaxial shapes, and particles of sample A are coarser and more rounded compared to sample B.

In addition to the Al-I composites, pure Al powder with nominal particle sizes in the range of 1 – 5 μm by Atlantic Equipment Engineers was used for selected oxidation experiments as a reference.

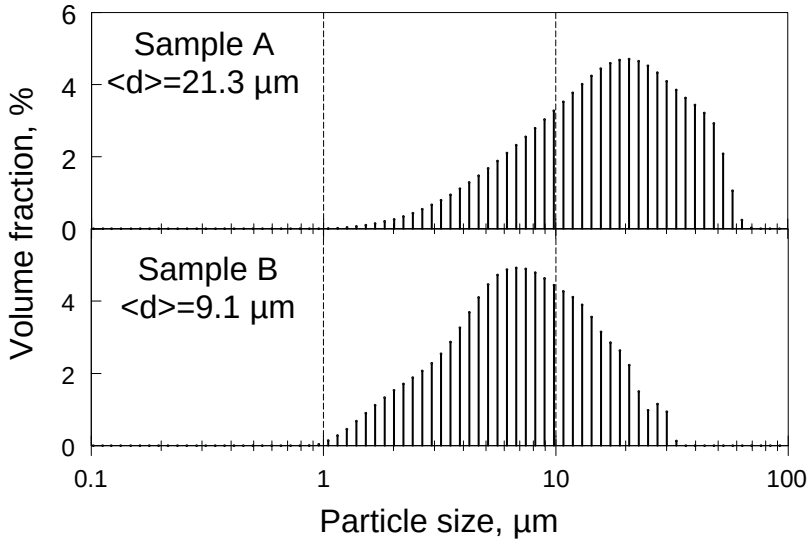

Fig. 6.1. Particle size distributions for samples A and B. Volume mean particle sizes are shown for each material

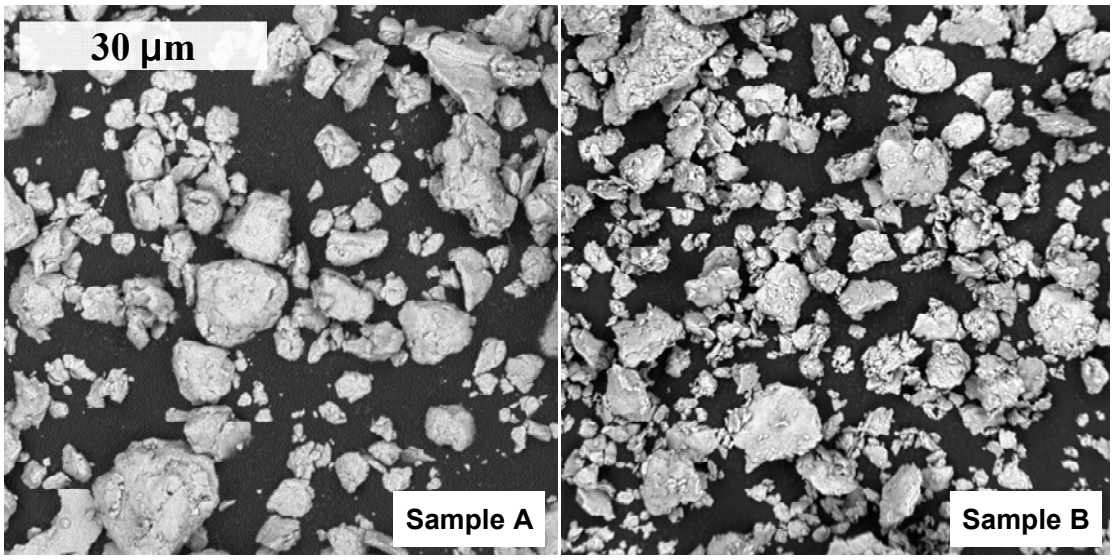

Fig. 6.2. SEM images of samples A and B; magnification is the same for both images.

Experimental

A TA Instruments model Q5000IR thermogravimetric analyzer (TGA) was used for both iodine release and oxidation measurements. Materials were placed in alumina pans. For iodine release measurements, the balance and the furnace were purged with argon at 20 and 50 ml/min, respectively. These relatively high flow rates were selected to protect the

balance from corrosive iodine, and to minimize the contamination of the furnace environment with traces of oxygen. The maximum temperature was limited to 1000 ºC (1273 K). The heating rates varied from 5 to 200 K min^{-1}. The mass of material used for iodine release kinetics measurements varied in the range of 1–20 mg.

Oxidation of Al-I composites was studied in oxygen-argon mixtures and in pure oxygen. The balance and the furnace of Q5000IR were purged with an oxidizing gas at 10 and 25 ml/min, respectively. Experiments were performed at heating rates varied from 5 to 200 K min^{-1}. The mass of material used in oxidation experiments varied in the range of 0.4 – 5 mg. A heated filament ignition test was used to characterize ignition of the prepared materials at heating rates not achievable by the thermo-analytical measurements. Details of this experimental technique are available elsewhere (Ward *et al*., 2006; Shoshin *et al*., 2006; Stamatis *et al*., 2009). A 0.5 mm diameter 4.5 cm long Nickel-Chromium alloy wire was used as the electrically heated filament. The filament served as a load in a circuit including a set of DC batteries and an adjustable resistor connected in series. A small amount of powder was mixed with a surfactant and hexane, and this slurry was coated onto the filament to form a thin layer with a coated portion of about 1 cm in length. Ignition was observed using a silicon photodiode (DET110 by Thorlabs, Inc.) equipped with an iris aimed at the powder coating from a distance of 4 – 5 cm. A high speed camera (MotionPro 500 by Redlake) was also used to observe the ignition in some experiments. The temperature history of the heated filament was measured using a high-speed infrared pyrometer (DP1581 by Omega Engineering, Inc.), which was focused on the uncoated surface of the filament adjacent to the powder coatings. The experiments were performed in air with varied filament heating rates.

Results

Iodine release

Mass reduction traces for samples A and B heated in argon at different heating rates are shown in Fig. 6.3. Consistent with a previous report (Zhang *et al*., 2010), there are several

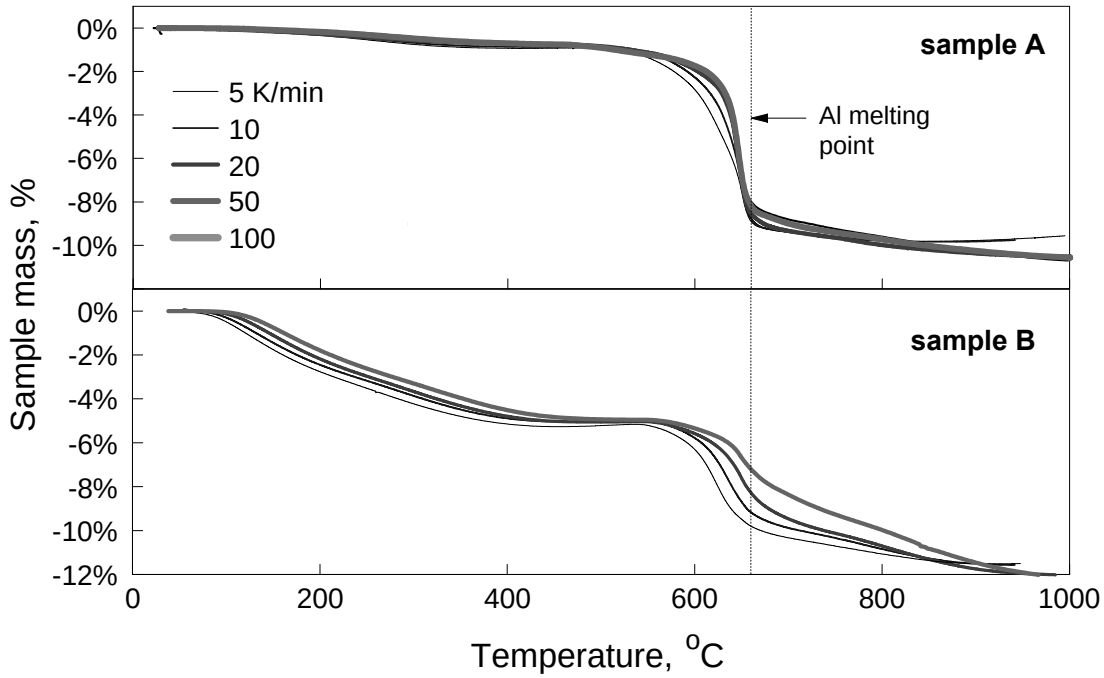

Fig. 6.3. Iodine release trace for sample A and B in TGA at different heating rates.

main mass reduction stages. Initial iodine release occurs well before Al melting, starting at a temperature as low as about 100ºC and continuing to up to about 400ºC. This iodine release stage is much stronger for sample B than for sample A. The second subsolidus iodine release stage begins in the vicinity of 600ºC. It overlaps with aluminum melting. The second iodine release stage is substantially stronger for sample A, for which the amount of iodine released in the initial stage is very small. Iodine release continues after melting; however, the measurements at elevated temperatures are increasingly affected by oxidation with residual oxygen and thus do not provide a reliable measure of the iodine release rate. The high-temperature iodine release from molten aluminum observed in these TGA experiments is also of little significance in terms of its effect on or interference with the material ignition (as shown below) and so it will not be analyzed further in this article.

To assess the kinetics of iodine release, consider Fig. 6.4 showing temperature derivatives of the TGA traces presented in Fig. 6.3. There are two clearly distinguished minima in the temperature range of 100 and 400ºC, when the first broad iodine release stage occurs. This iodine release stage is weak for sample A; nevertheless the two minima in the *dm/dT* trace

are clearly distinguished in the inset, showing fractions of the *dm/dT* traces at a magnified scale. Therefore, the first iodine release stage is further broken down into two steps. The temperatures at which the first and second steps occur correlate with the respective temperatures at which pure iodine and AlI_3 were observed to evaporate upon heating (Zhang *et al*., 2010). The second iodine release stage is represented by a single minimum in the *dm/dT* trace. For sample B, this minimum and the respective iodine release stage are nearly completed before the Al melting point. For sample A, the rate of iodine release appears to increase noticeably at the onset of aluminum melting, so that the shifts to higher temperatures at increased heating rates are smaller for the trailing edges of the respective minima of the *dm/dT* traces compared to those for the leading edges of the same minima.

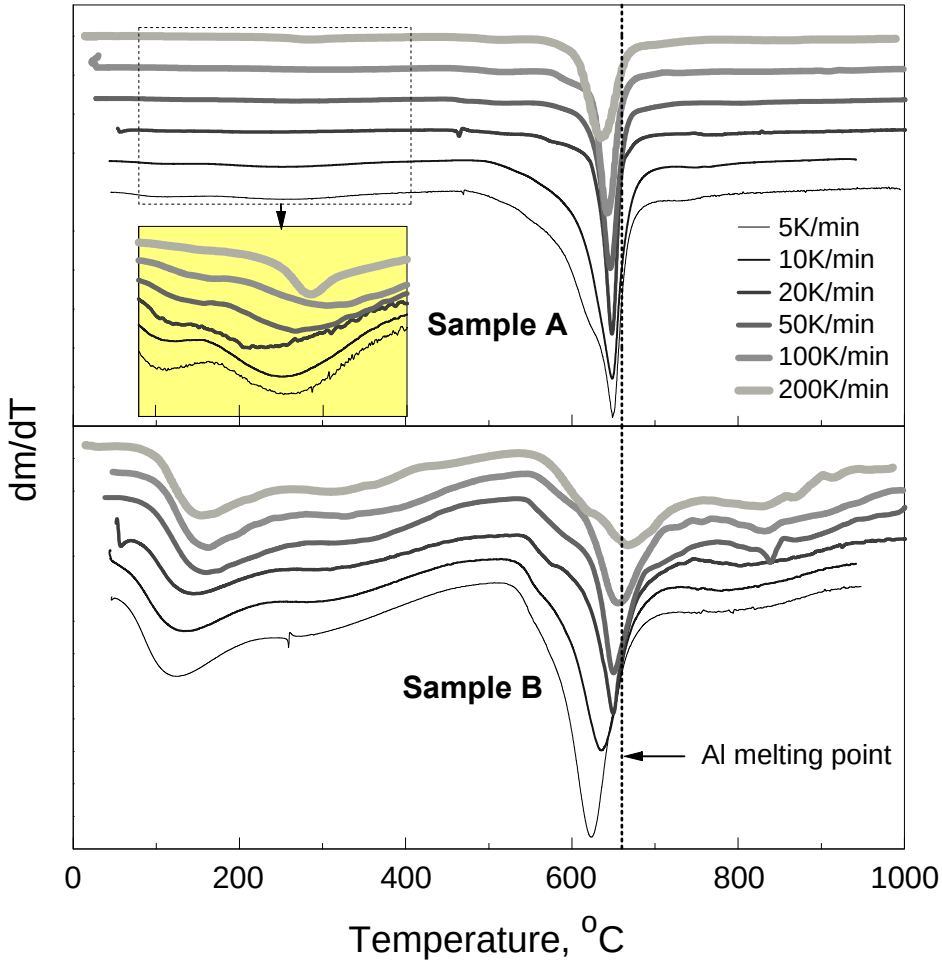

Fig. 6.4. Mass derivatives of iodine release for sample A and B in TGA at low temperature range for different heating rates.

The TGA measurements were processed to calculate the iodine release activation energy as a function of the reaction progress, assumed to change between 0 and 1 for the as-prepared sample and the sample heated to 1000ºC, respectively. The data processing used a model-free isoconversion method proposed by S. Vyazovkin (2001). Results from these calculations are shown in Fig. 6.5. For the first iodine release stage, the activation energy is generally low for both samples A and B. While less clearly distinguished, it appears that the first step has a somewhat lower activation energy (~ 50 kJ mol^{-1}) than the second one (~ 70 kJ mol^{-1}) for both samples. Specific values of the activation energies corresponding to the low temperature decomposition steps for samples A and B are very close to each other. The same activation energy values are also obtained using Kissinger method (Starink, 2003), following the minimum positions at various heating rates. Details of the Kissinger analysis are not shown for brevity.

For the second iodine release stage, (occurring at different reaction progress values for samples A and B), the activation energy increases for both materials. Note that the sharp spike in the activation energy immediately before it settles near 300 kJ mol^{-1} is an artifact caused by residual oxidation occurring in the TGA experiments despite continuous flushing the furnace with pure argon. This oxidation is detected by slight increase in the sample weight after the completion of the first iodine release stage. Note also that the interference of melting with the second iodine release stage for sample A results in a rapid increase of the apparent activation energy, as shown in Fig. 6.5.

The melting point does not depend on the heating rate so that, once again, very high apparent oxidation energies observed for sample A at high reaction progress values are not physical.

Oxidation

Oxidation of samples A and B was characterized by TGA at different heating rates in both an argon-oxygen mixture and pure oxygen; the results are shown in Fig. 6.6. The mass

changes result from the combined effects of iodine release (mass loss) and oxidation (mass gain). For all samples the mass keeps decreasing upon heating to 400ºC. In general there are four oxidation steps for both samples spread over broad temperature ranges from 400ºC to 1100ºC, which are better observed in the derivatives of mass change during oxidation (Fig. 6.7).

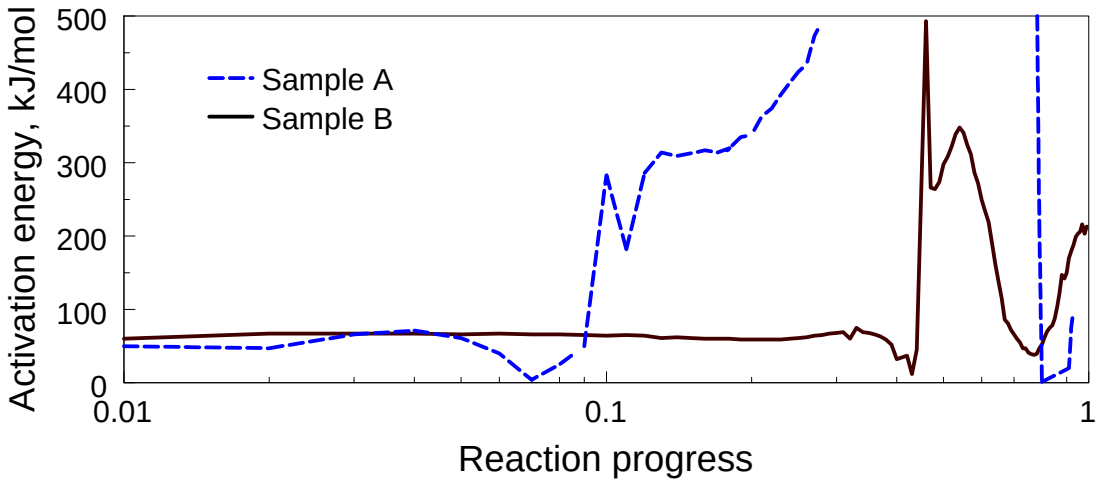

Fig. 6.5. Activation energy in function of reaction progress for samples A and B calculated using Vyazovkin method [14]. Note the logarithmic horizontal scale.

The first step starts around 400ºC with a slight weight gain. For sample B, the first step is not clearly seen from Fig. 6.6 and Fig. 6.7 because the mass loss due to iodine release offsets the mass gain due to oxidation. The second step starts around 600ºC where the sample mass sharply increases. The third step seems to be related to aluminum melting and does not shift with heating rates, unlike other, thermally activated reaction steps. As the heating rate increases, the second step shifts to higher temperatures and merges with the third step associated with Al melting. In the fourth step, oxidation occurs over a broad temperature range starting from 800ºC. For sample B the fourth step ends around 1100ºC; for sample A the end point is beyond the measured temperature range. Note that the weight increase is measured only when the weight gain from oxidation exceeds the weight loss from iodine release. Thus, the oxidation may be faster than what is directly implied by the measured weight gain.

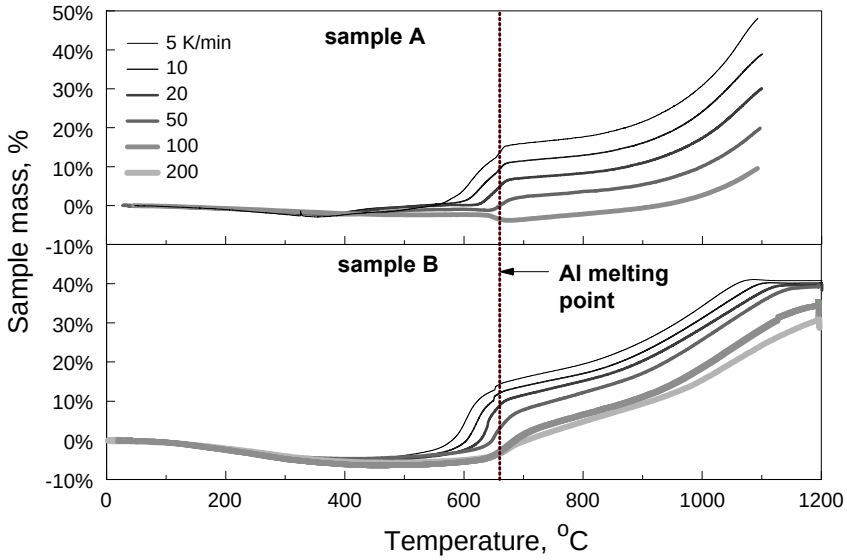

Fig. 6.6. Oxidation traces for samples A and B in TGA at different heating rates. The oxidation of sample A was measured in pure oxygen; the oxidation of sample B was measured in argon and oxygen mixture.

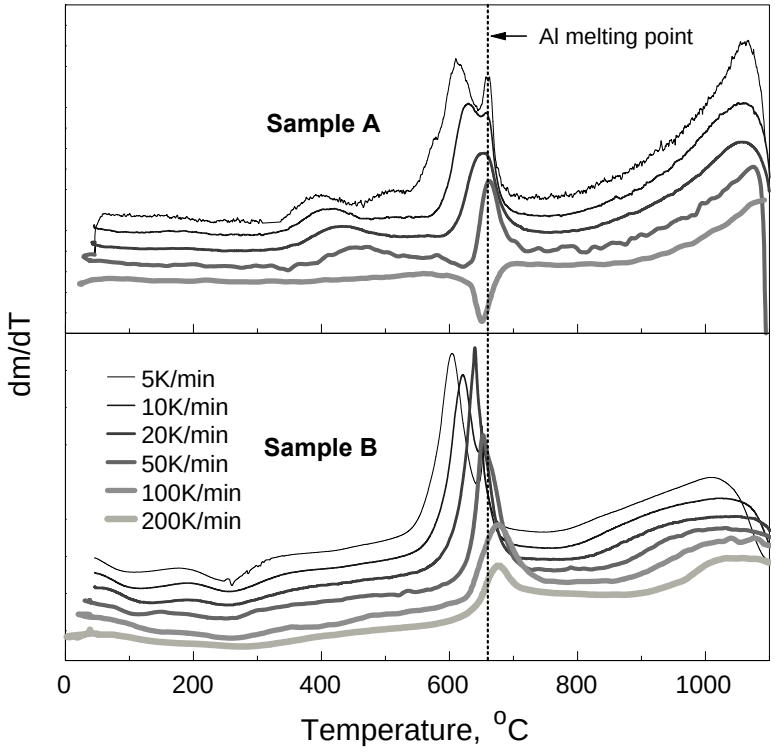

Fig. 6.7. Derivatives of mass change for oxidation of samples A and B at different heating rates.

The positions of the *dm/dT* peaks shifting to higher temperatures at greater heating rates were processed using the Kissinger method (Starink, 2003) to evaluate activation energies for different oxidation steps. Different oxidation steps were resolved better for different samples, respectively, so this processing was somewhat incomplete. The activation energies identified by this processing are shown in Table 6.1.

Table 6.1. Activation energies, kJ mol^{-1}, determined by Kissinger processing for different oxidation steps for Al-I composites.

Sample ID	A	B
Oxidation step		
1	144	-
2	289	287
4	-	506

To understand processes occurring during oxidation, XRD patterns were collected from powders by quenching sample B heated to 530, 640, 680 and 1200ºC. A low-background quartz sample holder was used to characterize small batches of material recovered after heating to intermediate temperatures. Fig. 6.8 shows the respective XRD patterns and the pattern of as-milled sample as reference. For this sample, peaks of iodine or iodine-containing phase cannot be clearly seen, and no iodine-containing phase was detected unambiguously as oxidation went on. Only aluminum reacting to form γ-alumina and α-alumina was observed from the XRD patterns.

To directly compare oxidation of Al-I composites with that of Al, the oxidation TGA traces shown in Fig. 6.6 were processed by subtracting the iodine release TGA traces recorded for the same material at the same heating rate in argon (see Fig. 6.3). The final processed oxidation traces for samples A and B are shown in Fig. 6.9. In addition, several oxidation traces directly measured for a pure Al powder are shown for comparison. A slow decrease in the processed TGA signal during the temperature ramp up to about 350ºC means that the iodine release at these low temperatures was slightly accelerated in the oxygen environment.

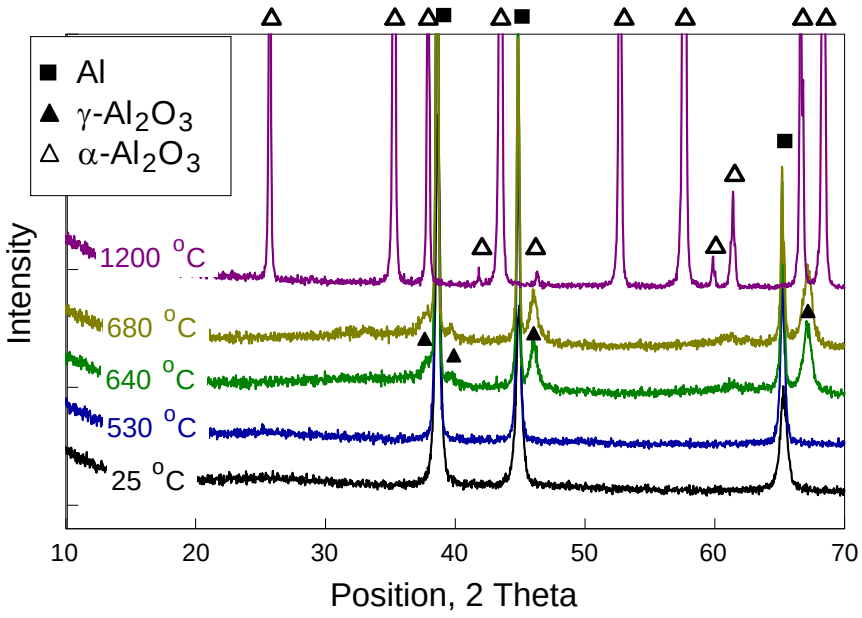

Fig. 6.8. XRD patterns of the powders produced by heating sample B in argon and oxygen mixture to and quenching at different temperatures.

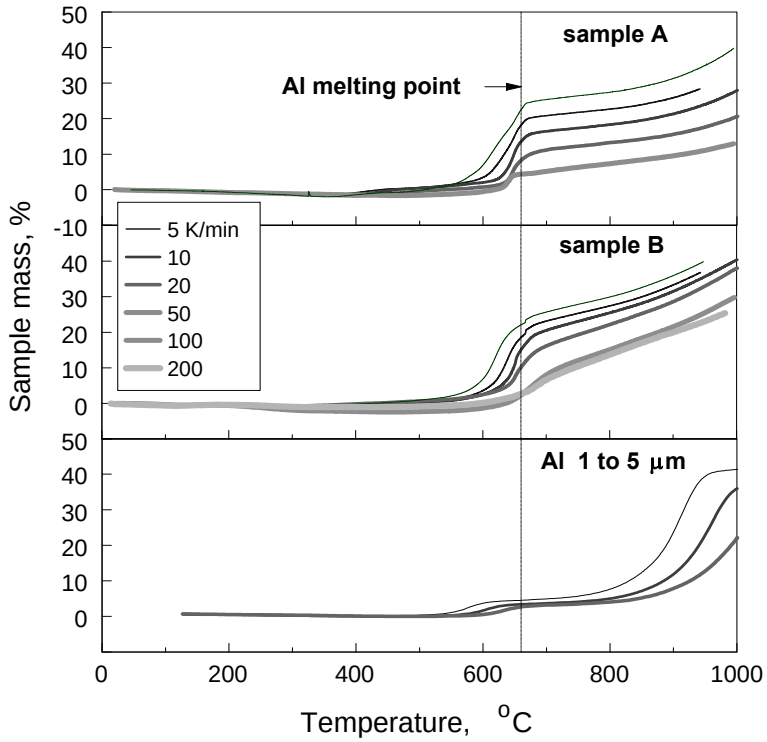

Fig. 6.9. The TGA oxidation traces of Al-I composites from which a TGA signal measured during heating the same samples in argon are subtracted (top) and TGA traces for the pure Al oxidation (bottom).

Although weight loss (dominated by the iodine release) was observed around the Al melting point for 100 K/min in the original oxidation trace (Fig. 6.6), the weight gain due to oxidation becomes noticeable after subtraction of the TGA curve measured in argon. Compared to the pure aluminum oxidation, oxidation for the composite materials starts at a lower temperature (400ºC) and a distinct oxidation event occurs around the aluminum melting point. It is apparent that oxidation for Al-I composites is generally accelerated compared to pure aluminum.

Ignition

Figure 6.10 illustrates the ignition temperature measurements and shows a temperature trace corresponding to a specific setting of the electric circuit and a photodiode signature for Al-I sample undergoing ignition. A photodiode signal for the blank filament without powder is also shown by Fig. 6.10 as a reference. The calibrated temperature range for the pyrometer is 530 – 930ºC. For Al-I powder, the ignition results in a sharp spike in the photodiode signal, which is observed just after 0.325 s in Fig. 6.10. At this time, the pyrometer output is within the calibrated range, and the ignition temperature is measured directly. For some runs ignition moment is beyond the calibrated pyrometer range; in such cases an extrapolation of the filament temperature based on the temperature ramp measured in the calibrated range is used. A linear extrapolation of the temperature ramp for the range of temperatures of interest in these experiments was supported by a detailed analysis of the heat transfer for the electrically heated filament placed in a convective environment (Ward, *et al*., 2006).

The filament ignition experiments were performed in air at different heating rates varying in the range of 1,000 to 220,000 K s^{-1}. Sample B exhibited clear ignition signatures and the time of ignition was readily detected by the photodiode. For sample A, clear ignition signatures were observed at heating rates from 5,000 to 8,000 K s^{-1}. For lower heating rates, (around 2,500 K s^{-1}) or higher heating rate (around 12,000 K s^{-1}), ignition of sample A could not be easily detected by the photodiode. A high speed video camera was used to aid in identifying the ignition moment. Figure 6.11 shows image sequences for the ignition or

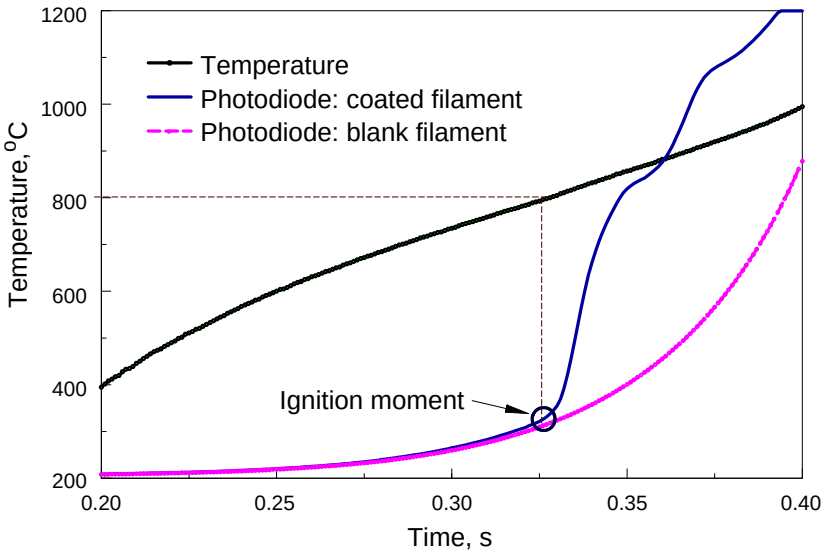

Fig. 6.10. Photodiode and temperature traces recorded during heated filament ignition experiment of Al-I composites. A blank filament without any powder coating was heated and the photodiode signal was recorded as a reference.

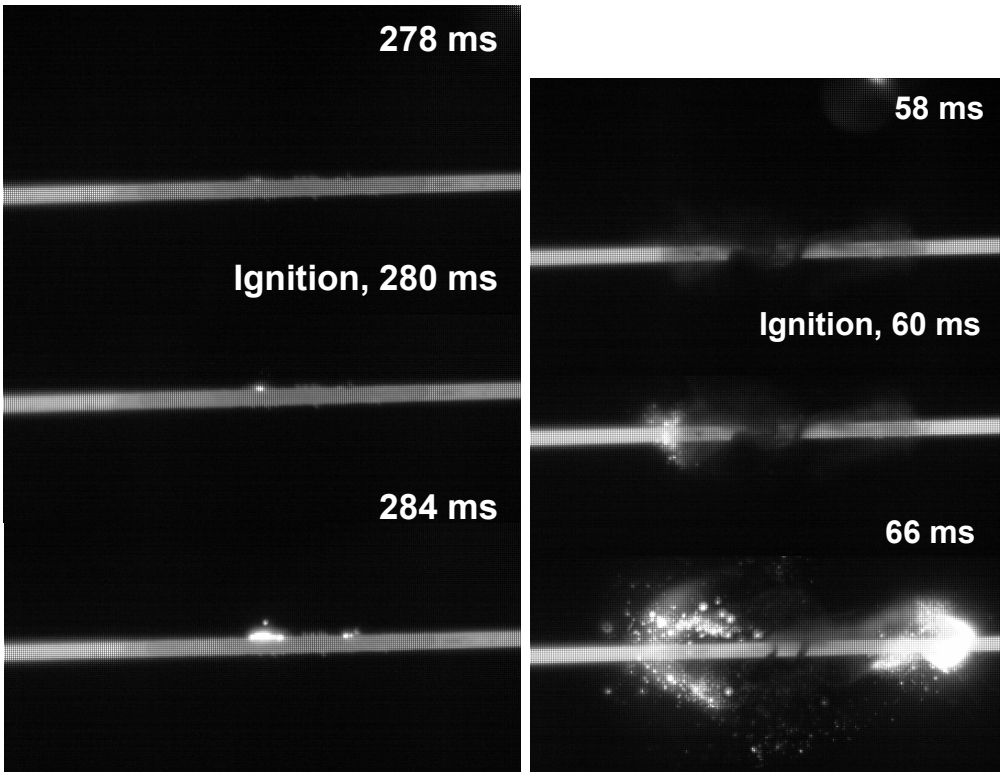

Fig. 6.11. Images recorded by the high speed camera for sample A undergoing ignition at 2,500 K s^{-1} (left), and at 12,000 Ks^{-1} (right). The filament diameter is 0.5 mm. The time delay for each frame is noted in the image.

sample A at low and high heating rates, respectively. As the filament is heating up, the coating surface looks darker than the uncoated filament, which may be attributed to the temperature gradient (the coated portion of the wire has a greater specific heat, and so it is heated to a lower temperatures compared to the blank wire). In addition, the emissivity of the coating may be different from that of the clean wire surface. Note that the difference in brightness between the coated portion of the filament and the clean surface is substantial at a high heating rate (right side of Fig. 6.11), and it is barely distinguishable for a low heating rate (left in Fig. 6.11), consistently with an expected stronger temperature gradient at the increased heating rates.

For the heating rate of 2,500 K s^{-1}, ignition is identified when a first bright spot is detected on the filament (cf. left in Fig. 6.11). As time goes on, multiple bright spots appear and ignition propagates over the coating. When the coated filament is heated at a higher rate of 12,000 K s^{-1} (right in Fig. 6.11), the time of ignition is identified when multiple bright particles appear to be lifted off the filament. This event always begins at the edges of the coated section of the wire, where the temperature is expected to be higher, and closer to that measured by the pyrometer. It is interesting that a visible smoke cloud is observed to be produced just before the ignition, as seen in the top image shown on the right in Fig. 6.11. Similar smoke clouds are observed in the video-images for the wire ignition experiments performed at heating rates of 8,000 – 12,000 K s^{-1}. This observation is hypothesized to be associated with iodine release, so that the mass-spectrometric identification of the emitted species could be of interest in the future.

Figure 6.12 shows the ignition temperatures of Al-I composites as a function of heating rate. In general it is observed that the ignition temperatures of the Al-I composites increase with increasing heating rates as is expected for a thermally activated ignition mechanism. Ignition temperatures measured for sample B are somewhat lower, and ignition can be observed in a wider range of heating rates compared to sample A. The difference in the ignition temperatures measured for samples A and B is relatively small and can be caused by a difference in the particle size distributions for the two materials (cf. Fig. 6.2.). The difference between the particle temperature and the filament temperature may be smaller

for finer particles (sample B), explaining a small decrease in the measured ignition temperature compared to sample A.

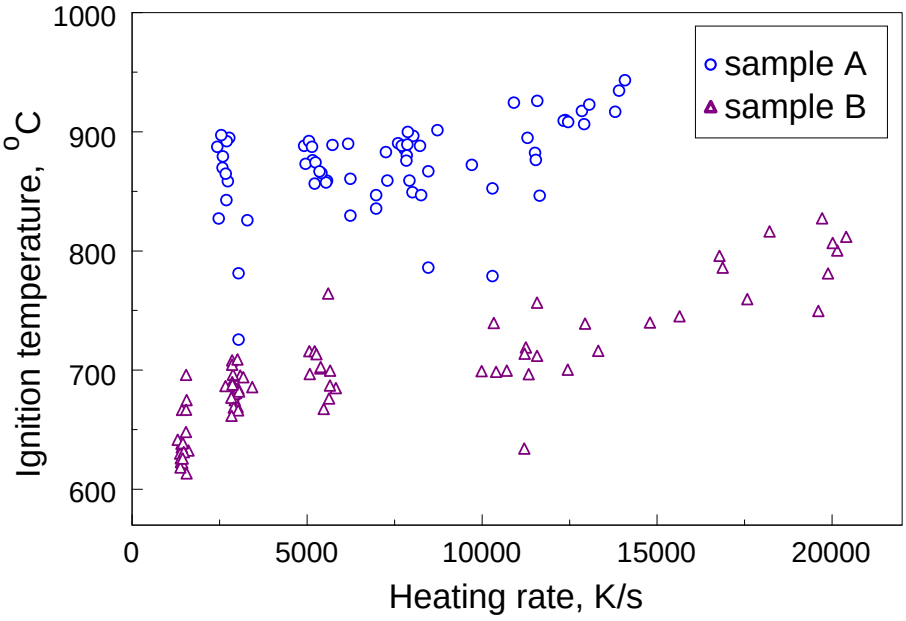

Fig. 6.12. Ignition temperatures measured for samples A and B at different heating rates.

Discussion

The results suggest that iodine is retained in the mechanically milled Al-I composites in at least three different forms. The correlation of temperatures for two initial iodine release steps (the first stage) with the volatilization temperatures of pure iodine and AlI_3 (Zhang *et al*., 2010; Gugelchuk, 2001) suggest that fractions of the iodine retained in Al can be described as representing elemental iodine and AlI_3, respectively. These compounds are only weakly bound to aluminum and, similarly to the respective separate phases of I and AlI_3, are volatilized upon moderate heating. It is expected that these compounds would result in relatively rapid aging and partial deterioration of the prepared composites upon storage and handling. Thus, sample A, releasing less iodine at low temperatures is considered to be more suitable for practical formulations. Iodine retained in the prepared materials at elevated temperatures and released just before, during, and after Al melting is

strongly bound to Al and is expected to survive storage and handling of these materials. The state of this iodine is unknown. It is possible that iodine is dissolved in the Al crystal lattice (e.g., with I atoms substituting for Al) or present as surface-stabilized nano-inclusions of pure iodine or AlI_3 embedded into aluminum matrix.

The differences in relative fractions of the iodine contained as weakly and strongly bound forms between samples A and B represent the major difference between these two materials. Indeed, quantitative differences in the iodine release and oxidation behaviors between these two samples can be readily traced to the difference in the weakly and strongly bound iodine forms. At the same time, qualitatively, the samples behave similar to each other, including consistency in the apparent activation energies assigned to different reactions.

Increasing the concentration of iodine strongly bound to Al while reducing the concentrations of the weakly bound forms behaving as pure iodine and AlI_3 are identified as objectives of further synthesis efforts aimed at development of practically useful Al-I composites.

It is interesting to consider whether the detected stages and steps of iodine release are correlating with the oxidation steps for the prepared materials. It is apparent that the first iodine release stage occurring at low temperatures does not directly correlate with the observed oxidation steps. Similarly, the initial oxidation step with the onset close to 400 ºC is not associated with any specific iodine release step. It is worth emphasizing that this initial oxidation step occurs earlier than for pure Al (cf. Fig. 6.8) and so the low-temperature oxidation rate for aluminum is clearly affected by the presence of iodine. Because no crystalline alumina phases are detected for the partially oxidized materials (Fig. 6.8), amorphous alumina is the likely product of oxidation at these temperatures, as is the case for pure Al (Trunov *et al*., 2005, 2006).

The second stage of iodine release does appear to correlate with the second oxidation step for Al-I composites. In both cases, the reactions start at about 500 – 600 ºC and in both cases, the activation energies are found to be close to 300 kJ/mol. Aluminum melting also

apparently interferes with both iodine release and the oxidation processes. Oxidation at these temperatures produces well-detectable quantities of γ-Al_2O_3. This product is also consistent with that observed for oxidation of pure Al at the same temperatures. Further oxidation results in formation of α-Al_2O_3, again, consistently with the oxidation of pure Al. Note that pure Al in O_2 does not oxidize appreciably immediately following its melting, while the oxidation rate increases rapidly at elevated temperatures. Conversely, Al-I composite materials oxidize relatively fast at the Al melting point. The oxidation rate increases only slightly (slower than for the pure molten Al) as the temperatures increase.

The acceleration in the pure aluminum oxidation upon melting has been previously observed in the presence of H_2O as an oxidizer (Schoenitz *et al*., 2009). It was hypothesized that presence of hydrogen alters properties of the protective alumina film resulting in disruption of its continuity when molten Al forms. It is possible that the presence of iodine has a similar effect on properties of alumina. It is also possible that iodine bound to crystalline Al is rapidly released upon Al melting; the release of gaseous iodine results in disrupting the alumina shell, which in turn leads to an enhanced transport of oxygen to the fresh aluminum surface.

Finally, it is interesting to consider possible correlations between the ignition kinetics and those of the various observed iodine release and oxidation events. Figure 6.13 shows ignition temperatures measured at different heating rates presented in the same Kissinger plot as the *dm/dT* minimum and maximum temperatures corresponding to individual iodine release and oxidation events, respectively. The kinetic trends following from TGA measurements are extrapolated as straight lines into the range of heating rates corresponding to the ignition experiments. It is apparent that the second iodine release step (corresponding to the release of the AlI_3-like form of iodine) correlates with the ignition data better than any other reactions observed in the TGA experiments. This observation is consistent with the observed "smoke" produced by the sample coated onto the heated filament just prior to its ignition (Fig. 6.11); the smoke may be formed by air moisture reacting with the generated iodine cloud. The second stage of iodine release, not shown in

Fig. 6.13, but effectively coinciding with step II of oxidation is projected to higher temperatures than the experimental ignition temperatures determined here.

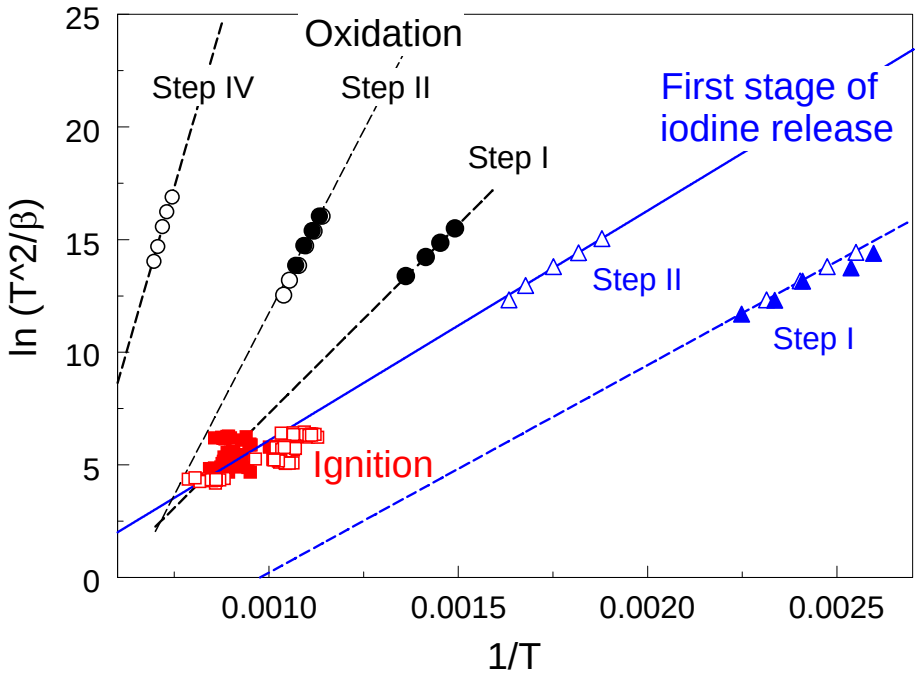

Fig. 6.13. Comparison of ignition temperatures measured at different heating rates with iodine release and oxidation steps observed in the TGA traces. Filled symbols represent sample A; open symbols represent sample B. Circles represent oxidation steps, triangles represent iodine release steps, and squares show ignition temperatures.

Thus, it is suggested that the second iodine release step which is not apparently accompanied by substantial oxidation, leads to ignition of the materials investigated in this project. Reducing the presence of weakly bound iodine forms in more stable materials can also alter their ignition behavior, which should be addressed in the future efforts.

Conclusions

Mechanical milling at cryogenic temperatures is successfully applied to prepare Al-I composite powders with iodine concentrations exceeding 10 wt %. Detailed TGA measurements suggest that iodine is present in the prepared composites in at least three different forms. Two weakly bound forms volatilize similarly to elemental iodine and AlI_3. A strongly bound form is retained in aluminum until the material is heated up to nearly the

Al melting point. Two different samples prepared in this effort contained different fractions of weakly and strongly bound iodine forms; however, the iodine release and oxidation behaviors were qualitatively similar for both samples. Oxidation of the prepared materials in O_2 occurs in several steps clearly distinguished by TGA. The low-temperature oxidation begins sooner than for pure aluminum. The second oxidation step is correlating with the release of strongly-bound form of iodine. Unlike for pure aluminum oxidizing in O_2, the second oxidation step is accelerated by Al melting. Ignition of the prepared materials occurs at substantially lower temperatures than for pure Al. It is observed that for the materials prepared in this study, the ignition kinetics correlates with that of the low-temperature release of iodine.

Chapter 7. Inactivation of aerosolized *Bacillus subtilis* spores and MS2 viruses caused by combustion of energetic materials

(to be submitted to a peer-reviewed journal)

Introduction

The focus of this grant was the development and evaluation of energetic materials with the added capability to effectively inactivate stress-resistant aerosolized microorganisms. The development effort was described in Chapters 5-6. This Chapter presents the experimental results on the inactivation of aerosolized bacterial spores and viruses due to their exposure to combustion environments, including hydrocarbon flame (with no powder) as well as different energetic formulations, including Al-I filled nano-composite material described in Chapters 5-6.

Method

The experimental set-up was described in Chapter 1. The challenge bioaerosol was generated from a surfactant-free, de-ionized water suspension using a six-jet Collison nebulizer (BGI Inc., Waltham, MA) operated at 6 L min^{-1}. Strong shear forces inside the nebulizer created by the high-velocity air jet enhanced de-agglomeration of biological particles. The aerosol generation protocol has previously been validated and used in several studies. The bioaerosol was diluted with HEPA-filtered dry air at flow rates of 12 and 30 L min^{-1} producing the total flows of Q=12+6=18 L min^{-1} and Q=30+6=36 L min^{-1}. After passing through a 10-mCi ^{85}Kr charge equilibrator (model 3012, TSI Inc., St. Paul, MN, USA), the bioaerosol entered the test chamber – a vertical cylindrical channel of 50 mm in inner diameter and 320 mm in height. The combustion or heating source (depending on type of the test) was installed along the axis of the chamber.

According to the project plan, two challenge bioaerosols were used: *B. subtilis* var. *niger* bacterial spores (obtained from the US Army Edgewood Chemical Biological Center, APG, MD) and MS2 bacteriophage viruses (obtained from the ATCC, Rockville, MD, USA).

For spores, the aerosol concentration and particle size distribution were determined in real time at the inlet and the outlet of the test chamber using an optical particle size spectrometer (Model 1.108, Grimm Technologies, Inc., Douglasville, GA, USA), which operated at a flow rate of 1.2 L min^{-1} and counted particles in 15 channels covering the optical size range of 0.3 to >10 μm. Following a 10-min nebilization period, a stable concentration of the challenge aerosol was achieved with the particle size distribution peaking at 0.7 – 0.8 μm (corresponding to the optical size of intact *B. subtilis* endospores).

After passing the test chamber and a U-shaped transportation line, the aerosol was transported through a 300-mm long cooling system that reduced the air flow temperature to the initial (room temperature) level. The spores were collected from the air flow downstream of the cooling system using three sterile 25 mm filter cassettes (SKC Inc., Eighty Four, PA, USA) equipped with identical 25-mm polycarbonate filters (Millipore Corp., Billerica, MA, USA) (pore size=0.4 μm); the viruses were collected 25-mm diameter gelatin filters (SKC Inc.). In most of the tests, the sampling time was 60 s and the sampling flow rate was 5 L min^{-1}. The filters were then removed and analyzed by cultivation using the standard techniques and protocols. The number of Colony Forming Units (CFU) or Plaque Forming Units (PFU) was detected for each test and control test.

The concentration of culturable spores (C_{CFU}) was determined as an average from the three filter samples obtained in each run. The experiments were conducted with and without combustion/heating. The culturable counts were compared for each test-control combination to determine the loss in spore culturability due to their specific exposure. Thus, the loss in culturability served as a surrogate for the viability loss.

The filters with collected MS2 viruses were removed, dissolved in sterile, filtered deionized water, and analyzed using a modified plaque assay. The PFU count was performed on

TYG agar plates from 1 mL aliquots of the original or diluted (up to 10^4) filter extracts. The concentration of viable viruses was determined as an average from the three filter samples obtained in each run. The lowest countable number was 1 PFU per plate. Some plates (representing the samples obtained under high thermal exposure conditions) showed zero count. Available analytical guidelines recommend using the Practical Quantification Limit (PQL)=5×LOD as the lowest level that can be reliably achieved within specific precision and accuracy limitations provided by routine laboratory operating conditions. Following these guidelines, we adopted 5×LOD per sample as the quantification limit for our analysis. Similarly, the upper limit of the reportable *IF* was derived from PQL and referred to as the highest practical quantification limit (HPQL).

In some instances, experimentally determined inactivation factors were corrected to account for the temperature profiles. These (corrected) *IF*-values are meant to serve as the lower approximation of the actual inactivation. The longitudinal and cross-sectional temperature profiles in the test chamber were determined through a separate series of experiments.

The following combustion environments were tested:

- hydrocarbon flame (no powder),
- B-Ti (burned in powder),
- Mg (burned in powder),
- 8Al MoO_3 (burned in powder)
- Al (burned in powder, large grain 8-10 μm),
- Al (burned in powder, finer grain 3-4.5 μm), and
- Al-I (burned in powder)

Results and conclusions

The combustion experiments were conducted to study the (i) inactivation of microorganisms pre-loaded on filters due to their exposure to combustion products (non-

desirable effect) and (ii) inactivation of the aerosolized microorganisms in the test chamber when passing the combustion zone (primary focus).

Figure 7.1 presents the experimental data. First, the inactivation factor measured with the *B. subtilis* endospores pre-loaded on the filters and exposed to the incoming combustion products was close to 1. This finding suggests that we achieved an important goal: the spores deposited on the filters are not affected by the incoming combustion products during the sample collection. This considerably improved our experimental protocol (as compared to using pellets) and allowed concentrating on the primary objective of this research – microbial inactivation in the aerosol phase. Second, as a background test, the inactivation was determined after the aerosolized spores were exposed to the burner-generated hydrocarbon flame, with no powder fed. This produced IF_{mean} of ~50. Third, the spores were challenged with combustion of non-iodinate powders, which were found to provide a range of inactivation factors of IF_{mean} = 231 to 856. It was clearly seen that the

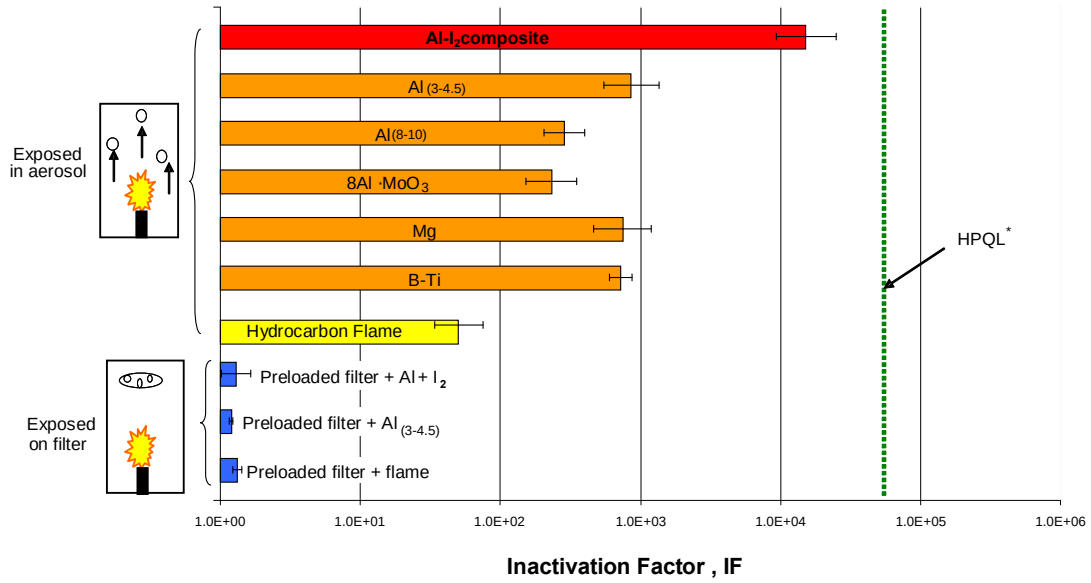

Figure 7.1. Inactivation factor (non-corrected) for viable aerosolized *B. subtilus* endospores exposed on filters and in aerosol phase to hydrocarbon flame and different powders. HPQL is the Highest Practical Quantification Limit.

powder combustion (even without iodine and at moderate feeding rates) increases the spore "kill" greatly. Forth, by testing with an aluminum-iodine composite, we found that a much more effective inactivation of airborne spores can be achieved (as compared to non-iodinated powders): the observed enhancement was almost two decades, and the inactivation exceeded 15,000. It is important to emphasize that this enhancement is not temperature-related because the temperature generated by burning Al-I powder was lower than those generated by most of other tested powders (Figure 7.2).

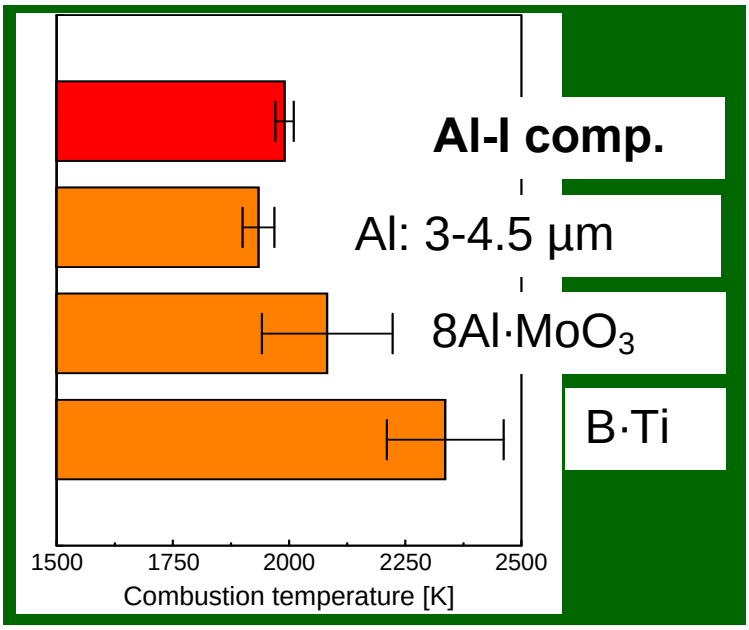

Figure 7.2. Temperatures measured in flames produced by different powders.

The aerosolized MS2 viruses (which are less stress-resistant than *B. subtilis* spores) were found to be effectively inactivated when exposed to combustion of both the iodinated and non-iodinated powders. The inactivation factors exceeded the quantification limit of our experimental protocol (see Figure 7.3).

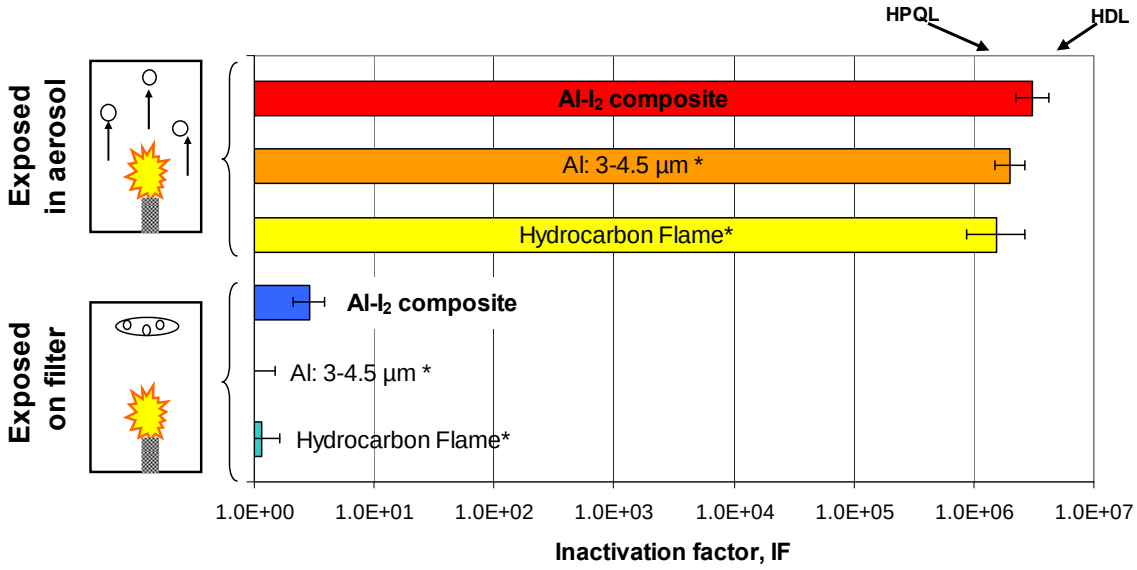

Figure 7.3. Inactivation factor (non-corrected) for viable aerosolized MS2 virions exposed on filters and in aerosol phase to hydrocarbon flame and different powders. HDL = Highest Detection Limit; HPQL is the Highest Practical Quantification Limit.

Chapter 8. Inactivation of aerosolized *Bacillus subtilis* spores exposed to "cold iodine" in air flow (a demonstration experiment).

Additional set of experiments were performed to explore the effect of iodine in the air flow on the spore inactivation. In these experiments, iodine was delivered to the exposure chamber directly, not through the combustion of iodinated powder. Figure 8.1 shows that exposure of BG spores to sublimated iodine at moderate release rates (12 mg s^{-1}) does not cause statistically significant inactivation (at exposure times below 1 s). Increase of the release rate of the "cold" iodine resulted in some inactivation but at or below IF~10. This is about an order of magnitude lower than the inactivation occurring in the air flow in presence of the hydrocarbon flame (with no powder combustion). However, once sublimated iodine is added to the above combustion environment, IF exceeds to $>10^4$, which demonstrates significant enhancement provided specifically by iodine to the spore "killing" and suggests that there may be a synergy between the effects of heat and chemical inactivation.

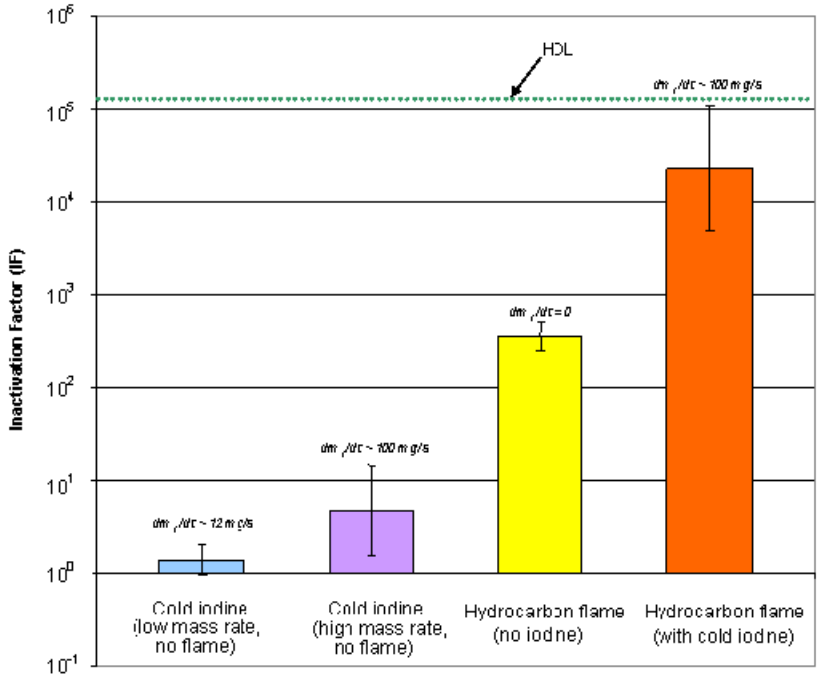

Figure 8.1. Biocidal effect of iodine released by sublimation.

References

Ababouch, L.H., Grimit, L., Eddafry, R., and Busta, F.F. (1995). Thermal inactivation kinetics of *Bacillus subtilis* spores suspended in buffer and in oils. *J. Appl. Bacteriol.* 78: 669-676.

Aizenberg, V., Reponen, T., Grinshpun, S.A. and Willeke, K. (2000). Performance of Air-O-Cell, Burkard, and Button Samplers for total enumeration of airborne spores. *Am. Ind. Hyg. Assoc. J*. 61: 855-864.

Amitai, G., Murata, H., Andersen, J.D., Koepsel, R.R., and Russell, A.J. (2010). Decontamination of chemical and biological warfare agents with a single multi-functional material. *A.J. Biomaterials.* 31: 4417-4425.

An, H.R., Mainelis, G., and Yao, M. (2004). Evaluation of a high-volume portable bioaerosol sampler in laboratory and field environments. *Indoor Air*. 14: 385-393.

Balazy, A., Toivola, M., Adhikari, A, Sivasubramani, S.K., Reponen, T., and Grinshpun, S.A. (2006). Do N95 respirators provide 95% protection level against airborne viruses and how adequate are surgical masks? *Amer. J. Infect. Control* 34: 51-57.

Baltschukat, K, and Horneck, G. (1991). Responses to accelerated heavy ions of spores of *Bacillus subtilis* of different repair capacity. *Radiat. Environ. Biophys.* 30: 87-103.

Barraza-Salas, M., Ibarra-Rodríguez, J. R., Mellado, S. J., Salas-Pacheco, J. M., Setlow, P., and Pedraza-Reyes, M. (2010). Effects of forespore-specific overexpression of apurinic/apyrimidinic endonuclease Nfo on the DNA-damage resistance properties of *Bacillus subtilis* spores. *FEMS Microbiol. Lett*. 302: 159-165.

Benjamin, S., and Belluck, D. (Eds). (2001). *A Practical Guide to Understanding, Managing, and Reviewing Environmental Risk Assessment Reports*, CRC Press, Boca Raton, FL.

Brock, T.D., Madigan, M.T., Markinko, J.M., and Parker, J. (1994). *Biology of Microorganisms*, 7th ed.; Prentice-Hall: Englewood Cliffs, NJ, Chapter 6.

Burton, N.C., Adhikari, A., Iossifova, Y., Grinshpun, S.A., and Reponen, T. (2008). Effect of gaseous chlorine dioxide on indoor microbial contaminants. *J. Air and Waste Management Assoc.* 58: 647-656.

Chen, R.-H., Suryanarayana, C., and Chaos, M., (2006). Combustion characteristics of mechanically alloyed ultrafine-grained Al-Mg powders. Adv. *Eng. Mater.* 8: 563-567.

Corbett, J. D. and Von Winbush, S. (1955). The solubility of some metals in their molten halides. *J. Am. Ceram. Soc*. 77: 3964-3966.

Curtiss, L. K. and Krueger, R.G. (1974). Localization of coliphage MS2 A-protein, *J. Virol.* 14: 503-508.

Daniels, J.K., Caldwell, T.P., Christensen, K.A., and Chumanov, G. (2006). Monitoring the kinetics of *Bacillus subtilis* endospore germination via surface-enhanced Raman scattering spectroscopy. *Anal. Chem.* 78: 1724-1729.

del Carmen Huesca Espitia, L., Caley, C., Bagyan, J., and Setlow, P. (2002). Base-change mutations induced by various treatments of *Bacillus subtilis* spores with and without DNA protective small, acid-soluble spore proteins. *Mutat. Res.* 503: 77–84.

de Jong, J.C., Harmsen, M., and Trouwborst (1975). Factors in the inactivation of Encephalomyocarditis virus in aerosols, *Infect. & Immun.* 12: 29-35.

Dreizin, E.L. and Schoenitz, M. (2009). Nano-composite energetic powders prepared by arrested reactive milling. US Patent 7,524,355 B2.

Dubovi, E.J. and Akers, T.G. (1970). Airborne stability of tailless bacterial viruses S-13 and MS-2, *Appl. Microbiol.* 19: 624-628.

Eninger, R., Hogan, C.J., Biswas, P., Adhikari, A., Reponen, T. and Grinshpun, S.A. (2009). Electrospray versus nebulization for aerosolization and filter testing with virus particles. *Aerosol Sci. Technol.* 43: 298–304.

Fairhead, H., Setlow, B., and Setlow, P. (1993). Prevention of DNA Damage in spores and in vitro by small, acid-soluble proteins from Bacillus species. *J. Bacteriol.* 175: 1367-1374.

Farley, C. and Pantoya, M. (2010). Reaction kinetics of nanometric aluminum and iodine pentoxide. *J. Therm. Anal. Calorim*., in press.

Franz, D.R., Parrott, C.D., and Takafuji, E.T. (1997). The U.S. biological warfare and biological defense programs. *Medical Aspects of Chemical and Biological Warfare* (Edited by Sidell, F.R., Takafuji, E.T. and Fraz, D.R.), Borden Institute, Walter Reed Army Medical Center, Washington, D.C.

Green, L.H. and Green G.M. (1968). Direct method for determining the viability of a freshly generated mixed bacterial aerosol. *Appl. Environ. Microbiol*. 16: 78-81.

Grinshpun, S.A., Adhikari, A., Honda, T., Kim, K.Y., Toivola, M., Rao, K.S.R., and Reponen, T. (2007). Control of aerosol contaminants in indoor air: combining the particle concentration reduction with microbial inactivation. *Environ. Sci. Technol.* 41: 606-612.

Grinshpun, S. A., Adhikari, A., Li, C., Reponen, T., Yermakov, M., Schoenitz, M., Dreizin, E., Trunov, M., and Mohan, S. (2010a). Thermal inactivation of airborne viable *Bacillus subtilis* spores by a short-term exposure in axially heated air flow. *J. Aerosol Sci.* 41: 352–363.

Grinshpun, S.A., Adhikari, A., Li C., Yermakov, M., Reponen, L., Johansson, E. and Trunov M. (2010b). Inactivation of aerosolzed viruses in continuous air flow with axial heating, *Aerosol Sci. Technol.* 44: 1042-1048.

Grinshpun, S.A., Mainelis, G., Trunov, M., Adhikari, A., Reponen, T., and Willeke, K. (2005). Evaluation of ionic air purifiers for reducing aerosol exposure in confined indoor spaces, *Indoor Air*. 15: 235-245.

Grinshpun, S.A., Mainelis, G., Trunov, M., Górny, R.L., Sivasubramani, S.K., Adhikari, A., and Reponen, T. (2005). Collection of airborne spores by circular single-stage impactors with small jet-to-plate distance. *J. Aerosol Sci.,* 36: 575-591.

Gugelchuk, M., (2001). Aluminum Iodide. *Encyclopedia of Reagents for Organic Synthesis. John Wiley & Sons Ltd.;* DOI: 10.1002/047084289X.ra083

Havelaar, A. H., van Olphen, M., and Drost, Y.C. (1993). F-specific RNA bacteriophages are adequate model organisms for enteric viruses in fresh water. *Appl. Environ. Microbiol.* 59: 2956–2962.

Henderson, D.A. (2004). The threat of aerosolized biological weapons. *ASHRAE J.* 46: 50-53.

Heinrich, J. , Hölscher, B., Douwes, J., Richter, K., Koch, A., Bischof, W., Fahlbusch, B., Kinne, R.W., and Wichmann, H.E. (2003). INGA Study Group, Reproducibility of allergen, endotoxin and fungi measurements in the indoor environment, *J. Expos. Anal. Environ. Epidemiol.* 13: 152-160.

Helfinstine, S. L., Vargas-Aburto, C., Uribe, R. M., and Woolverton, C. J. (2005). Inactivation of *Bacillus* Endospores in envelopes by electron beam irradiation. *Appl. Environ. Microbiol.* 71: 7029-7032.

Hiatt, C.W. (1964). Kinetics of the inactivation of viruses, *Bacteriol. Rev.* 28:150–163.

Hill, S.C., Pinnick, R.G., Niles, S., Pan, Y.-L., Holler, S., Chang, R.K., Bottiger, J., Chen, B.T., Orr, C.-S., Feather, G., and Snyder, A.P. (1999). Real-time measurement of fluorescence spectra from single airborne biological particles. *Field Analytic. Chem. Technol.* 3: 221-239.

Hitchcock, P.J., Mair, M., Inglesby, T.V., Gross, J., Henderson, D.A., O'Toole, T., Ahern-Seronde, J., Bahnfleth, W.P., Brennan, T., Burroughs, H.E.B., Davidson, C., Delp, W., Ensor, D.S., Gomory, R., Olsiewski, P., Samet, J.M., Smith, W.M., Streifel, A.J., Hogan, C. J., Kettleson, E. M., Lee, M. -H., Ramaswami, B., Angenent, L. T., and Biswas, P. (2005). Sampling methodologies and dosage assessment techniques for submicrometre and ultrafine virus aerosol particles, *J. Appl. Microbiol.* 99: 1422-1434.

Holman, J.P. (2002). *Heat Transfer*, 9nd ed., McGraw-Hill, Boston, MA.

Hung, L.L., Miller, J.D., and Dillon, H.K. (2005). Field Guide for the Determination of Biological Contaminants in Environmental Samples. *AIHA - American Industrial Hygiene Association. 2nd Edn. (Eds.)* AIHA, Fairfax, Virginia.

ISO - International Organization for Standardization 10705-2:2000 (2000). Water quality - Detection and enumeration of bacteriophages - Part 2: Enumeration of somatic coliphages.

Johnson, B., Martin, D.D., and Resnick, I.G. (1994). Efficacy of selected respiratory protective equipment challenged with *Bacillus subtilis* subsp. *niger*. *Appl. Environ. Microbiol.* 60: 2184-2186.

Johnson, C. E.; Higa, K. T., and Albro, W. R. (2008). Nanothermites with condensable gas Products. *Proceedings of the 35th International Pyrotechnics Seminar.* 35: 159-168.

Johnson, H.R., Hooker, J.M., Francis, M.B., and Clark, D.S. (2007). Solubilization and stabilization of bacteriophage MS2 in organic solvents. *Biotechnol. Bioengin.* 97: 224-234.

Jones, M.V., Bellamy, K., Alcock, R., and Hudson, R. (1991). The use of bacteriophage MS2 as a model system to evaluate virucidal hand disinfectants, *J. Hosp. Infect.* 17: 279–285.

Jung, J.H., Lee, C.H., Lee, J.E., Lee, J.H., Kim, S.S., and Lee, B.U. (2009a). Design and characterization of a fungal bioaerosol generator using multi-orifice air jets and a rotating substrate. *J Aerosol Sci.,* 40: 72-80.

Jung, J.H., Lee, E.L., and Kim, S.S. (2009b). Thermal effects on bacterial bioaerosols in continuous air flow, *Sci. Total Environ.* 407: 4723-4730.

Jung, J.H., Lee, J.E., Lee, C.H., Kim, S.S., and Lee, B.U. (2009c). Treatment of fungal bioaerosols by a high-temperature, short-time process in a continuous flow system, *Appl. Environ. Microbiol.* 75: 2742-2749.

Kawabata, N. and Kawato, S. (1998). Removal of airborne bacteria by filtration using a composite microporous membrane made of a pyridinium-type polymer showing strong affinity with microbial cells. *Epidemiol.. & Infect.* 121: 349-356.

Kempf, M.J., Schubert, W.W., and Beaudet, R.A. (2008). Determination of lethality rate constants and D-values for *Bacillus atrophaeus* (ATCC 9372) spores exposed to dry heat from 115ºC to 170ºC. *Astrobiology.* 8: 1169-1182.

Koch, A. (2006). US makes quiet progress on 'agent defeat'. *Jane's Defence Weekly* JAN.: 405-406.

Laflamme, C., Lavigne, S., Ho, J., and Duchaine, C. (2004). Assessment of bacterial endospore viability with fluorescent dyes. *J. Appl. Microbiol.* 96: 684-692.

Larson, A. C. and Von Dreele, R. B. (2004). General Structure Analysis System (GSAS). *Los Alamos National Lab. Rept*. LAURL, pp. 86-748.

Lee, Y.H. and Lee, B.U. (2006). Inactivation of airborne *E. coli* and *B. subtilis* bioaerosols utilizing thermal energy. *J. Microbiol. Biotechnol.* 16: 1684-1689.

Lemke, K.H., Rosenbauer, R.J., and Bird, D.K. (2009). Peptide synthesis in early Earth hydrothermal systems, *Astrobiology.* 9: 141-146.

Li, C. S., Hao, M. L., Lin, W. H., and Chang, C.W. (1999). Evaluation of microbial samplers for bacterial microorganisms, *Aerosol Sci. Technol.* 30: 100–108.

Lin, C.Y. and Li, C.S. (2002). Control effectiveness of ultraviolet germicidal irradiation on bioaerosols. *Aerosol Sci. Technol*. 36: 474-478.

Lin, X., Reponen, T., Willeke, K., Wang, Z., Grinshpun, S.A., and Trunov, M. (2000). Survival of airborne microorganisms during swirling aerosol collection. *Aerosol Sci. Technol.* 32: 184-196.

Luna, V. A., Cannons, A. C., Amuso, P. T., and Cattani, J. (2008). The inactivation and removal of airborne Bacillus atrophaeus endospores from air circulation systems using UVC and HEPA filters. *J. Appl. Microbiol.* 104: 489–498.

Mainelis, G., Grinshpun, S., Willeke, K., Reponen, T., Ulevicius, V., and Hintz, P. (1999). Collection of airborne microorganisms by electrostatic precipitation. *Aerosol Sci. Technol.* 30: 127-144.

Martirosyan, K.S., Wang, L,. and Luss, D. (2009). Novel nanoenergetic system based on iodine pentoxide. *Chem. Phys. Let.* 483: 107-110.

Ma, Y., Zhang, G.-J., Shi, X.-M., Xu, G.-M., and Yang, Y. (2008). Chemical mechanisms of bacterial inactivation using dielectric barrier discharge plasma in atmospheric air. *IEEE Transact. Plasma Sci.* 36: 1615-1620.

McBean, E.A. and Rovers, F.A. (1998). *Statistical Procedures for Analysis of Environmental Monitoring Data and Risk Assessment*. Prentice Hall, Upper Saddle River, NJ.

Molin, G. and Östlund, K. (1975). Dry-heat inactivation of *Bacillus subtilis* spores by means of infra-red heating. *Antonie van Leeuwenhoe*. 41: 329-335**.**

Mullican, C.L., Buchanan, L.M., and Hoffman, R.K. (1971). Thermal inactivation of aerosolized *Bacillus subtilis* var. *niger* spores. *Appl. Microbiol.* 22: 557-559.

Munakata, N., Morohoshi, F., Saitou, M., Yamazaki, N., and Hayashi, K. (1994). Molecular chacaterization of thirteen *gyrA* mutations conferring nalidixic acid resistance in Bacillus subtilis. *Mol. Gen. Genet.* 244: 97-103.

Muranyi, P., Wunderlich, J., and Heise, M. (2007). Sterilization efficiency of a cascaded dielectric barrier discharge. *J. Appl. Microbiol.* 103: 1535–1544.

Nadasi, E., Varjas, T., Prantner, I., Virag, V.. and Ember, I. (2007). Bioterrorism: Warfare of the 21st century. *Gene Ther. Mol. Biol*. 11: 315-320.

Nelson, R.W. (2004). Nuclear ‘‘bunker busters’’ would more likely disperse than destroy buried stockpiles of Biological and chemical agents. *Sci. Global Secur.* 12: 69-89.

Nicholson, W.L., Munakata, N., Horneck, G., Melosh, H.J., and Setlow, P. (2000). Resistance of *Bacillus* endospores to extreme terrestrial and extraterrestrial environments, *Microbiol. Mol. Biol. Rev.* 64: 548-572.

Northrop, J., and Slepecky, R. A. (1967). Sporulation mutations induced by heat in *Bacillus subtilis, Science.* 155: 838-839.

Obrey, S., Pachecho, A. N., Foley, T. J., Higa, K. T., and Johnson, C. E. (2008). Sensitivity, ignition and flame propagation in new nano-aluminum iodate nanoenergetic material. *Proceedings of JANNAF Meeting, (May 2008, Boston, MA).*

O'Callaghan, R., Bradley, R., and Paranchych, W. (1973). Controlled alterations in the physical and biological properties of R17 bacteriophage induced by gunaidine hydrochloride, *Virology* 54: 476-494.

Pfeifer, J. and Kessler, H.G. (1994). Effect of relative humidity of hot air on the heat resistance of *Bacillus cereus* spores. *J. Appl. Bacteriol.* 77: 121-128.

Price, E.W. (1984). Combustion of metalized propellants. *Progr. Astronaut. Aero.* 90: 479-513.

Rengasamy, S., Fisher, E., and Shaffer, R.E. (2010). Evaluation of the survivability of MS2 viral aerosols deposited on filtering face piece respirator samples incorporating antimicrobial technologies, *Amer. J. Infect. Control.* 38: 9-17.

Reponen, T., Willeke, K., Ulevicius, V., Grinshpun, S.A. and Donnelly, J. (1997). Techniques for dispersion of microorganisms into air. *Aerosol Sci. Technol.* 27: 405-421.

Riemenschneider, L., Woo, M.-H., Wu, C.-Y., Lundgren, D., Wander, J., Lee, J.-H., Li, H.-W, and Heimbuch, B. (2010). Characterization of reaerosolization from impingers in an effort to improve airborne virus sampling. *J. Appl. Microbiol.* 108: 315-324.

Roth, S., Feichtinger, J., and Hertel, C. (2010). Characterization of Bacillus subtilis spore inactivation in low-pressure, low-temperature gas plasma sterilization processes. *J. Appl. Microbiol.*108: 521-531.

Russell, A.D. (2003). Similarities and differences in the responses of microorganisms to biocides. *J. Antimicrob.Chemoth.* 52: 750-763..

Santos I., Haemmerich D., Pinheiro C.S. and Rocha, A. F. (2008). Effect of variable heat transfer coefficient on tissue temperature next to large vessel during radiofrequency tumor ablation. *BioMedical Engineering Online*. **7**:21 (available http://www.biomedical-engineering-online.com/content/7/1/21)

Schoenitz, M., Chen, C-M., and Dreizin, E.L. (2009). Oxidation of aluminum particles in the presence of water. *J. Phys. Chem*. B.113: 5136-5140.

Schoenitz, M. and Dreizin, E.L. (2003). Structure and properties of Al-Mg mechanical alloys. *J. Mater. Res*. 18: 1827-1836.

Schoenitz, M. and Dreizin, E.L. (2004). Oxidation processes and phase changes in metastable Al-Mg alloys. *J. Propuls. Power.* 20: 1064-1068.

Shoshin, Y. L. and Dreizin, E.L. (2006). Particle combustion rates for mechanically alloyed Al-Ti and aluminum powders burning in air. *Combust. Flame.* 145: 714-722.

Shoshin, Y. L., Trunov, M.A., Zhu, X., Schoenitz, M., and Dreizin, E.L. (2006). Ignition of aluminum-rich Al-Ti mechanical alloys in air. *Combust. Flame.* 144: 688–697.

Setlow, B. and Setlow, P. (1995). Small, acid-soluble proteins bound to DNA protect *Bacillus subtilis* spores from killing by dry heat. *Appl. Environ. Microbiol.* 61: 2787–2790.

Setlow, P. (1995). Mechanisms for the prevention of damage to the DNA in spores of *Bacillus* species, *Annual Rev. Microbiol.* 49: 29–54.

Setlow, P. (2006). Spores of *Bacillus subtilis*: their resistance to and killing by radiation, heat and chemicals. *J. Appl. Microbiol.* 101: 514-525.

Shafaat, H. S., and Ponce, A. (2006). Applications of a rapid endospore viability assay for monitoring UV inactivation and characterizing Arctic Ice Cores. *Appl. Environ. Microbiol.* 72: 6808-6814.

Stamatis, D., Jiang, Z., Hoffmann, V.K., Schoenitz, M., and Dreizin, E.L. (2009). Fully dense, aluminum-rich Al-CuO nanocomposite powders for energetic formulations. *Combust. Sci. Technol.* 181: 97-116.

Starink, M.J. (2003). The determination of activation energy from linear heating rate experiments: A comparison of the accuracy of isoconversion methods. *Thermochim. Acta*. 404: 163-176.

Stonehouse, N.J., and Stockley, P.G. (1993). Effects of amino acid substitution on the thermal stability of MS2 capsids lacking genomic RNA, *FEBS Lett.* 334: 355-359.

Stumbo, C.R. (1973). *Thermobacteriology in Food Processing*. Academic Press, London.

Sullivan K. T., Piekiel N. W., Chowdhury S., Wu C., Johnson C.E., and Zachariah M. R. (2010). Novel nanoenergetic system based on iodine pentoxide. *Combust. Sci. Technol*., in press.

Suryanarayana, C. (2001). Mechanical alloying and milling. *Prog. Mater*. Sci. 46: 1-184.

Suryanarayana, C. (2008). Recent developments in mechanical alloying. *Rev. Adv. Mater. Sci*. 18: 203-211.

Tan, B., Peng, R., Chen, X., Li, H., Yu, W., and Chu, S. (2006). Evaluation of destruction methods of chemical and biological warfare agents. *J. Chongqing University (Natural Science Edition)* [in Chinese] 29: 127-131.

Tanooka, H., Munakata, N., and Kitahara, S. (1978). Mutation induction with UV- and X-radiations in spores and vegetative cells of *Bacillus subtilis*. *Mutaion Research.*49: 179-186.

Thomas L.C. (1992). *Heat Transfer*, 2nd ed., Prentice Hall: Englewood Cliffs, NJ.

Trunov, M.A., Schoenitz, M., and Dreizin, E.L. (2006). Effect of polymorphic phase transformations in alumina layer on ignition of aluminium particles. *Combust. Theor. Model*. 10: 603-623.

Trunov, M.A., Schoenitz, M., Zhu, X., Dreizin, E.L. (2005). Effect of polymorphic phase transformations in Al2O3 film on oxidation kinetics of aluminum powders. *Combust. Flame*. 140: 310-318.

Tseng, C.-C., and Li, C.-S. (2005). Collection efficiencies of aerosol samplers for virus-containing aerosols, *J. Aerosol Sci*. 36: 593–607.

Ulevicius, V., Willeke, K., Grinshpun, S.A., Donnelly, J., Lin, X., and Mainelis, G. (1997). Aerosolization of particles by bubbling liquid: characteristics and generator development. *Aerosol Sci. Technol.* 26: 175-190.

Umbrajkar, S.M., Seshadri, S., Schoenitz, M., Hoffmann, V.K., and Dreizin E.L. (2008). Aluminum-rich Al-MoO_3 nanocomposite powders prepared by arrested reactive milling. *J. Propulsion Power* 24: 192-198.

Vadhe, P.P., Pawar, R.B.; Sinha, R.K.; Asthana, S.N.; and Rao, S. (2008). Cast aluminized explosives (review). *Combust. Explo. Shock Waves*.44: 461-477.

Verreault, D., Moineau, S., and Duchaine, C. (2008). Methods for sampling of airborne viruses. *Microbiol. Mol. Biol. Rev.* 72: 413-444.

Vyazovkin, S. (2001). Modification of the integral isoconversional method to account for variation in the activation energy. *J. Comput. Chem.* 22: 178.

Ward, T.S., Trunov, M.A., Schoenitz, M., and Dreizin, E.L. (2006). Experimental methodology and heat transfer model for identification of ignition kinetics of powdered fuels. *Int. J.l Heat Mass Tran.* 49: 4943-4954.

Wayman, C., Gordon, E., and King, G. (1999). The method detection limit and practical quantitation level: their derivations and regulatory implications. *Proceedings of Waste Management Conference* (WM'99**,** Tucson, AZ, February 28 **-** March 4**,** 1999).

White, R.H. and Woods, J.E. (2006). Improving performance of HVAC systems to reduce exposure to aerosolized infectious agents in buildings; recommendations to reduce risks posed by biological attacks. *Biosecur. Bioterror.* 4: 41-54.

Wood, J.P., Lemieux, P., Betancourt, D., Kariher, P., and Griffin, N. (2008). Pilot-scale experimental and theoretical investigations into the thermal destruction of a *Bacillus anthracis* surrogate embedded in building decontamination residue bundles. *Environ. Sci. Technol.* 42: 5712-5717.

www.omega.com/temperature/Z/pdf/z088-089.pdf, *Table of Total Emissivity,* pp. Z-88 – Z89, accessed on August 17, 2009.

Zamenhof, S. (1960). Effects of heating dry bacteria and spores on their phenotype and genotype. *Proc. Natl. Acad. Sci. USA* 46: 101-105.

Zhang, S., Schoenitz, M., Dreizin, E.L. (2010). Mechanically alloyed Al-I composite materials. *J. Phys. Chem*. Solids. 71: 1213.

Zhang, S., Schoenitz, M., and Dreizin, E. L. (2010). Preparation and characterization Al-I nanocomposite powders as fuel additives with biocidal combustion products. 48th AIAA Aerospace Sciences Meeting (Orlando, Florida, Jan. 4-7, 2010), #AIAA-2010-618.

Zheng, L.B., Donovan, W.P., Fitz-James, P.C., and Losick, R. (1988). Gene encoding a morphogenic protein required in the assembly of the outer coat of the *Bacillus subtilis* endospore. *Genes & Development*. 2: 1047-1054.

Zhu, X., Schoenitz, M., and Dreizin, E.L., (2006). Oxidation of mechanically alloyed Al-rich Al-Ti powders. *Oxid. Met.* : 65357-65376.

Zhu, X., Schoentiz, M., Dreizin, E.L., (2007). Mechanically alloyed Al-Li powders. *J. Alloys Compd.* 432: 111-117.

Zytkovic, T. H. and Halvorson, H.O. (1972). Some characteristics of dipicolinic acid-less mutant spores of *Bacillus cereus, Bacillus megaterium* and *Bacillus subtilis*. *Spores V*. (Edited by H. O. Halvorson, R. Hanson, and L. L. Campbell), American Society for Microbiology, Washington, D.C.: 49–52

DEPARTMENT OF DEFENSE

DEFENSE TECHNICAL
INFORMATION CENTER
8725 JOHN J. KINGMAN ROAD,
SUITE 0944
FT. BELVOIR, VA 22060-6201
ATTN: DTIC/OCA

DEPARTMENT OF DEFENSE CONTRACTORS

EXELIS, INC.
1680 TEXAS STREET, SE
KIRTLAND AFB, NM 87117-5669
ATTN: DTRIAC